STEERING LAW DESIGN FOR REDUNDANT SINGLE GIMBAL CONTROL MOMENT GYRO SYSTEMS

by

NAZARETH SARKIS BEDROSSIAN

BSME University of Florida
(1984)

SUBMITTED IN PARTIAL FULFILLMENT
OF THE REQUIREMENTS FOR THE
DEGREE OF

MASTER OF SCIENCE

IN MECHANICAL ENGINEERING

at the

MASSACHUSETTS INSTITUTE OF TECHNOLOGY

August 1987

c Charles Stark Draper Laboratory Inc., 1987

Signature of Author __
Department of Mechanical Engineering
August 7, 1987

Certified by __
Edward V. Bergmann
Technical Supervisor, CSDL

Certified by __
Professor Derek Rowell
Thesis Supervisor

Accepted by _____
Professor Ain A. Sonin
Chairman, Departmental Graduate Committe

MASSACHUSETTS INSTITUTE
OF TECHNOLOGY

NOV 0 4 1987

LIBRARIES
Archives

ACKNOWLEDGEMENTS

First and foremost, I would like to thank the Charles Stark Draper Laboratory for affording me the opportunity to continue my graduate education at MIT, and providing the excellent environment, abundant resources, and generous financial support, which have made this thesis much easier. I am especially gratefull to Dave Redding for having enough faith in me, and for providing guidance and advice. Ed Bergmann deserves special mention for allowing me the freedom to explore this thesis area. I would also like to thank Prof. Rowell for overseeing this thesis.

This research benefited enormously from discussions with Joe Paradiso. He was always available to listen and provide valuable suggestions about the subject matter. He also deserves my sincere gratitude for painstakingly reviewing this thesis from cover to cover, and providing constructive criticism. I would like to thank my officemate Brent Appleby, for providing a sounding board for my ideas as well as valuable advise, and assisting with the development of the simulation package. I would also like to thank Marty Matuski, Neil Adams, Phil Hattis, Greg Barton and his fan, Greg Chamitoff, and John Dzielski for helpful discussions. Also Bob Boucher and the consulting staff deserve special praise for their invaluable assistance in preparing this document.

I would like to thank my parents for their love and guidance throughout the years. Finally, I can never thank enough my wife Melinda, who has supported me with such remarkable patience and sensitivity.

This report was prepared at The Charles Stark Draper Laboratory, Inc. under contract NAS9-17560 with the National Aeronautics and Space Administration.

Publication of this report does not constitute approval by the Charles Stark Draper Laboratory or NASA of the findings or conclusions contained herein. It is published solely for the exchange of ideas.

TABLE OF CONTENTS

LIST OF ILLUSTRATIONS

CHAPTER 1

INTRODUCTION

Single gimbal Control Moment Gyros (CMGs) are angular momentum storage devices that can apply torque to a vehicle without expending consumables. Single gimbal CMGs have significant advantages over double gimbal CMGs in spacecraft attitude control; i.e. mechanical simplicity and ability to provide torque amplification. Despite these advantages, single gimbal CMGs are plagued by singular states which preclude torque generation in a certain direction, and thus lead to loss of three-axis control of the vehicle. These conditions, if not properly addressed, severely limit the usable momentum capability of the CMG system. Hardware limits on gimbal rates entail that neighborhoods of singular states be considered in the control law design, since they represent regions of limited torque capability, thus require high gimbal rates to generate the requisite torque.

Although the extra degrees of freedom provided by adopting redundant CMG systems can be used to avoid these singular states, the use of redundant CMG systems does not elliminate the singularity problem. Since the specific arrangement of the gimbals affects the type and number of singularities, one may reduce the possibility of encountering singular states within the CMG momentum workspace through modifications and improvements in CMG design. Control laws designed to manage single gimbal systems, however, must nonetheless account for these singular states in order to extract maximum performance.

A method for resolving this redundancy is required for the proper formulation and design of spacecraft attitude control systems, which define a required output torque from the single gimbal CMG system as a function of the state of the vehicle. These

methods are refered to as Steering laws because they address the kinematic relationship between gimbal rates and total CMG output torque. Intelligent design of a Steering law warrants careful examination of the singular states mentioned above. These two themes comprise the central thrust of this thesis.

The general objective of this thesis is to study the control of kinematically redundant single gimbal CMGs. To this end there are two major objectives. The first goal includes the detailed analysis of singular states and development of a method that distinguishes between different types of singularities. The second goal is the development of a general Steering law for 4-Pyramid mounted single gimbal CMGs. An overview of the thesis is presented below:

In Chapter 2, single gimbal CMG fundamentals will be reviewed, and the mechanical analog to the CMG system, the robotic manipulator, will be presented. A simple method of generating an orthogonal null-space basis to the Jacobian matrix will also be given.

In Chapter 3, the control architecture for spacecraft equipped with single gimbal CMGs will be reviewed. The desirability to accomodate occasional errors in torque delivered by the CMG system will be discussed.

In Chapter 4, the singular states of single gimbal CMGs will be classified, and a test for null motion near a singular configuration will be presented. Examples of different types of singularities will be presented for both the CMG system and a planar

manipulator, and the relationship between the singularity measure and the null-space of the Jacobian matrix will be examined.

In Chapter 5, various torque-input Steering laws will be reviewed, and alternative singularity avoidance methods will be proposed. Performance of these candidate methods will be examined and compared in computer simulations using the 4-CMG system.

In Chapter 6, a method of singularity avoidance based on the SR-inverse will be proposed. This approach will be compared to the methods introduced in Chapter 5, and simulation results will be presented to verify its performance.

Finally, in Chapter 7, concluding remarks and recommendations will be given.

CHAPTER 2

SINGLE GIMBAL (SG) CONTROL MOMENT GYRO (CMG) FUNDAMENTALS

2.1 CHARACTERISTICS OF SG SYTEMS

A single gimbal CMG consists of a flywheel spinning at a constant rate about an axis that is gimballed to allow changes in the spin direction. An example of such a device is shown in Figure 2-1. The CMG is a constant magnitude angular momentum storage device since the flywheel rate is held constant. As can be seen from the figure, the momentum vector is restricted to lie in the plane of rotation. The gimbal is rigidly attached to the spacecraft and is able to rotate about the gimbal axis. A coordinate system attached to each gimbal is defined by the orthonormal basis vectors:

$$\left\{ \hat{\theta}_i, \hat{h}_i, \hat{j}_i \right\}$$

where $\hat{\theta}_i =$ *Unit vector along gimbal axis*

$\hat{h}_i =$ *Unit vector along angular momentum*

$\hat{j}_i =$ *Unit vector given by* $\hat{\theta}_i \times \hat{h}_i$

For each CMG, the gimbal angle θ_i is measured with respect to the reference coordinate frame with positive angular displacement defined by the gimbal axis direction. The reference frame is defined by the initial orientation of the gimbal-fixed frame and is denoted by $\left\{ \hat{\theta}_i, \hat{h}_i{}^0, \hat{j}_i{}^0 \right\}$. The expression for the unit vectors $\left\{ \hat{h}_i, \hat{j}_i \right\}$ in this reference frame is given by:

$$\begin{aligned} \hat{h}_i &= \cos\theta_i \hat{h}_i{}^0 + \sin\theta_i \hat{j}_i{}^0 \\ \hat{j}_i &= -\sin\theta_i \hat{h}_i{}^0 + \cos\theta_i \hat{j}_i{}^0 \end{aligned} \qquad (2\text{-}1)$$

This is shown in Figure 2-1.

For a system of n single gimbal CMGs, the total system angular momentum is the vector sum of the individual momenta, i.e.

$$\underline{h}(\underline{\theta}) = \sum_{i=1}^{n} \underline{h}_i(\theta_i) \tag{2-2}$$

where $\underline{h}(\underline{\theta}) =$ *Total system angular momentum*

$\underline{h}_i(\underline{\theta}_i) =$ *Angular momentum of* i^{th} *CMG*

$\theta_i =$ i^{th} *gimbal angle*

The expression for the angular momentum of the i^{th} CMG with respect to the reference coordinate frame is given by:

$$\underline{h}_i = h_i \hat{h}_i$$

where $h_i =$ *Magnitude of* i^{th} *CMG angular momentum*

2.2 PRINCIPLE OF OPERATION

The principle governing the operation of a CMG system is that torque is the time rate of change of angular momentum. Since the magnitude of the angular momentum of a CMG is constant, torque is produced by rotation of the momentum vector. The direction of the output torque is given by the right-hand rule, i.e. gimbal axis "crossed" into momentum direction. This is shown in Figure 2-2. The CMG output torque is given by:

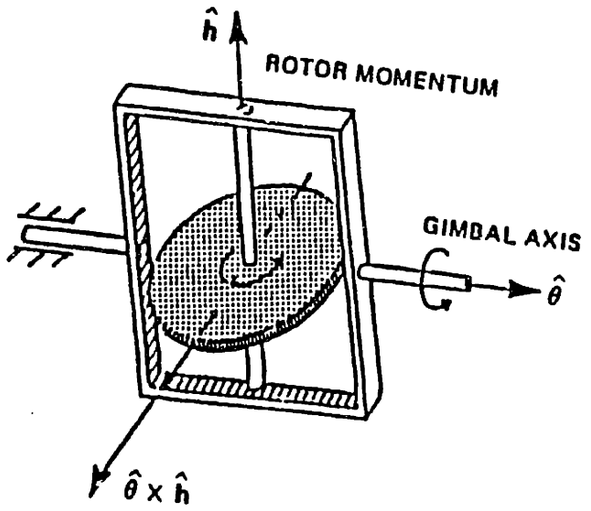

Figure 2-1. Single Gimbal CMG (Part 1 of 2)

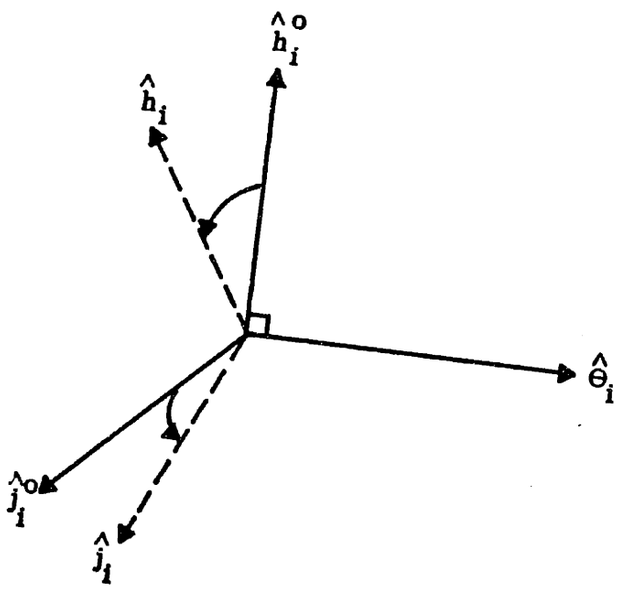

Figure 2-1. Reference Gimbal Coordinate Frame. (Part 2 of 2)

$$\underline{T} = \dot{\underline{h}} = \underline{\dot{\theta}} \times \underline{h}$$

As in the case of the angular momentum, the output torque of a CMG lies in the plane of rotation. It is also clear that the torque direction is perpendicular to the momentum direction. This type of device can be thought of as a two-sided actuator due to its ability to produce a torque in opposite directions, as opposed to an individual jet which can provide a torque in only one direction.

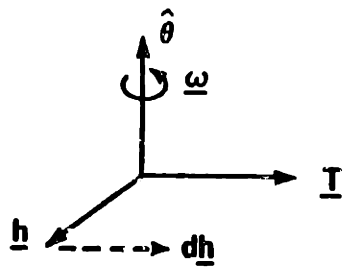

Figure 2-2. CMG Output Torque

For spacecraft three-axis control, at least three single gimbal CMGs are required. If the CMG system in question has more actuators (gimbals) than rotational degrees of freedom, it is termed redundant. The degree of redundancy is given by the difference between the number of CMGs and the number of degrees of freedom to be controlled.

2.3 MECHANICAL ANALOG

In order to visualize motions of a CMG system, the concept of the momentum

linkage [1] is introduced and the analogy to a robotic manipulator is proposed. Consider the CMG system as an open-loop kinematic chain or linkage made up of equal "length" momentum links, placed in arbitrary order, with one link attached to a grounded pivot. The "length" of each link is given by the magnitude of each CMG angular momentum, considered equal in this case. The individual links are constrained to rotate in a fixed plane determined by the corresponding gimbal axes. The motivation for this concept derives from the expression for the total angular momentum of a CMG system as the vector sum of individual momenta. The summation operation in this case is commutative. For a robotic manipulator, the end-effector position is the vector sum of the individual link displacements. It is proposed that a correspondence exists between link displacements for a manipulator and individual momenta for a CMG system. The first part of the analog then, is the correspondence between angular momentum for a CMG system and displacement for a manipulator.

The momentum linkage can be defined as a commutative linkage with links made up of individual momenta, $\underline{h}_i$ [1]. The total system momentum corresponds to the position of the momentum linkage tip in momentum space which is a Euclidean 3-space E^3. We can think of the momentum linkage as a manipulator whose end-effector position corresponds to total angular momentum. The workspace of this manipulator naturally corresponds to the momentum volume and the boundary of the workspace is defined as the momentum envelope or locus of all points traced out by the maximally stretched momentum linkage. An example of the momentum envelope for 4-Pyramid mounted CMGs is shown in Figure 2-3, [1]. The holes or funnels represent windows on the envelope. These regions represent unattainable momentum

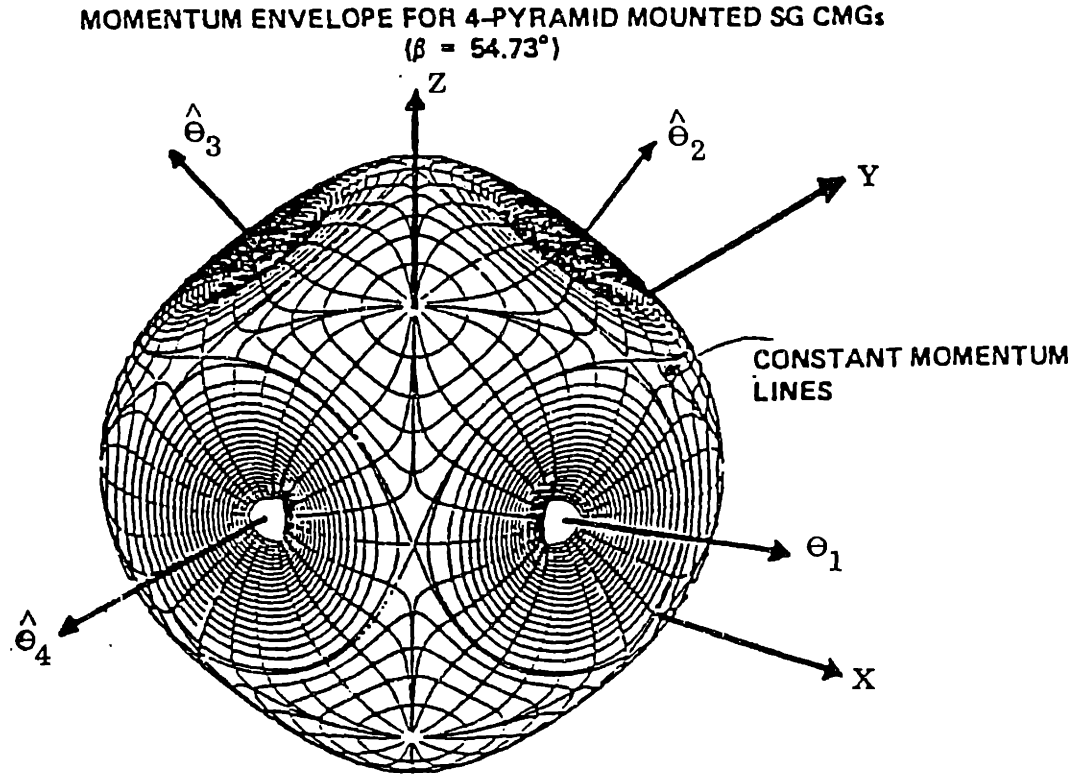

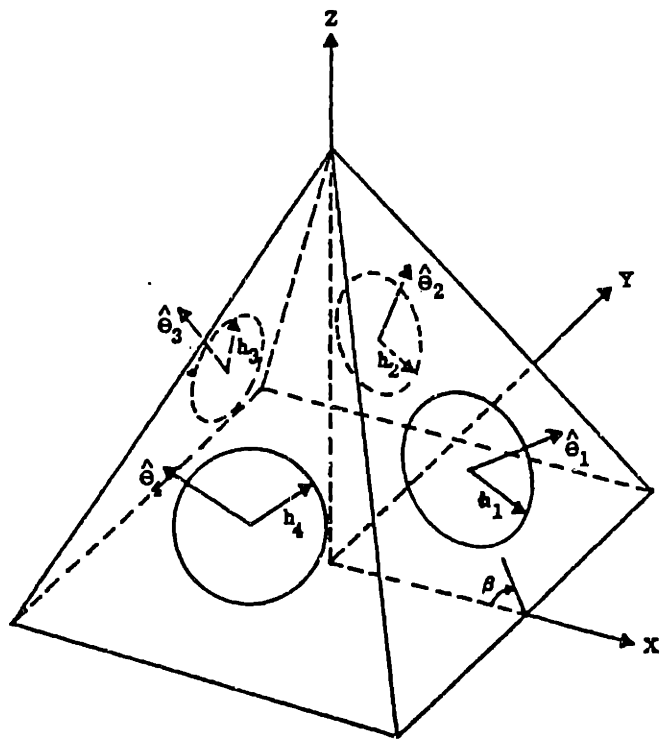

Figure 2-3. Momentum Envelope For 4-Pyramid Mounted CMGs

states, because the normal to the window is aligned with a gimbal axis. The funnel then is part of the boundary to the momentum volume.

The momentum linkage concept was used in [1] to describe the total angular momentum of a CMG system and to describe the boundary surface or momentum envelope as the surface generated by the stretched momentum linkage. The linkage concept was also used to describe null motion of a CMG system, which are discussed in the next section.

2.4 TORQUE AND NON-TORQUE PRODUCING MOTIONS

The output torque for a system of n CMGs is given by the time rate of change of the total system angular momentum relative to a frame of reference of interest, in this case the spacecraft body-fixed coordinate frame, which is given by:

$$\underline{T} = \dot{\underline{h}}(\underline{\theta}) = J(\underline{\theta})\,\dot{\underline{\theta}} \tag{2-3}$$

where $J(\underline{\theta}) \equiv \left[\, \underline{j}_1(\theta_1), \ldots, \underline{j}_n(\theta_n) \,\right]$, *Instantaneous Jacobian matrix* $(3 \times n)$

$$\underline{j}_i(\theta_i) = \frac{\partial \underline{h}}{\partial \theta_i} = \frac{\partial \underline{h}_i}{\partial \theta_i}, \quad \textit{Jacobian columns}$$

It is seen that the total output torque for a system of CMGs is given by the sum of the individual gimbal torques. Extending the momentum linkage concept to this case, the motion (rotation) of each link corresponds to the output torque for each CMG. To draw the analogy to the robotic manipulator, it is noted that for the manipulator the end-effector velocity is the vector sum of the individual link velocities. Just as the

individual link displacements correspond to angular momenta, link velocities correspond to individual CMG output torques, thus the total output torque for a system of CMGs corresponds to the velocity of the momentum linkage tip in E^3. So far it has been established that for the mechanical analog to a CMG system (the robotic manipulator), link lengths correspond to magnitude of individual CMG angular momenta, and end-effector position and velocity to total angular momentum and total output torque for the CMG system. What remains to complete the analogy is to show an equivalence in the singularity problem for a manipulator and the CMG system.

We now turn our attention to torque and non-torque producing link motions (or gimbal rates). First, the linkage concept will be used to describe torque and non-torque producing motions, and then an analytic description in terms of gimbal rates will be presented.

Using the momentum linkage concept, it is seen that the total output torque of a CMG system corresponds to the velocity of the linkage tip. If the linkage tip is stationary, no net torque is applied to the spacecraft. Torque producing motions are those link motions for which the tip of the momentum linkage moves. On the other hand, relative motions of the links that do not affect the location of the linkage tip do not produce a net torque on the spacecraft, and are termed non-torque producing motions. These motions can be visualized by treating the linkage tip as a virtual pivot, which fixes the tip location, and moving the remaining links. The linkage can attain any kinematically admissible configuration or "closure", by relative link motions as long as the linkage tip remains stationary. These relative motions are termed "admissible". An example of such a motion for the mechanical analog is shown in Figure 2-4. The cho-

sen analog is a 3-link planar manipulator that possesses one degree of redundancy, since only two degrees of freedom are to be controlled.

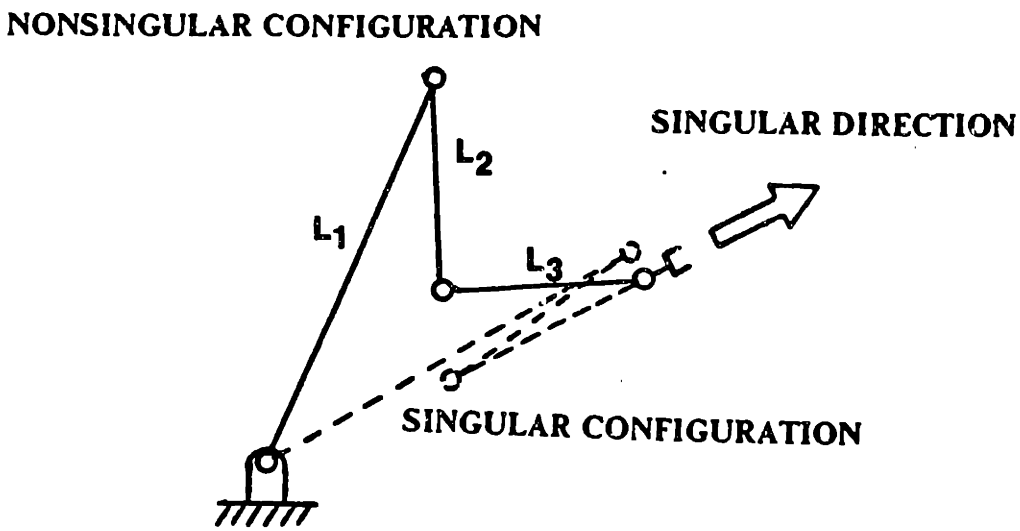

Figure 2-4. Example Of Null Motion For Mechanical Analog

To express torque producing and non-torque producing motions in terms of gimbal rates, we can see that torque producing motions consist of gimbal rates that result in movement of the linkage tip, and gimbal rates that do not affect the location of the linkage tip are called non-torque producing rates. This concept is naturally expressed by the general solution to the non-homogeneous system of linear equations in (2-3). The general solution can be represented as:

$$\dot{\underline{\theta}} = \dot{\underline{\theta}}_P + \dot{\underline{\theta}}_H$$

$$\text{where} \quad \dot{\underline{\theta}}_P = \text{Particular solution} \left(J(\underline{\theta})\, \dot{\underline{\theta}}_P = \underline{T} \right)$$

$$\dot{\underline{\theta}}_H = \text{Homogeneous solution} \left(J(\underline{\theta})\, \dot{\underline{\theta}}_H = \underline{0} \right)$$

The particular solution expresses the torque producing gimbal rates, and the homogeneous solution the non-torque producing gimbal rates or "null motion". The term "null motion" arises from the fact that the solution to the homogeneous system consists of gimbal rates that lie in the null-space of the Jacobian matrix, and therefore produce no instantaneous torque ("instantaneous" because the Jacobian matrix is evaluated using the instantaneous values of the gimbal angles). These "null motions" are the variations of "admissible" relative link motions. This property of null motion can be exploited to reconfigure the linkage or momentum state of the CMG system without altering its total momentum. Correspondingly, torque producing gimbal rates lie in the row space or orthogonal complement of the null-space of the Jacobian. The solution-space to the non-homogeneous problem can be regarded as 2-dimensional, with an orthogonal basis consisting of the torque and non-torque producing solutions.

The system of linear equations (2-3) can be solved as long as the rank of the Jacobian matrix is 3. If the rank is less than 3, the CMG system cannot produce a torque along all three axes of the spacecraft, and three-axis controllability is lost. The CMG system is termed singular when the rank of the Jacobian is less than 3, i.e. the matrix is singular. This essentially defines the singularity problem for CMGs. In this situation no output torque is available along an axis or direction. This information will now be used to establish the equivalence of the singularity problem of a CMG system to that of a corresponding manipulator.

We have seen that velocity for a manipulator is analogous to torque for a CMG system. The Jacobian matrix for a manipulator transforms joint rates to end-effector velocity whereas for a CMG system the Jacobian transforms gimbal rates to torque. When the manipulator Jacobian loses rank (becomes singular), motion in a particular direction is not possible. An example of a singular configuration for a planar manipulator is shown in Figure 2-4. The singularity analog is established by noting that for a manipulator no motion is possible in a certain direction, whereas for a CMG system no torque is possible in a certain direction. The singularity problem for both systems is similar. Of course the elements of the manipulator Jacobian will not be the same as those for a CMG, although the general structure is the same. A summary of the analogy between a manipulator and a CMG system is given in Table 2-1. The conclusion from the above discussion is that manipulators and CMG system have similar singularity problems and results from one area may be applicable to the other.

2.5 EXAMPLES OF SG CMG SYSTEM AND PLANAR MANIPULATOR

In order to clarify some of the concepts presented in the previous sections, specific examples of a CMG system and a planar manipulator will be presented in this section. We will consider a 4-Pyramid mounted SG CMG system and a planar 3-link manipulator. These particular examples will be used throughout, to illustrate concepts and applications.

2.5.1 4-Pyramid Mounted SG CMG System

The 4-Pyramid type CMG system consists of 4 single gimbal CMGs each positioned on one face of a 4-sided pyramid such that the momentum vector lies in this

Table 2-1. Analogy Of Manipulator To SG CMG System

MANIPULATOR		⇔	SG CMG SYSTEM	
Position	$\underline{x} = \underline{x}(\underline{q})$		Momentum	$\underline{h} = \underline{h}(\underline{\theta})$
Velocity	$\dot{\underline{x}} = J(\underline{q})\,\dot{\underline{q}}$		Torque	$\dot{\underline{h}} = J(\underline{\theta})\,\dot{\underline{\theta}}$
Acceleration	$\ddot{\underline{x}} = J(\underline{q})\,\ddot{\underline{q}} + \dot{J}(\underline{q})\,\dot{\underline{q}}$		Torque	$\ddot{\underline{h}} = J(\underline{\theta})\,\ddot{\underline{\theta}} + \dot{J}(\underline{\theta})\,\dot{\underline{\theta}}$

Singularity

No motion possible in a certain direction	No torque possible in a certain direction

plane. An example of this mounting configuration in the spacecraft body fixed coordinate frame $\{ X,Y,Z \}$ is shown in Figure 2-5. If the skew angle β equals 54.73 degrees, the gimbal axes lie along the main diagonals of a cube.

We will express the angular momentum of each CMG with respect to the spacecraft coordinate system. These are given by:

$$\underline{h}_1 = h \begin{bmatrix} -c\beta \sin\theta_1 \\ \cos\theta_1 \\ s\beta \sin\theta_1 \end{bmatrix} \quad \underline{h}_2 = h \begin{bmatrix} -\cos\theta_2 \\ -c\beta \sin\theta_2 \\ s\beta \sin\theta_2 \end{bmatrix}$$

$$\underline{h}_3 = h \begin{bmatrix} c\beta \sin\theta_3 \\ -\cos\theta_3 \\ s\beta \sin\theta_3 \end{bmatrix} \quad \underline{h}_4 = h \begin{bmatrix} \cos\theta_4 \\ c\beta \sin\theta_4 \\ s\beta \sin\theta_4 \end{bmatrix}$$

where $s\beta = \sin\beta$
$c\beta = \cos\beta$
$h =$ *Angular momentum magnitude*

The total angular momentum of this system is:

$$\underline{h} = \underline{h}_1 + \underline{h}_2 + \underline{h}_3 + \underline{h}_4 \tag{2-4}$$

The output torque of the CMG system is obtained by differentiating (2-4) in the spacecraft frame of reference:

$$\dot{\underline{h}} = \dot{\underline{h}}_1 + \dot{\underline{h}}_2 + \dot{\underline{h}}_3 + \dot{\underline{h}}_4 = J(\underline{\theta})\,\dot{\underline{\theta}} \tag{2-5}$$

The Jacobian matrix has the form:

$$J(\underline{\theta}) = h\begin{bmatrix} -c\beta\cos\theta_1 & \sin\theta_2 & c\beta\cos\theta_3 & -\sin\theta_4 \\ -\sin\theta_1 & -c\beta\cos\theta_2 & \sin\theta_3 & c\beta\cos\theta_4 \\ s\beta\cos\theta_1 & s\beta\cos\theta_2 & s\beta\cos\theta_3 & s\beta\cos\theta_4 \end{bmatrix} \quad (2\text{-}6)$$

A method for constructing the null-vector(s) of the Jacobian matrix using the concept of the generalized cross-product in n-dimensions is presented in the next section. It will be shown that much insight about the properties of the null-space can be gained through this construction method.

2.5.2 Null-Space Of Jacobian Matrix And The Generalized Cross-Product

It has been shown that the null-space of the Jacobian contributes the homogeneous or non-torque producing solution to (2-3). The null-space basis vectors are essential, because the homogeneous solution can be written as a linear combination of these vectors, as well as providing more insight into the kinematics of the CMG system. The dimension of the null-space or nullity [2] is:

$$n(J) = n - r(J) \quad (2\text{-}6)$$

$$\begin{aligned} \textit{where} \quad n(J) &= \textit{Nullity of Jacobian} \\ r(J) &= \textit{Rank of Jacobian} \\ n &= \textit{Dimension of Jacobian domain space} \end{aligned}$$

For this CMG configuration, $n = 4$. When the Jacobian is non-singular, its nullity is 1, and when it is singular its nullity is 2 (due to non-coplanar gimbal mounting). The null-space basis vectors can be determined by row-echelon reduction of the Jacobian to produce its dependent columns, which then can be used to span the null-space. This is

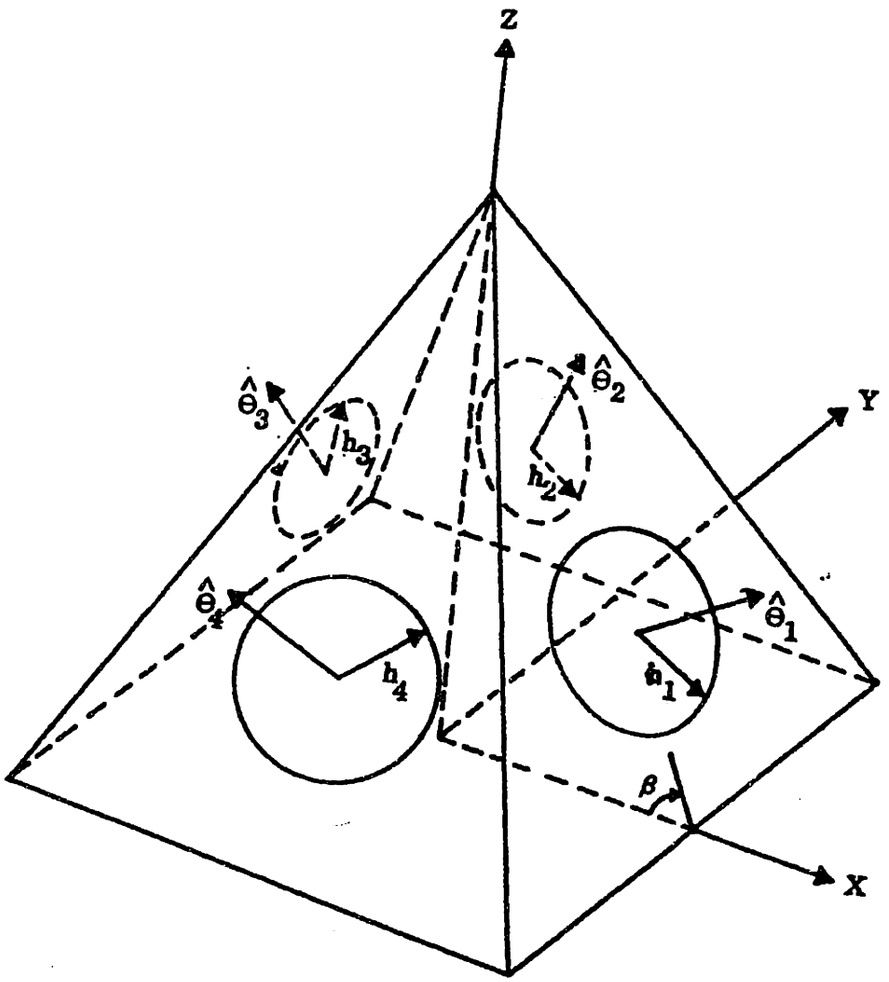

Figure 2-5. 4-Pyramid Mounted Single Gimbal CMG System

a numerical method and does not provide a closed form expression for the basis vectors. A closed form expression can be generated by use of the generalized vector cross-product in n-dimensions [1] . This method generates an orthogonal basis by forming $n - rank(J)$ vectors that are orthogonal to the linearly independent row vectors of the Jacobian and to each other. This approach is preferred over the row-echelon method; not only because a closed form solution is obtained, but also for the general insight that it provides about null motion.

To motivate this approach, it is noted that the rank of a matrix is given by either the column rank or the row rank, since the column rank equals the row rank [2]. Let $\underline{v}$ denote an n-dimensional null-vector of $J(\underline{\theta})$. This vector must satisfy $J(\underline{\theta})\,\underline{v} = 0$. For the case when $J(\underline{\theta})$ is nonsingular, it has three linearly independent row and column vectors, and $rank(J) = 3$. Therefore, the nullity is 1, and $\underline{v}$ must be orthogonal to the row vectors of $J(\underline{\theta})$. To carry out the cross-product in n-dimensions, it is noted that the cross product of two vectors in 3-dimensions can be written in terms of their components as a 3×3 determinant. These components are the 2×2 minors of this 3×3 matrix. Let us illustrate this by an example. Consider two 3-dimensional vectors $\underline{a}, \underline{b}$ expressed in a rectangular coordinate system with unit vectors $\{\hat{i}, \hat{j}, \hat{k}\}$. Then we can write:

$$\underline{a} = a_x \hat{i} + a_y \hat{j} + a_z \hat{k}$$
$$\underline{b} = b_x \hat{i} + b_y \hat{j} + b_z \hat{k}$$

The cross-product of $\underline{a}$ and $\underline{b}$ is given by:

$$\underline{a} \times \underline{b} = \left(a_y b_z - a_z b_y\right)\hat{i} + \left(a_z b_x - a_x b_z\right)\hat{j} + \left(a_x b_y - a_y b_x\right)\hat{k}$$

This result can be written as the determinant

$$\underline{a} \times \underline{b} = \begin{vmatrix} \hat{i} & \hat{j} & \hat{k} \\ a_x & a_y & a_z \\ b_x & b_y & b_z \end{vmatrix} = \begin{vmatrix} \hat{i} & \hat{j} & \hat{k} \\ \underline{c}_x & \underline{c}_y & \underline{c}_z \end{vmatrix}$$

We can see that the cross-product can be written in terms of the 2×2 minors of the determinant matrix:

$$\underline{a} \times \underline{b} = M_3\hat{i} - M_2\hat{j} + M_1\hat{k}$$

$$\begin{aligned} \textit{where} \quad M_1 &= |\, \underline{c}_x \;\; \underline{c}_y \,| \quad \textit{first minor} \\ M_2 &= |\, \underline{c}_x \;\; \underline{c}_z \,| \quad \textit{second minor} \\ M_3 &= |\, \underline{c}_y \;\; \underline{c}_z \,| \quad \textit{third minor} \end{aligned}$$

The null-vector for the case of nonsingular $J(\underline{\theta})$ can now be computed using this method. Let the 4-dimensional gimbal angle space $\underline{\theta}$ be defined by the unit vectors $\left\{\hat{\theta}_1, \hat{\theta}_2, \hat{\theta}_3, \hat{\theta}_4\right\}$. The cross-product in 4-dimensions operates on the 3 linearly independent row vectors of $J(\underline{\theta})$. The determinant matrix is given by:

$$\begin{vmatrix} \hat{\theta}_1 & \hat{\theta}_2 & \hat{\theta}_3 & \hat{\theta}_4 \\ \underline{j}_1 & \underline{j}_2 & \underline{j}_3 & \underline{j}_4 \end{vmatrix} \tag{2-8}$$

In terms of the Jacobian minors, the null-vector becomes:

$$\underline{v} = M_4 \hat{\theta}_1 - M_3 \hat{\theta}_2 + M_2 \hat{\theta}_3 - M_1 \hat{\theta}_4$$

or

$$\underline{v} = \begin{bmatrix} M_4 \\ -M_3 \\ M_2 \\ -M_1 \end{bmatrix} \tag{2-9}$$

where $M_1 = | \underline{j}_1 \ \underline{j}_2 \ \underline{j}_3 |$

$M_2 = | \underline{j}_1 \ \underline{j}_2 \ \underline{j}_4 |$

$M_3 = | \underline{j}_1 \ \underline{j}_3 \ \underline{j}_4 |$

$M_4 = | \underline{j}_2 \ \underline{j}_3 \ \underline{j}_4 |$

This method can also be used when the Jacobian is singular. In that case, $J(\underline{\theta})$ will only have two linearly independent row vectors, thus in order to apply this method, these row vectors must first be determined. The next step would be to take the 3-dimensional cross-product using only the first three elements of the row vectors in order to generate a vector in 3-space that is orthogonal to the truncated row vectors. Then, a 4-dimensional cross-product is taken using the two linearly independent row vectors and the vector just generated with a zero fourth element. In this way, the two orthogonal null-space basis vectors are generated. We can apply this approach in a similar fashion to systems with more than 4 CMGs.

Considerable insight can be gleaned from the form of the null-vector and the Jacobian minors. In general, this expression (2-9) for the null vector is valid when $J(\underline{\theta})$ is nonsingular, and it is a function of the gimbal angles. The minors of the Jacobian matrix have a very interesting physical meaning. A minor is zero when the columns of the minor matrix or 3×3 Jacobian sub-matrix are dependent. This means the sub-ma-

trix is singular, and its columns do not span E^3. The rank of this submatrix has dropped from 3 to 2. Physically, it means that the 3 CMGs corresponding to this sub-matrix can no longer produce torque along all three spacecraft axes, hence three-axis controllability is lost for this CMG sub-system. We can thus think of the minors as controllability tests for sub-systems of 3 CMGs taken together according to the columns in the corresponding minor. For example, sub-system 1 corresponding to M_1 would be comprised of CMGs 1, 2, and 3. It is clear that when all 4 sub-systems lose three-axis controllability, the spacecraft is not controllable by the CMG system. An alternate statment is that the rank of a matrix is the order of the largest nonsingular square sub-matrix formed from this matrix [2]. Thus the Jacobian is singular when all 3×3 minors are 0, i.e. there is no nonsingular sub-matrix of order 3. It is also evident that when one of the minors is zero, one of the elements of the null-vector is zero, which implies that no null motion is available from the corresponding CMG.

2.5.3 Planar 3-Link Manipulator

A planar 3-link manipulator with 1 degree of redundancy is shown in Figure 2-6. The choice for generalized coordinates in this case are the absolute joint angles. This choice of coordinates is made to keep the analogy to the CMG system transparent. The link length choice is dictated by the requirement that the manipulator possess the same number of equivalent types of singularities. We could have chosen equal length links for the manipulator to match the choice of equal magnitude angular momenta, but this would have resulted in a manipulator that would not possess all types of singularities encountered in the CMG system. Specifically, internal Elliptic type singulari-

ties would not be encountered for this manipulator (the various types of singularities will be defined in Chapter 4).

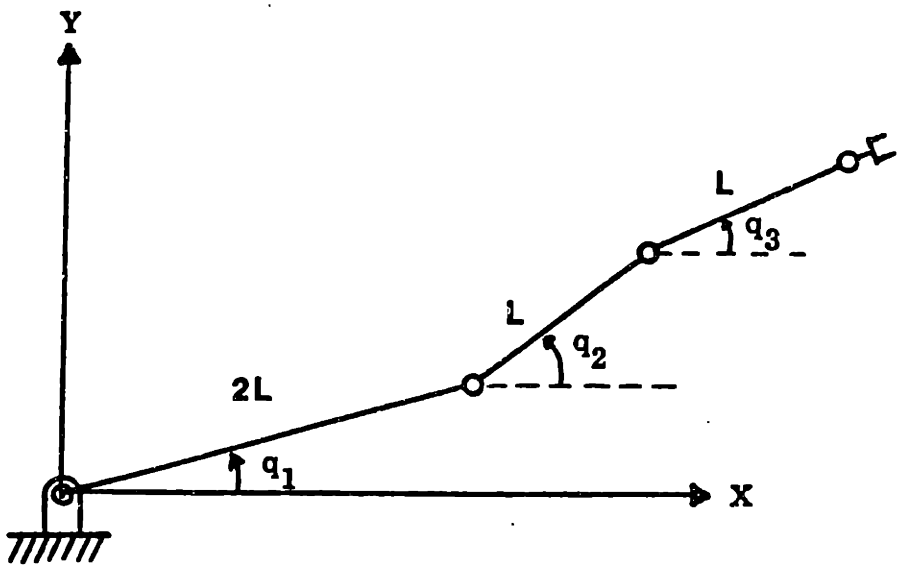

Figure 2-6. Planar 3-Link Manipulator

The motion of the manipulator is described by the generalized coordinates $\{ q_1, q_2, q_3 \}$ relative to a fixed coordinate frame $\{ X, Y \}$. The displacement of the end-effector is denoted $\underline{x}$, while the individual link displacements are defined by $\underline{x}_i$. The link displacements are:

$$\underline{x}_1 = 2l \begin{bmatrix} \cos q_1 \\ \sin q_1 \end{bmatrix} \quad \underline{x}_2 = l \begin{bmatrix} \cos q_2 \\ \sin q_2 \end{bmatrix} \quad \underline{x}_3 = l \begin{bmatrix} \cos q_3 \\ \sin q_3 \end{bmatrix}$$

where l = *Link length*

The end-effector position is given by:

$$\underline{x} = \underline{x}_1 + \underline{x}_2 + \underline{x}_3 \tag{2-10}$$

The end-effector velocity thus becomes:

$$\dot{\underline{x}} = \dot{\underline{x}}_1 + \dot{\underline{x}}_2 + \dot{\underline{x}}_3 = J(\underline{q})\,\dot{\underline{q}}. \tag{2-11}$$

The Jacobian matrix for the manipulator is:

$$J(\underline{q}) = l\begin{bmatrix} -2\sin q_1 & -\sin q_2 & -\sin q_3 \\ 2\cos q_1 & \cos q_2 & \cos q_3 \end{bmatrix} \tag{2-12}$$

Comparing the manipulator results to the 4-CMG system, we can easily see an analogy. Observe that the manipulator Jacobian has a similar form to the CMG Jacobian with this choice of generalized coordinates. Specifically, the manipulator columns are the partial derivatives with respect to the generalized coordinates of the individual joint displacements, as was analogously true for the CMG system. It is also noted that if the Jacobian is differentiated again, with respect to the generalized coordinates, its columns will be the negative of the link displacements. This is due to the cyclic nature of the trigonometric functions, governing the generalized coordinates, hence is also true for the CMG Jacobian. Finally, it is emphasized that the planar manipulator of Figure 2-6 is not the exact analog to the 4-CMG system because its Elliptic type internal singularity is actually a degenerate Hyperbolic singularity. This will become clear in Chapter 4. The exact analog can be obtained by projecting the gimbal motions in the

3 orthogonal planes formed by the spacecraft coordinate system. A manipulator with varying link lengths can then be defined such that its motion recovers the motion of the gimbals in each plane. A simple example would be to project the motion of gimbal #1 in the $X - Y$ plane. The path of the gimbal in this plane is elliptic because the projection varies. A link with varying length can be used to duplicate this motion in the plane.

The null-vector for the manipulator Jacobian can also be constructed using the generalized cross-product approach. Let the 3-dimensional joint angle space be defined by the unit-vectors $\{\hat{q}_1, \hat{q}_2, \hat{q}_3\}$. The cross-product in 3-dimensions operates on the 2 linearly independent rows of $J(\underline{q})$. The determinant matrix is:

$$\begin{vmatrix} \hat{q}_1 & \hat{q}_2 & \hat{q}_3 \\ \underline{j}_1 & \underline{j}_2 & \underline{j}_3 \end{vmatrix} \tag{2-13}$$

In terms of the manipulator Jacobian minors, the null-vector becomes:

$$\underline{v} = M_3 \hat{q}_1 - M_2 \hat{q}_2 + M_1 \hat{q}_3$$

or

$$\underline{v} = \begin{bmatrix} M_3 \\ -M_2 \\ M_1 \end{bmatrix} \tag{2-14}$$

where $M_1 = | \underline{j}_1 \; \underline{j}_2 |$

$M_2 = | \underline{j}_1 \; \underline{j}_3 |$

$M_3 = | \underline{j}_2 \; \underline{j}_3 |$

Equivalent comments apply to the manipulator null-vector as for the CMG null-vector. The physical meaning of the minors in this case represents relative folding of the links. When a minor has 0 value, the columns of the corresponding sub-matrix of order 2 are not linearly independent; the sub-matrix has rank 1. This implies that the velocity capability of these two links is restricted to a line rather than a plane whenever the minor is nonzero, therefore the links are colinear or folded. The value of each minor thus represents the degree of folding of the corresponding pair of links. In this case there are 3 distinct combinations of pairs of links; when all three combinations are singular, the Jacobian is also singular, thus motion is restricted to a line. The general concepts of controllability, capability for null motion, etc. naturally carry over from the previous discussion about the CMG Jacobian null-space and will not be repeated here.

CHAPTER 3

SPACECRAFT CONTROL ARCHITECTURE

3.1 SPACECRAFT ATTITUDE MANEUVERS

Spacecraft attitude control may be realized through angular momentum exchange between the spacecraft and momentum storage devices such as single gimbal CMGs, which can be used to provide control torques for attitude control of space vehicles. A most common example is the reorientation of a spacecraft. The most general prescription for an attitude maneuver is to specify the desired final state (attitude and rate) given the initial state of the spacecraft. The controller must then be able to satisfy this request using CMGs as actuators.

An attitude maneuver can be accomplished in various ways. The methods to accomplish these maneuvers can be classified as kinematic or dynamic, depending on the criteria used. An example of a kinematic approach is an eigenaxis or single-axis rotation, because this results in the smallest rotation angle required for the maneuver. A single-axis feedback controller based on this approach is used on the Space Shuttle [3]. On the other hand, the ORA controller [4] is an example of a dynamic approach. It uses a feedforward-feedback model-following controller structure for fuel-optimal maneuvers, which are not constrained to rotations about a single axis. This approach reduces fuel consumption, hence it is superior to the kinematic method. For the case of spacecraft with CMGs, a model following controller (dynamic method) could also be used, as long as the model or desired trajectory is constructed in a way that reflects the unique properties of CMG actuated spacecraft.

One method of generating a desired trajectory that is globally "optimal" in a certain sense, using the calculus of variations, is described in [5]. The optimization problem requires the design of an optimal terminal controller, with only some of the states specified at a fixed terminal time. These specified states are chosen to be the spacecraft initial and teminal attitude and rate. The assumption of no external torques implies that the terminal CMG state is not constrained, since that would violate conservation of angular momentum for the combined system.

Performance criteria of interest include minimization of gimbal rates, minimization of final spacecraft state error from the desired value, and maintaining CMG 3-axis controllability over the entire trajectory. Redundancy resolution can be accomplished in a global sense by parametrizing CMG 3-axis controllability over the whole spacecraft trajectory. Solution of this problem, however, is very difficult because some of the Lagrange multipliers have no boundary conditions at either end (i.e. initial and terminal conditions), since we have specified the values of the corresponding states at both ends. An intial control history is required to solve this optimization problem.

To represent the attitude of a spacecraft, Euler parameters $\{ \eta, \underline{\varepsilon} \}$ or quaternions will be used. Let the underscore represent a vector expressed in the spacecraft fixed frame. The rate of change of the Euler parameters is given by [6]:

$$\begin{aligned} \dot{\eta} &= -\frac{1}{2} \underline{\varepsilon}^T \underline{\omega} \\ \dot{\underline{\varepsilon}} &= \frac{1}{2} \left[\underline{\varepsilon}^{\times} + \eta \underline{1} \right] \underline{\omega} \end{aligned} \tag{3-1}$$

Let $\underline{q}$ represent the quaternion,

$$\underline{q} = \begin{bmatrix} \eta \\ \underline{\varepsilon} \end{bmatrix}$$

then we can rewrite (3-1) as:

$$\dot{\underline{q}} = E(\underline{q})\,\underline{\omega} \tag{3-2}$$

The equations of motion for the combined spacecraft-CMG system are obtained from the total angular momentum expression. Let the superscript I denote a quantity expressed in an inertial frame. The total angular momentum expressed in an inertial frame is given by:

$$\underline{H}_T^I = \underline{H}^I + \underline{h}^I \tag{3-3}$$

where $\underline{H}^I$ = *Spacecraft angular momentum* $\left(\underline{H}^I = \mathrm{I}\,\underline{\omega}^I\right)$

$\underline{h}^I$ = *Total CMG angular momentum*

Expressing the time rate of change of the absolute total angular momentum of the combined system in the spacecraft fixed body axes, we obtain:

$$\dot{\underline{H}} + \underline{\omega} \times \underline{H} + \dot{\underline{h}} + \underline{\omega} \times \underline{h} = \underline{T} \tag{3-4}$$

where $\underline{T}$ = *External torques on spacecraft*

Rewriting (3-4) with $\dot{\underline{h}} = J\,\dot{\underline{\theta}}$, and including (3-2) we obtain the dynamical equations governing this system:

$$\begin{aligned} \dot{\underline{q}} &= E(\underline{q})\,\underline{\omega} \\ \dot{\underline{\omega}} &= -\mathrm{I}^{-1}\left[\,\underline{\omega}\times(\mathrm{I}\underline{\omega} + \underline{h}(\underline{\theta}))\,\right] - \mathrm{I}^{-1}J(\underline{\theta})\,\dot{\underline{\theta}} + \mathrm{I}^{-1}\underline{T} \end{aligned} \tag{3-5}$$

3.2 CONTROL ARCHITECTURE

Attitude maneuvers of spacecraft equipped with CMGs are usually accomplished using a dual-level control architecture. This is because we can consider the attitude maneuver as consisting of two parts; first, the necessary torque required from the CMG actuators to accomplish the maneuver must be determined, and second, this torque must be generated by the redundant system of CMGs. These two levels of the controller are defined as:

a) **Outer Control Loop**

b) **Inner Control Loop**

The general objectives of the control system for the combined spacecraft-CMG system can be stated as:

a) Spacecraft reorientation accomplished using SG CMGs.

b) CMG system must supply a commanded torque while avoiding singular configurations.

c) Spacecraft controllability must be maintained at all times.

It has been shown that single gimbal CMG systems are plagued by singular states. For this reason, the Inner Control Loop must be capable of generating the required torque while simultaneously avoiding singular configurations. This is not an easy task. This problem might be made more tractable if the Outer Control Loop design takes this adverse feature of single gimbal CMGs into account; specifically, the design of the Outer controller must tolerate occasional errors in torque delivered by the CMG system, or limit the CMG torque command to avoid approaching vicinities of singular CMG orientations. The capability of accomodating errors in the torque request. is required due to reduced effectiveness of the CMG system near singular configurations. The Outer controller should also not constrain the CMG system to produce a given torque if this can lead to a singularity which the Steering law is not capable of avoiding. In addition, the non-spherical nature of the SG CMG momentum envelope must specifically be taken into account for maneuvers which move the CMG system near saturation.

All currently proposed SG CMG Steering laws (including those presented in this thesis) are unable to guarantee continuously flawless singularity avoidance, although various techniques (discussed in Chapters 5 and 6) do aid in reducing singular encounters. Because of this, any Outer controller must be prepared to occasionally deal with singularity related phenomena as discussed above. For reorientation maneuvers, the vehicle trajectory may be as general as possible, since the only constraints are the two boundary conditions; the initial and final states of the spacecraft. The choice of intermediate points is arbitrary, and thus may be chosen, if required, to aid in avoiding singular CMG configurations.

3.3 OUTER CONTROL LOOP

The function of the Outer Control Loop is to generate torque commands that accomplish the spacecraft attitude maneuver. Two possibilites for this controller were mentioned in the previous section. The model following controller can be implemented in different ways; two examples are the Sliding Mode Controller (SMC) and optimal tracking method. An example of the Sliding Mode approach applied to spacecraft using CMGs can be found in [7], where the control input $\underline{\tau}$ is defined as the output torque of the CMG system:

$$\underline{\tau} = J(\underline{\theta})\,\dot{\underline{\theta}}$$

The advantages of this approach are real-time implementation and a globally stable controller based on Lyapunov stability analysis, despite the presence of model imprecision and disturbance torques.

A derivation of the optimal tracking method for spacecraft using CMGs can be found in [5]. The solution to the tracking problem leads to a full-state feedback control law where the optimal control has a feedforward-feedback structure. The major advantage of this approach is that performance criteria of interest can be included in the objective function. This approach is not considered real-time implementable however, since it requires numerical solution (an initial control history is required to start the numerical process).

3.4 INNER CONTROL LOOP

The function of the Inner Control Loop is to generate gimbal angle rate commands that cause the CMG system to produce the desired torque requested by the Outer Control Loop. It must also resolve the redundancy present in the CMG system. In the literature, this is usually referred to as a Steering law. This is not the only approach available. The Steering law may also be formulated to generate gimbal angle commands in response to angular momentum requests [8]. The Steering law thus exploits the kinematic relationship between CMG gimbal rates and the rate of change of total CMG angular momentum in the rotating frame of reference (spacecraft body fixed frame).

The requirements that a successful Steering law must meet are:

a) Generate the required torque.
b) Steer the gimbal angle trajectories away from undesirable configurations.
c) Meet any constraints placed on the CMG system, such as maximum gimbal rates, gimbal stops etc.

An undesirable configuration is one for which the CMG system is unable to produce any torque along a particular direction in E^3 . This is equivalent to loss of spacecraft three-axis controllability, thus conditions a) and b) are not independent in the sense that the ability to produce a required torque implies that the CMG system is not in an undesirable configuration.

To produce a desired torque requires the solution of the underdetermined system of sinultaneous linear equations given by:

$$J(\underline{\theta})\,\dot{\underline{\theta}} = \underline{\tau} \tag{3-6}$$

The general solution to a non-homogeneous system of linear equations such as (3-6), can be formed from the solution to the homogeneous system, and any particular solution, as was discussed in Chapter 2. When the rank of the Jacobian matrix is 3, infinitely many solutions to (3-6) exist. In this case, the particular solution is almost always obtained using the Moore-Penrose pseudoinverse [2] , which is given by:

$$\dot{\underline{\theta}}_P = J^T(J\,J^T)^{-1}\,\underline{\tau} \tag{3-7}$$

To illustrate the properties of (3-7), a derivation based on orthogonal projections is presented in the next section. To motivate this derivation the properties of the the Moore-Penrose pseudoinverse are presented below:

a) $\dot{\underline{\theta}}_P$ is orthogonal to $\dot{\underline{\theta}}_H$. Therefore, $< \dot{\underline{\theta}}_P, \dot{\underline{\theta}}_H > \; = 0$.

b) The particular solution is the minimum norm solution to (3-6), as can be seen from the Pythagorean theorem:

$$|\,\dot{\underline{\theta}}\,|^2 = |\,\dot{\underline{\theta}}_P\,|^2 + |\,\dot{\underline{\theta}}_H\,|^2$$

Since the particular and homogeneous solutions are orthogonal to each other, the norm of the solution will be smallest when the homogeneous solution is zero.

3.4.1 Derivation Of The Moore-Penrose Pseudoinverse Using Orthogonal Projections

From the fundamental theorem of linear algebra [9], the row space of any matrix is perpendicular to its nullspace. Since the torque producing solution lies in the row space of J, we can write the general solution to (3-6) in the form:

$$\dot{\underline{\theta}} = \dot{\underline{\theta}}_R + \dot{\underline{\theta}}_N$$

$$\textit{where} \quad \dot{\underline{\theta}}_R = \textit{Torque producing solution} \; (J\dot{\underline{\theta}}_R = \underline{\tau})$$

$$\dot{\underline{\theta}}_N = \textit{Homogeneous solution} \; (J\dot{\underline{\theta}}_N = \underline{0})$$

The torque producing solution can now be written as a linear combination of the row-space basis vectors. Since the Jacobian matrix is nonsingular, it has 3 linearly independent row vectors. The row space is spanned by these vectors (which become the columns of J^T), thus we can write the torque producing solution as:

$$\dot{\underline{\theta}}_R = \sum_{i=1}^{3} \alpha_i \underline{R}_i = J^T \underline{\alpha} \tag{3-8}$$

$$\textit{where} \quad \underline{R}_i^T = i^{th} \textit{ Jacobian row vector}$$

Substituting (3-8) in (3-6) we obtain

$$J J^T \underline{\alpha} = \underline{\tau}$$

from which we can solve for $\underline{\alpha}$:

$$\underline{\alpha} = (J J^T)^{-1} \underline{\tau} \tag{3-9}$$

To obtain the final result for $\underline{\dot{\theta}}_R$ we substitute (3-9) into (3-8) to get:

$$\underline{\dot{\theta}}_R = J^T(JJ^T)^{-1}\underline{\tau} \tag{3-10}$$

This is the desired final result. By picking the particular solution as (3-10), the properties of the Moore-Penrose pseudoinverse are satisfied. Since the pseudoinverse provides the minimum 2-norm solution, an alternative derivation can be obtained using Lagrange multipliers to solve the following problem:

$$\min \quad \frac{1}{2}\underline{\dot{\theta}}^T\underline{\dot{\theta}}$$

$$\textit{subject to} \quad J\underline{\dot{\theta}} = \underline{\tau}$$

$$\textit{with} \quad \textit{Hamiltonian} \quad H = \frac{1}{2}\underline{\dot{\theta}}^T\underline{\dot{\theta}} + \lambda^T(\underline{\tau} - J\underline{\dot{\theta}})$$

This minimization will yield $\underline{\dot{\theta}} = \underline{\dot{\theta}}_R$, as defined in (3-10).

The homogeneous solution can be written as a linear combination of the Jacobian null space basis vectors.

$$\underline{\dot{\theta}}_H = \sum_{i=1}^{n-r(J)} \lambda_i(t)\,\underline{v}_i \tag{3-11}$$

where $\lambda_i(t)$ = *Time varying scalar weighting factor*
$\underline{v}_i$ = *n – dimensional Jacobian null space basis vector*
$r(J)$ = *Rank of Jacobian*

The computation of the null space basis vectors is carried out using the generalized cross-product approach as presented in Chapter 2. The scalar weighting factor deter-

mines the magnitude and sign of the contribution of each null space basis vector to the homogeneous solution. These are the free design parameters, to be selected in a manner that the performance criteria for the Steering law are accomplished.

Because $\underline{\dot{\theta}}_R$ is orthogonal to $\underline{\dot{\theta}}_N$, any general solution to (3-6) can be written in terms of the Moore-Penrose pseudoinverse and any homogeneous solution. An alternative approach for a Steering law utilizing linear programming is discussed in the next section.

3.5 REDUNDANCY RESOLUTION VIA LINEAR PROGRAMMING

Another way of addressing the singularity avoidance and steering problem is to assign gimbal rates via linear programming, as described in [10]. The instantaneous torque output of each gimbal is used to form a set of activity vectors that are used to satisfy spacecraft rate-change requests by solving for approximate gimbal displacements, or torque requests by solving for instantaneous gimbal rates. The linear program intrinsically incorporates upper bounds on the CMG selection that limit allowed gimbal displacements and rates while optimizing an objective function to encourage avoidance of singular configurations and gimbal stops. Unfortunately, this method like all available methods, cannot avoid all internal singularities due to the use of a gradient-based objective (to be discussed in Chapter 5). Linear programming has been applied to double gimbal CMGs, however, with considerable success.

This approach can also account for hybrid control of spacecraft using both jets and CMGs. It is highly adaptable to hardware failures, variations in CMG system defi-

nition, and changes in vehicle mass properties. A major advantage of this approach is that performance criteria can be explicitly and dynamically taken into account merely by altering the linear objective functions and imposed upper bounds.

CHAPTER 4

SINGULAR CONTROL MOMENT GYRO (CMG) CONFIGURATIONS

4.1 DEFINITION OF SINGULARITY

Spacecraft attitude control systems utilizing single gimbal CMGs must effectively address the singularity conditions inherent with this type of actuators. These conditions prevail when the CMG system is in a configuration that precludes torque generation in a certain direction, i.e. spacecraft three-axis controllability is lost. These conditions, if not properly addressed, severely limit the usable momentum capability of the CMG system. Not only must the singularities themselves be avoided; neighborhoods of singular states represent regions of limited torque capability, thus require high gimbal rates to generate the requisite torque. Hardware limits on gimbal rates therefore entail that these neighborhoods also be considered in the control law design.

The requirement of spacecraft three-axis controllability is expressed by the rank of the CMG system Jacobian matrix. If the rank of the Jacobian is less than 3, the CMG system is unable to produce torque along a direction $\underline{u}$, referred to as the singular direction in E^3. This is summarized below:

Singular State: A singular state can be defined as a set of gimbal angles for which the CMG system is unable to produce torque along the singular direction $\underline{u}$. This occurs whenever $rank(J) < 3$, the number of controlled axes.

For 3-axis control the maximal rank of the Jacobian is 3 and the minimal rank is 2, because the gimbal axes, $\hat{\theta}_i$, are not mounted coplanar. For example, if $rank(J) = 2$,

the resultant otput torque lies in a plane which is spanned by the columns of the Jacobian matrix. The singular direction $\underline{u}$ is then perpendicular to this plane. This condition can be stated as:

$$\underline{j}_i(\theta_i)^T \cdot \underline{u} = 0 \qquad (i = 1,2,...,n) \tag{4-1}$$

The gimbal angles corresponding to a singular configuration can be computed using (4-1) and the expression for the Jacobian columns with respect to the reference gimbal coordinate frame (2-1). The i^{th} column of the Jacobian matrix is:

$$\underline{j}_i = h\left[\ \cos\theta_i \hat{j}_i^{\,0} - \sin\theta_i \hat{h}_i^{\,0}\ \right] \tag{4-2}$$

Combining (4-1) with (4-2) we obtain

$$\underline{j}_i \cdot \underline{u} = \cos\theta_i (\hat{j}_i^{\,0} \cdot \underline{u}) - \sin\theta_i (\hat{h}_i^{\,0} \cdot \underline{u}) = 0 \tag{4-3}$$

the solutions of which are the singular gimbal angles. These angles are obtained from:

$$\theta_i^S = \tan^{-1}\left[\ \frac{\varepsilon_i \hat{j}_i^{\,0} \cdot \underline{u}}{\varepsilon_i \hat{h}_i^{\,0} \cdot \underline{u}}\ \right] \tag{4-4}$$

$$\begin{aligned} \textit{where} \quad \theta_i^S &= \textit{Singular gimbal angle (2 solutions)} \\ \varepsilon_i &= \pm 1 \end{aligned}$$

The two solutions obtained from (4-4) correspond to the two extreme projections of the i^{th} angular momentum vector on the singular direction. These are the maximum positive and maximum negative projections, therefore there corresponds two solutions

for each singularity and momentum vector associated with maximum positive (+) and maximum negative (-) projections along the singular direction. Examples of the various sign patterns can be found in [11] . The singularity problem can thus be summarized for a n-CMG system: There exist 2^n combinations of gimbal angles for which the CMG system cannot produce torque about any given direction in space [1] .

All singular states can be classified according to their location in the total CMG angular momentum envelope:

a) **Surface or Saturation Singularities**

b) **Internal Singularities**

   i) **Elliptic or Unescapable**

   ii) **Hyperbolic**

4.2 SATURATION SINGULARITY

As the name suggests, a Saturation singularity corresponds to a configuration for which the CMG system has projected its maximum momentum capability along a certain direction. A Saturation singularity can be defined as the set of gimbal angles for which the total momentum of the CMG system lies on the momentum envelope (implying that the momentum linkage tip has reached the momentum envelope). The mechanical analog to this type of a singularity is a completely stretched manipulator.

Deeper insight about the Saturation singularity can be gained by examining the behaviour of the momentum linkage. The momentum envelope, which is generated by

motion of the maximally stretched linkage, is the set of radius vectors from zero momentum to the saturation surface. The direction of the maximal stretch is termed the "saturation direction", and the singular direction is given by the outward normal to the momentum envelope at the point of contact of the linkage tip. These directions are illustrated in Figure 4-1, which depicts the projection of the momentum envelope on the $Z - X$ plane [12]. Since the linkage tip is restrained to move either on the envelope or inside, no motion is possible beyond the envelope in the outward normal direction. Motion along the inward normal is also instantaneously not possible, since the Jacobian is still singular. To be more precise, the singular direction is an axis along which instantaneous CMG output torque capability is entirely lost. Torque can only be generated along the tangent plane to the envelope, which has as its normal vector the singular direction at the point of the linkage tip contact. In this case, the CMG system is termed saturated with reference to the direction $\underline{u}$, since the system has projected its maximum available momentum in this direction. We can summarize the criteria for a Saturation singularity as:

a) $Rank(J) < 3$

b) $All\ \underline{h}_i \bullet \underline{u} > 0 \quad (i = 1,...,n)$

An example of this type of singularity for the Pyramid mounted 4-CMG system and the 3-link planar manipulator is shown in Figure 4-2. From the figure, we can see that all the gimbals have projected their maximum momentum capability along the singular direction. From the manipulator example, it is intuitively clear that there can be no relative motion of the links which does not affect the end-effector location. There is

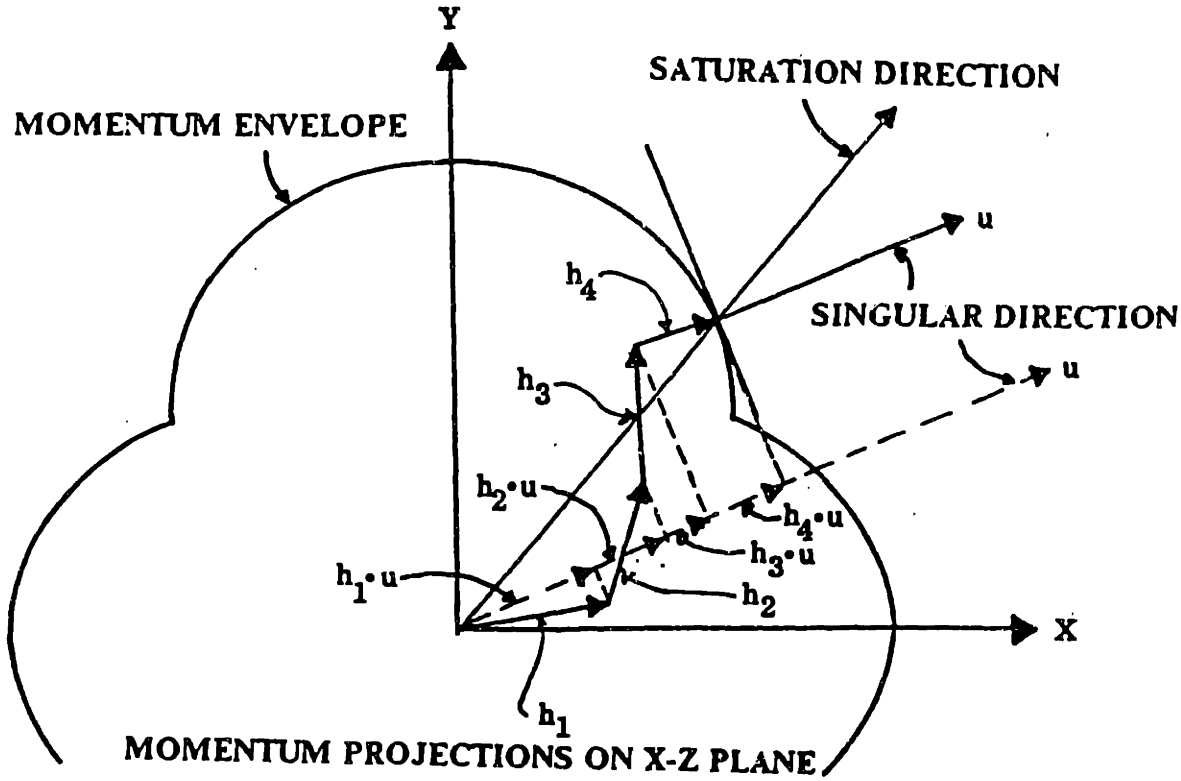

Figure 4-1. Saturation Singularity Projections For 4-SG CMG System

no null motion possible for this type of singularity. A degenerate case where null motion would be possible can be imagined if the ground pivot allowed rotation about the singular direction, but this is excluded for this type of manipulator. The same comments apply to the CMG system; For a maximally projected CMG linkage, no null motion is possible (no degenerate case exists for the CMG system).

From the above discussion, it can be seen that a Saturation singularity corresponds to the physical capabilities of the CMG system. Thus, the term "desaturation" refers to the process by which the resultant momentum vector is removed or retracted from the envelope or surface without net momentum transfer to the spacecraft. To accomplish this task, an external torque (such as jet firings or gravity gradient/aerodynamic torques) is required to cancel the torque exerted on the spacecraft while desaturating the CMG system. Saturation states cannot be avoided by the Steering law alone; A

momentum management procedure such as [13], [14] must be used to command the spacecraft attitude such that the CMGs remain unsaturated.

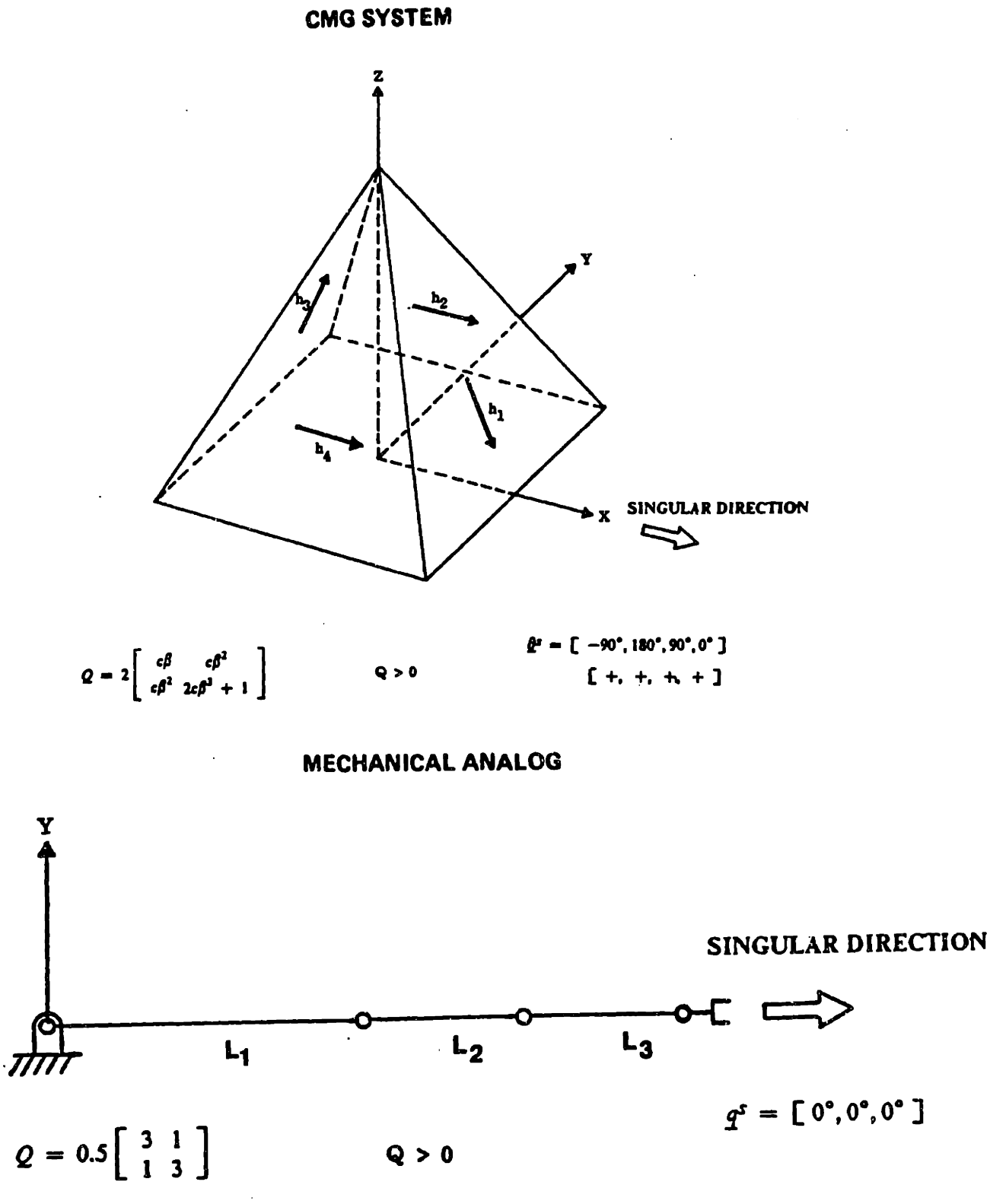

Figure 4-2. Example Of Saturation Singularity

4.3 INTERNAL SINGULARITIES

Any singular state for which the total angular momentum vector (or linkage) is not completely stretched is defined by default to be an Internal singularity. These states can be generated from the Saturation singularity by reversing one or more angular momentum vectors so that they point opposite to the singular direction. For a 4-CMG system, these singularities can be grouped into two categories. One category consists of an even number of positive and negative projections, and the other category is made up of an odd number of positive and negative projections. The mechanical analog to this situation is a manipulator with folded links. Some singularities can offer the possibility of escape through null motion, therefore it is useful to investigate the conditions under which singular configurations can be removed by null motion alone, and thus classify Internal singularities according to whether a null motion escape is possible.

The term "escape" used in this context needs to be defined carefully. The term escape will be defined in the following manner:

Escape By Null Motion: A singular CMG system can be reconfigured by null motion into a non-singular configuration, if one exists for the same total angular momentum.

The implications of this statement are twofold.

a) A non-singular configuration is reachable by null motion from the singular-configuration; i.e. the CMG system can be reconfigured in a continuous manner

using null motion only. To state it succinctly, the two solution sets are not disjoint with respect to null motion.

b) The rank of the Jacobian can be affected (increased) by these null motion. The singularity measure (to be introduced later) is increased also (can be made non-zero).

An immediate consequence of these statements is that Saturation singularities are not escapable. This will be established rigorously in the next section, when a test for the possibility of null motion near a singularity is presented. It should also be emphasized that the mere possibility of null motion at a singularity does not automatically imply that the singularity is escapable. An example of this was given in the degenerate Saturation singularity discussion for the manipulator.

4.3.1 Test For Possibility Of Null Motion Near A Singularity

Valuable insight can be gained by investigating the conditions under which null motion is possible near a singularity. A method to examinine the behaviour of a CMG system using null motion near a singular state can be found in [1]. A similar approach based on this method will now be presented. Let $\underline{h}^s(\underline{\theta}^s)$ denote a singular CMG configuration. Expanding the total CMG angular momentum about about this singular configuration, $\underline{\theta}^s$, we obtain:

$$\underline{h}(\underline{\theta}) - \underline{h}(\underline{\theta}^S) = \sum_{i=1}^{n} \left[\frac{\partial \underline{h}_i}{\partial \theta_i}\Big|_{\theta_i^s} \delta\theta_i + \frac{1}{2}\frac{\partial^2 \underline{h}_i}{\partial \theta_i^2}\Big|_{\theta_i^s} \delta\theta_i^2 + H.O.T. \right] \qquad (4\text{-}5)$$

The first partial on the right hand side of (4-5) is just the i^{th} column vector of the Jacobian. The expression for the second partial is given by:

$$\dot{\underline{j}}_i = \frac{\partial \underline{j}_i}{\partial \theta_i}\dot{\theta}_i = \dot{\theta}_i \hat{\theta}_i \times \underline{j}_i = -\dot{\theta}_i h_i \hat{h}_i$$

$$\frac{\partial^2 \underline{h}_i}{\partial \theta_i^2} = \frac{\partial \underline{j}_i}{\partial \theta_i} = -h_i \hat{h}_i = -\underline{h}_i$$

If we now take the inner product of (4-5) with the singular direction, $\underline{u}$, the first term on the right hand side drops out because the singular direction is orthogonal to the Jacobian columns, i.e. $\underline{j}_i(\theta_i^S) \bullet \underline{u} = 0$. The resulting expression is:

$$\underline{u} \bullet \left[\underline{h} - \underline{h}^S \right] = -\frac{1}{2} \sum_{i=1}^{n} \underline{h}_i^S \bullet \underline{u}\ \delta\theta_i^2 \tag{4-6}$$

Recognizing that the right hand side of (4-6) is a quadratic form, it can be written as:

$$\underline{u} \bullet \left[\underline{h} - \underline{h}^S \right] = -\frac{1}{2} \delta\underline{\theta}^T P\, \delta\underline{\theta} \tag{4-7}$$

$$where \quad P = diag(\underline{h}_i^S \bullet \underline{u}) \quad . i = 1,2,...,n$$

The diagonal matrix P will be refered to as the projection matrix, since its elements represent the projections of the singular angular momentum vectors onto the singular direction.

The governing equation for the null motion test is expressed by (4-7). In order to examine the behaviour of (4-7) for null motion near a singularity, the variations in gim-

bal angles $\delta\theta_i$ are defined to be null motion. For null motion, $\underline{h} = \underline{h}^s$ by definition, since null motion do not affect the total angular momentum of the system. Therefore, (4-7) becomes (neglecting the constant):

$$\delta\underline{\theta}^T P \, \delta\underline{\theta} = 0 \qquad (4\text{-}8)$$

The null motion can be expressed as a linear combination of the null-space basis vectors as in [15]. The gimbal angle variations can then be expressed in this basis as:

$$\delta\underline{\theta} = \sum_{i=1}^{n-r(J)} \lambda_i \underline{v}_i = N\underline{\lambda} \qquad (4\text{-}9)$$

where λ_i = *Scalar weighting factor*
$\underline{v}_i$ = *Null space basis vector* (n − *dimensional*)
$r(j)$ = *Rank of Jacobian matrix*

Substituting (4-9) in (4-8) , we obtain the desired final result:

$$\underline{\lambda}^T Q \underline{\lambda} = 0$$
$$\text{where} \quad Q = N^T P N \qquad (4\text{-}10)$$

This quadratic form can now be used to test the possibility of null motion near a singularity. Two possibilities exist:

a) **Definite Q**

b) **Indefinite or Semi-Definite Q**

4.3.1.1 Definite Q

If Q is definite, the quadratic form is definite, and in order to satisfy (4-10) we must have $\underline{\lambda} = 0$. This implies that no null motion is possible at this singular configuration, therefore no escape is possible from this singularity by null motion. Near a singularity of this type, the CMG system cannot be reconfigured by null motion into a non-singular configuration; the two configurations are disjoint solutions to the total system momentum. This result can be used to identify unescapable singularities.

When P is definite, Q is also definite. This corresponds to the case of a Saturation singularity, for which all angular momenta have maximum positive projections on the singular direction. All the elements of the diagonal projection matrix are positive. This type of singularity was defined in [1] as Elliptic, because the quadratic in (4-7) has the form of an elliptic conic section, an ellipsoid. Using this notation for the case of definite Q, the singularity will be defined as Elliptic or unescapable. For Q to be definite, it is not neccessary that all momenta have positive projections on the singular directions; i.e. P can be indefinite. Odd numbers of positive and negative projections usually result in a definite quadratic form. A case for an even number of projections has not been found for which the quadratic form is definite.

4.3.1.2 Indefinite Or Semi-Definite Q

The other possibility for (4-10) is to be either indefinite or semi-definite. It is indefinite when the eigenvalues of Q are both positive and negative, and is positive (negative) semidefinite if Q has non-negative (non-positive) eigenvalues, i.e. has at least

one zero eigenvalue [2] . In this case, $\underline{\lambda} \neq 0$ satisfies (4-10). This implies that null motion is possible at this singularity, therefore null motion may provide a possibility of escape. In order to definitely state that escape is possible, degenerate solutions must be excluded. Degenerate solutions are those for which rigid body rotation is possible which does not affect the total system momentum. The term rigid body is used to indicate the fact that the the singular configuration remains undisturbed during these null motion. An example of this was given in "4.2 Saturation Singularity" for a manipulator. In that case, the rigid body is the stretched linkage which can rotate about the stretch axis. Similarly, it may be possible that the momentum linkage could possess configurations for which rigid body rotations are possible.

This type of singularity was defined in [1] as Hyperbolic because the quadratic in (4-7) has the form of a hyperbolic conic section, a hyperboloid. Using this notation, a singularity for which Q is either semi-definite or indefinite will be defined as Hyperbolic.

Applying the above conclusions, the results of the null motion test can be used to classify the two possibilities which exist for an Internal singularity:

a) **Elliptic or Unescapable Singularity (Q Definite)**

b) **Hyperbolic Singularity (Q Indefinite or Semi-Definite)**

It is evident that Hyperbolic singularities offer the possibility of escape through null motion. These cases must be examined for degenerate solutions to determine the possibility of escape. Examples of the various singularities are presented in the next section.

4.4 EXAMPLES OF INTERNAL SINGULARITIES

In this section, examples of the two different types of Internal singularitites are presented for the 4-Pyramid CMG system and the planar 3-link manipulator introduced in Chapter 2. All the relevant computations for the null motion test are presented in each case. The choice of singular direction, for both systems is the spacecraft X-axis, i.e. $\underline{u} = \hat{X}$. For simplicity, $h = l = 1$.

4.4.1 Example Of Elliptic Or Unescapable Internal Singularity

A particular example of an Internal Elliptic singularity is shown in Figure 4-3. The 4-Pyramid CMG system will be discussed first. The configuration for this singularity is defined by the gimbal angles: $\underline{\theta}^s = [\ -90°, 0°, 90°, 0°\ ]^T$. It is seen that there are an odd number of equal sign momentum projections along the singular direction $\underline{u} = \hat{X}$. The sign pattern of these projections is $[\ +, -, +, +\ ]$ for this singularity.

The row-echelon form of the Jacobian matrix evaluated at these gimbal angles is:

$$J = \begin{bmatrix} 1 & 0 & 1 & 2c\beta \\ 0 & 1 & 0 & 1 \\ 0 & 0 & 0 & 0 \end{bmatrix}$$

The linearly independent (but non-orthogonal) null-space basis vectors can be obtained from the row-echelon form. These two null-vectors can be constructed from the dependent columns of the Jacobian:

$$\underline{v}_1 = \begin{bmatrix} -1 \\ 0 \\ 1 \\ 0 \end{bmatrix} \quad \underline{v}_2 = \begin{bmatrix} -2c\beta \\ -1 \\ 0 \\ 1 \end{bmatrix} \quad or\ N = \begin{bmatrix} -1 & -2c\beta \\ 0 & -1 \\ 1 & 0 \\ 0 & 1 \end{bmatrix}$$

To obtain the projection matrix, the inner product of each CMG angular momentum with the singular direction is evaluated at these gimbal angles. The projection matrix for this case becomes:

$$P = \begin{bmatrix} c\beta & 0 & 0 & 0 \\ 0 & -1 & 0 & 0 \\ 0 & 0 & c\beta & 0 \\ 0 & 0 & 0 & 1 \end{bmatrix}$$

Carrying out the matrix multiplications in (4-10), the expression for the symmetric Q matrix is:

$$Q = 2\begin{bmatrix} c\beta & c\beta^2 \\ c\beta^2 & 2c\beta^3 \end{bmatrix} \qquad c\beta > 0$$

For Q to be definite, all of its pivots must be non-zero and of the same sign. The upper-triangular form of Q is:

$$Q = 2\begin{bmatrix} c\beta & c\beta^2 \\ 0 & c\beta^3 \end{bmatrix}$$

Both pivots, $c\beta$, $c\beta^3$, are positive, thus $Q > 0$, i.e. is positive definite. This singularity is then of Elliptic type, hence unescapable by null motion.

CMG SYSTEM

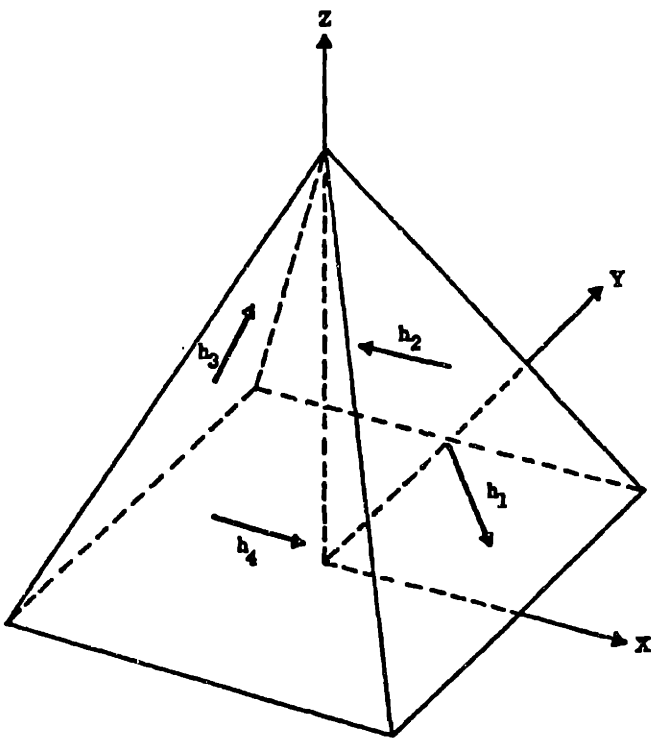

$$Q = 2\begin{bmatrix} c\beta & c\beta^2 \\ c\beta^2 & 2c\beta^2 \end{bmatrix} \qquad Q > 0 \qquad \beta^T = [\,-90°, 0°, 90°, 0°\,]^T$$

$$[\,+,-,+,+\,]$$

MECHANICAL ANALOG

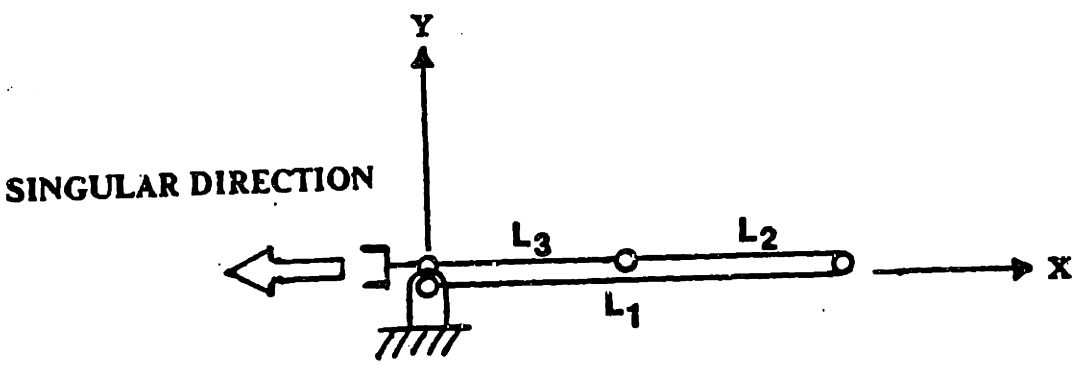

$$q^s = [\,0°, 180°, 180°\,]^T$$

$$Q = \begin{bmatrix} -1 & 1 \\ 0 & 0 \end{bmatrix} \qquad Q \leq 0$$

Figure 4-3. Example Of Elliptic Internal Singularity

An example of an unescapable singularity for the manipulator is shown in Figure 4-2. The singularity is defined by the joint angles: $\underline{q}^S = [\, 0°, 180°, 180° \,]^T$. The sign pattern of the projections in the singular direction $\underline{u} = \hat{X}$ becomes $[\, -, +, + \,]$.

The row-echelon form of the Jacobian and the null-space basis are given by:

$$J = \begin{bmatrix} 1 & -0.5 & -0.5 \\ 0 & 0 & 0 \end{bmatrix} \quad N = \begin{bmatrix} 0.5 & 0.5 \\ 1 & 0 \\ 0 & 1 \end{bmatrix}$$

The projection and Q matrices are:

$$P = \begin{bmatrix} 2 & 0 & 0 \\ 0 & -1 & 0 \\ 0 & -1 & -1 \end{bmatrix} \quad Q = 0.5 \begin{bmatrix} -1 & 1 \\ 1 & -1 \end{bmatrix}$$

The upper-triangular form is:

$$Q = \begin{bmatrix} -1 & 1 \\ 0 & 0 \end{bmatrix}$$

The pivots are -1, 0. Thus the quadratic form is negative semi-definite, $Q \leq 0$, which suggests that this singularity is Hyperbolic and null motion is possible. This is a degenerate singularity however, because rigid body motion is possible by null motion, since the manipulator can be rotated as a rigid body about the grounded pivot without affecting the location of the tip. As a consequence, escape from this singularity is not possible by null motion.

4.4.2 Example Of Hyperbolic Internal Singularity

An example of an Internal Hyperbolic singularity is shown in Figure 4-4. The singular configuration for the CMG system is defined by the gimbal angles: $\underline{\theta}^s = [\, 90°, 180°, -90°, 0° \,]$. The sign pattern of the projections for this singularity is $[\, -, +, -, + \,]$.

The row-echelon form of the Jacobian and the non-orthogonal null-space basis are given by:

$$J = \begin{bmatrix} 1 & 0 & 1 & -2c\beta \\ 0 & 1 & 0 & -1 \\ 0 & 0 & 0 & 0 \end{bmatrix} \quad N = \begin{bmatrix} -1 & 2c\beta \\ 0 & 1 \\ 1 & 0 \\ 0 & 1 \end{bmatrix}$$

The projection and Q matrices become:

$$P = \begin{bmatrix} -c\beta & 0 & 0 & 0 \\ 0 & 1 & 0 & 0 \\ 0 & 0 & -c\beta & 0 \\ 0 & 0 & 0 & 1 \end{bmatrix} \quad Q = 2\begin{bmatrix} -c\beta & c\beta^2 \\ c\beta & 1 - 2c\beta^3 \end{bmatrix}$$

The upper triangular form of Q is:

$$Q = 2\begin{bmatrix} -c\beta & c\beta^2 \\ 0 & 1 - c\beta^3 \end{bmatrix}$$

The pivots are $-c\beta$, $1 - c\beta^3$. Since $0 < c\beta < 1$, then $1 - c\beta^3 > 0$, and the quadratic form is indefinite. For this case null motion is possible, and the singularity

can also be escaped. Currently, the degeneracy of the Hyperbolic singularity is resolved by simulation. This will be discussed in Chapter 5.

For the manipulator the singular configuration is defined by the joint angles: $\underline{q}^s = [\, 0°, 180°, 0° \,]$.

The row-echelon form of the Jacobian matrix and the null-space basis are:

$$J = \begin{bmatrix} 1 & -0.5 & 0.5 \\ 0 & 0 & 0 \end{bmatrix} \quad N = \begin{bmatrix} 0.5 & -0.5 \\ 1 & 0 \\ 0 & 1 \end{bmatrix}$$

The projection and Q matrices become:

$$P = \begin{bmatrix} 2 & 0 & 0 \\ 0 & -1 & 0 \\ 0 & 0 & 1 \end{bmatrix} \quad Q = 0.5 \begin{bmatrix} -1 & -1 \\ -1 & 3 \end{bmatrix}$$

The upper-triangular form is:

$$Q = 0.5 \begin{bmatrix} -1 & -1 \\ 0 & 4 \end{bmatrix}$$

The pivots are -1, 4, therefore the quadratic form is indefinite. In this case null motion is possible as well as escape from the singularity.

4.5 EXAMPLE OF SATURATION SINGULARITY

In this section a similar analysis is carried out for the Saturation singularity exam-

CMG SYSTEM

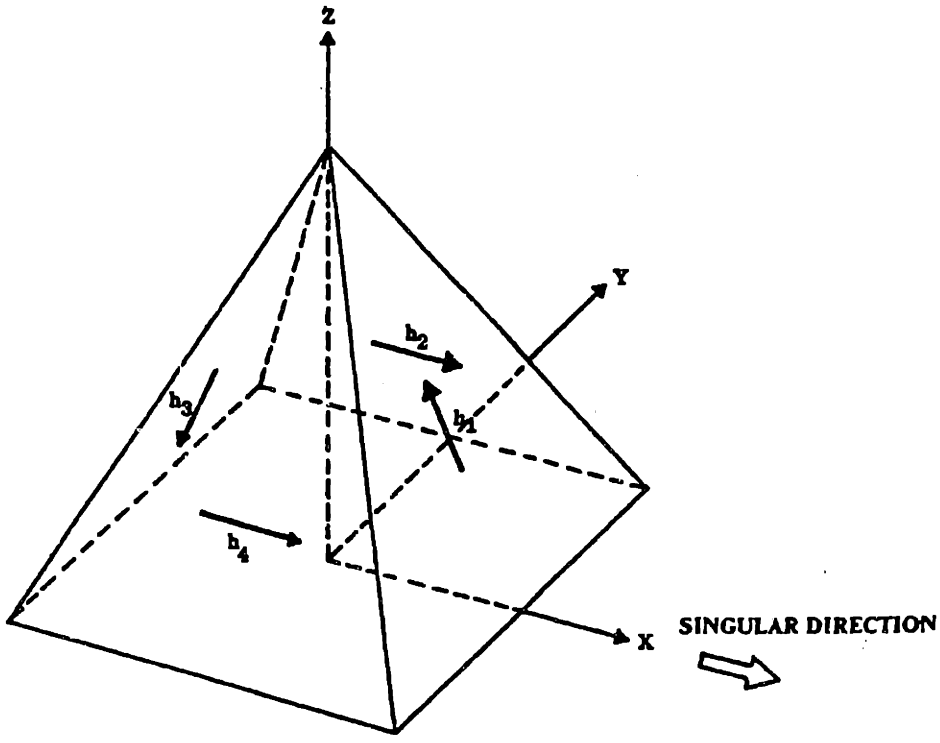

$$Q = 2\begin{bmatrix} -c\beta & c\beta^2 \\ c\beta & 1 - 2c\beta^3 \end{bmatrix}$$

INDEFINITE Q

$$\underline{\theta}^s = [\,90°, 180°, -90°, 0°\,]$$

$$[\,-,+,-,+\,]$$

MECHANICAL ANALOG

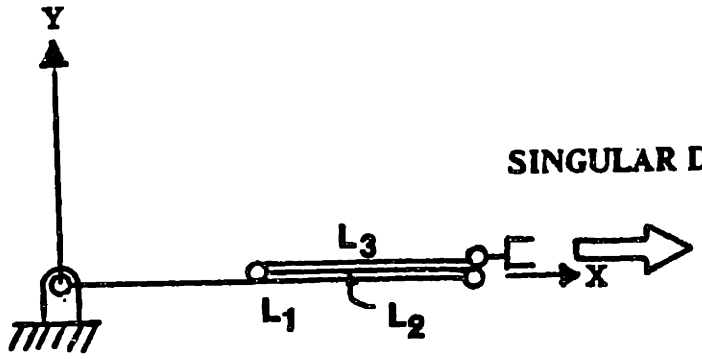

$$\underline{\theta}^s = [\,0°, 180°, 0°\,]$$

$$Q = 0.5\begin{bmatrix} -1 & -1 \\ -1 & 3 \end{bmatrix}$$

INDEFINITE Q

Figure 4-4. Example Of Hyperbolic Internal Singularity

ple used in Figure 4-2. The singular configuration for the CMG system is defined by the gimbal angles: $\underline{\theta}^s = [\ -90°, 180°, 90°, 0°\ ]$.

The row-echelon form of the Jacobian and its corresponding null-space basis is given by:

$$J = \begin{bmatrix} 1 & 0 & 1 & 2c\beta \\ 0 & 1 & 0 & -1 \\ 0 & 0 & 0 & 0 \end{bmatrix} \quad N = \begin{bmatrix} -1 & -2c\beta \\ 0 & 1 \\ 1 & 0 \\ 0 & 1 \end{bmatrix}$$

The Q matrix and its upper-triangular form are:

$$Q = 2\begin{bmatrix} c\beta & c\beta^2 \\ c\beta^2 & 2c\beta^3 + 1 \end{bmatrix} \quad Q = 2\begin{bmatrix} c\beta & c\beta^2 \\ 0 & c\beta^3 + 1 \end{bmatrix}$$

The pivots are $c\beta$ and $c\beta^3 + 1$. Both are positive, thus $Q > 0$, i.e. is positive definite. This suggests that the singularity is of Elliptic type and is unescapable by null motion. No null motion whatsoever is possible for this case, as earlier observed to be a property of the Saturation singularity.

In the case of the manipulator, the singularity is defined by the joint angles: $\underline{q}^s = [\ 0°, 0°, 0°\ ]$. The row-echelon form of the Jacobian and its null-space basis are:

$$J = \begin{bmatrix} 1 & 0.5 & 0.5 \\ 0 & 0 & 0 \end{bmatrix} \quad N = \begin{bmatrix} -0.5 & -0.5 \\ 1 & 0 \\ 0 & 1 \end{bmatrix}$$

The Q matrix and its upper-triangular form are:

$$Q = 0.5\begin{bmatrix} 3 & 1 \\ 1 & 3 \end{bmatrix} \quad Q = 0.5\begin{bmatrix} 3 & 1 \\ 0 & 8/3 \end{bmatrix}$$

The pivots are 3, 8/3. Both pivots are positive, and $Q > 0$. The singularity is therefore Elliptic, and no null motion is possible.

4.6 MEASURE OF SINGULARITY

We have seen that the rank of the Jacobian matrix is an indicator of the singularity of the CMG system. This information can be used to define an index, the singularity measure m, which shows how close the CMG system is to being singular. In the literature, m^2 is also refered to as the CMG "gain" [15]. The derivation of the singularity measure presented here employs the Singular Value Decomposition (SVD) of the Jacobian matrix, which is given by:

$$J(\underline{\theta}) = U \Sigma V^T \tag{4-11}$$

where U *is a* 3×3 *orthonormal matrix*
V *is a* $n \times n$ *orthonormal matrix*

$$\Sigma = \begin{bmatrix} \sigma_1 & 0 & 0 & \\ 0 & \sigma_2 & 0 & [\,0\,] \\ 0 & 0 & \sigma_3 & \end{bmatrix}$$

$\sigma_i \neq 0$ *singular values*

For a matrix to be nonsingular, all of its singular values must be greater than zero [2], therefore the product of the singular values can be used as a singularity measure. This is given by:

$$m = \sqrt{\det\, J J^T} = \prod_{i=1}^{3} \sigma_i \tag{4-12}$$

Equation (4-12) is easily verified by substituting the SVD definition (4-11) for the Jacobian:

$$\begin{aligned} m &= \sqrt{\det\left[(U \Sigma V^T)(V \Sigma^T U^T) \right]} \\ &= \sqrt{\det(U \Sigma \Sigma^T U^T)} \\ &= \sqrt{\det U \ \det \Sigma \Sigma^T \ \det U^{-1}} \\ &= \sqrt{\prod_{i=1}^{3} \sigma_i^2} \\ m &= \prod_{i=1}^{3} \sigma_i \end{aligned}$$

Since, m is a measure of spacecraft 3-axis controllability, the CMG system approaches a singular state as $m \rightarrow 0$. The parameter m^2 has been used as an objective function for a singularity-avoidance Steering law using single-gimbal CMGs [15], and m has been used for double-gimbal CMG Steering laws [16]. For redundant manipulators, this measure was called *manipulability* [17]. In the next section, a convenient formula is presented to evaluate the singularity measure.

4.6.1 Formula For The Singularity Measure

The numerical computation of the singularity measure can become difficult, even for a CMG system with only one degree of redundancy. The computational burden may be reduced by using the Binet-Cauchy formula [8] :

$$m = \sqrt{\sum_{i=1}^{\binom{N}{3}} M_i^2} \qquad \binom{N}{3} = \frac{N(N-1)(N-2)}{3!}, \quad N \geq 3 \tag{4-13}$$

$$\textit{where} \quad M_i = \binom{N}{3} \textit{ distinct Jacobian minors of order } 3$$

For the Pyramid mounted 4-CMG system, the measure can be written as:

$$m = \sqrt{M_1^2 + M_2^2 + M_3^2 + M_4^2} \tag{4-14}$$

The evaluation of the singularity measure is much simpler by this formula, since the order 3 minors of the Jacobian matrix are dimensioned smaller as well as having simple entries than the square matrix formed from ($J J^T$). Since this formula expresses the measure in terms of all distinct minors of order 3 which are extractable from the Jacobian, we can see from (4-14) that individual minors can be zero, (implying loss of three-axis controllability for the corresponding sub-system of 3 CMGs) while the system as a whole remains non-singular.

A new measure of distance from singular points was recently proposed for redundant manipulators [18]. This new measure is defined in terms of the product of non-singular Jacobian minors. Since the minors represent the relative folding of all sub-groups of links, this measure reflects the number of relatively unfolded (non-colinear) groups of links remaining in the manipulator system. This approach can analogously be used in CMG Steering laws. However, since keeping the product of minors non-zero precludes the switching of solutions (or linkage configuration) it is felt that this approach is not appropriate for CMG Steering laws.

This switching of solutions is determined by the singular minors, that is gimbal angles for which $M_i = 0$, define the boundary between one form of joint configuration and another form. In nonredundant systems, this boundary is defined by $\det(J) = 0$. This fact can be most easily understood by refering to the planar 3-link manipulator (introduced in Chapter 2) in Figure 4-5, which shows the transition from one joint configuration or closure (A) to another closure (C) through the switch configuration (B) while the total system is nonsingular through the switch. It is seen that the switch boundary occurs when links #2 and #3 are colinear, which implies that $M_3 = |\underline{j}_2\, \underline{j}_3| = 0$ at the boundary, while the other two minors are nonzero. This switching is undesirable in manipulators because it leads to repeatability problems. On the other hand, in CMG systems this switching is desirable for singularity avoidance.

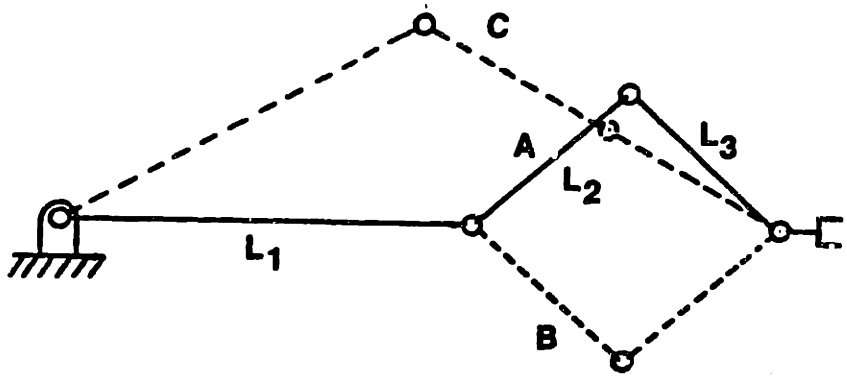

Figure 4-5. Transition Between Two Joint Closures Via Singular Minor

4.6.2 Singularity Measure And Null-Space Of Jacobian

We have seen that the singularity measure of the Jacobian can be expressed in terms of its minors. It has also been shown that the Jacobian null-space can likewise be expressed in terms of the minors. What then, is the relationship between the two, if any? In order to examine the relationship, we will use the 4-CMG system as an example (what follows is actually valid for any system with one degree of redundancy). The definition below provides some illumination:

Definition: For any non-singular real matrix J of dimension $m \times (m+1)$

$$\det(J J^T) = |\underline{v}|^2$$
$$\textit{where} \quad \underline{v} = \textit{Jacobian null} - \textit{vector}$$

Proof: Using the notation of Chapter 2 and the Jacobian matrix of the 4-CMG system, we can write:

$$\det(J J^T) = M_1^2 + M_2^2 + M_3^2 + M_4^2$$

$$|\underline{v}|^2 = \underline{v}^T \cdot \underline{v} = \begin{bmatrix} M_4, & -M_3, & M_2, & -M_1 \end{bmatrix} \begin{bmatrix} M_4 \\ -M_3 \\ M_2 \\ -M_1 \end{bmatrix} = M_1^2 + M_2^2 + M_3^2 + M_4^2$$

Armed with this definition, the null-vector of the Jacobian can be better understood; this understanding will be vital in the design of the Steering law. The fundamental attributes of the null-vector, its magnitude and direction, for non-singular systems of single-degree redundancy can be summarized as follows:

Magnitude Of Null-Vector: The magnitude of the null-space basis vector is identical to the singularity measure, m, thus is directly related to the nearness of a singularity.

Direction Of Null-Vector: The direction of null motion is defined by the non-zero distinct minors of order 3 extractable from the Jacobian matrix. The availability of null motion from each CMG is also determined by these non-zero minors.

The above statements dictate that the amount of null motion available from each gimbal is governed by both the singularity measure and its corresponding minor. On the other hand, the possibility of extracting null motion from each CMG is determined only by the value of the corresponding minor.

CHAPTER 5

KINEMATIC REDUNDANCY RESOLUTION METHODS

5.1 GENERAL SOLUTION METHODS

In this chapter, various torque-input Steering laws will be reviewed, and their performance evaluated. Alternative methods of singularity avoidance will also be proposed, and their behaviour likewise examined. The results of Chapter 4 will be used extensively to evaluate and understand the performance of the different Steering laws. It will be shown that existing singularity avoidance methods do not avoid Elliptic type internal singularities.

Kinematic methods of redundancy resolution require the solution of an underdetermined system of linear simultaneous equations (the torque equation) involving the instantaneous Jacobian matrix of the CMG system.

$$J(\underline{\theta})\,\dot{\underline{\theta}} = \underline{\tau} \tag{5-1}$$

These methods are refered to as local, because they yield gimbal rate solutions to the instantaneous torque request. Redundancy is also resolved instantaneously, based on some criteria that hopefully steer the gimbal angles away from internal singular configurations while simultaneously satisfying the torque request, $\underline{\tau}$. Local methods have the advantage that real-time implementation is readily feasible.

The general solution to (3-6) was shown in Chapter 3 to be formed from the Moore-Penrose pseudoinverse and any homogeneous solution. This form can be further classified into the following three categories:

a) **Pseudoinverse (Moore-Penrose) Method**

$$\dot{\underline{\theta}} = J^T(J\,J^T)^{-1}\,\underline{\tau} \tag{5-2}$$

b) **Weighted Pseudoinverse**

$$\dot{\underline{\theta}} = W^{-1}J^T(J\,W^{-1}J^T)^{-1}\,\underline{\tau} \tag{5-3}$$

c) **Pseudoinverse With Null Motion**

i) Projection Matrix

$$\dot{\underline{\theta}} = J^T(J\,J^T)^{-1}\,\underline{\tau} + \gamma\left[\,\underline{1} - J^T(J\,J^T)^{-1}J\,\right]\underline{d} \tag{5-4}$$

ii) Null Vector

$$\dot{\underline{\theta}} = J^T(J\,J^T)^{-1}\,\underline{\tau} + \sum_{i=1}^{n-r(J)} \lambda_i\,\underline{v}_i \tag{5-5}$$

To illustrate the properties of the various methods, computer simulations using the Pyramid mounted 4-CMG system will be used.

5.1.1 Simulation Parameters To Exercise Steering Laws

To illustrate the singularity avoidance properties of the various solution methods, a constant torque request along the spacecraft $\hat{X}$-axis will be used. This direction is chosen because it will force the CMG system through the Elliptic internal singularity

which was analyzed in Chapter 4. Since the Elliptic singularity represents the worst type of singular configuration, it can be used as a measure of the singularity avoidance capability of the particular method used in the Steering law. Also, the torque request is aligned with the singular direction, which represents the worst possible combination. It should be noted that non-degenerate Hyperbolic internal singularities can be avoided by any of the above methods; this will be shown by computer simulation.

During the course of the computer simulations, it was found that the method used to calculate the pseudoinverse could affect the gimbal angle trajectories. The first method which was used, numerically evaluated the pseudoinverse using symbolic expressions for the adjoint of the square matrix ($J J^T$) and its determinant. This square matrix is ideally symmetric, however, during computation it was observed that there were slight discrepancies between the off-diagonal terms due to truncation errors. For this reason, the dyadic form of ($J J^T$) was used instead (as in [1]) to obtain a closed form solution for the torque producing gimbal rates. This solution is given by:

$$\dot{\theta}_1^T = \frac{1}{m^2}\left\{ M_1 \left| \underline{j}_2\ \underline{j}_3\ \underline{\tau} \right| + M_2 \left| \underline{j}_2\ \underline{j}_4\ \underline{\tau} \right| + M_3 \left| \underline{j}_3\ \underline{j}_4\ \underline{\tau} \right| \right\}$$

$$\dot{\theta}_2^T = \frac{1}{m^2}\left\{ -M_1 \left| \underline{j}_1\ \underline{j}_3\ \underline{\tau} \right| - M_2 \left| \underline{j}_1\ \underline{j}_4\ \underline{\tau} \right| + M_4 \left| \underline{j}_3\ \underline{j}_4 \underline{\tau} \right| \right\}$$

$$\dot{\theta}_3^T = \frac{1}{m^2}\left\{ M_1 \left| \underline{j}_1\ \underline{j}_2\ \underline{\tau} \right| - M_3 \left| \underline{j}_1\ \underline{j}_4\ \underline{\tau} \right| - M_4 \left| \underline{j}_2\ \underline{j}_4\ \tau \right| \right\}$$

$$\dot{\theta}_4^T = \frac{1}{m^2}\left\{ M_2 \left| \underline{j}_1\ \underline{j}_2\ \underline{\tau} \right| + M_3 \left| \underline{j}_1\ \underline{j}_3\ \underline{\tau} \right| + M_4 \left| \underline{j}_2\ \underline{j}_3\ \underline{\tau} \right| \right\}$$

where M_i = *Jacobian minors of order* 3

$\dot{\theta}_i^T$ = *Torque producing gimbal rates*

This approach was found to yield more accurate results than the symbolic inverse.

The CMG dynamics were integrated at a simulation interval of 0.01 sec, unless otherwise stated. The gimbal rates were integrated using the routine DVERK from the IMSL library, which performs a fifth-sixth order Runge-Kutta numeric integration. A tolerance value of 0.0001 was used. Programs were written in double precision Fortran 77. The torque request and angular momentum magnitudes were set equal to unity (i.e. $h = 1$, $|\underline{\tau}| = 1$), and no rate limits were enforced. The applied torque request vector was:

$$\underline{\tau} = \begin{bmatrix} 1 \\ 0 \\ 0 \end{bmatrix}$$

The initial gimbal angles for all simulations were each set to 0.

5.2 PSEUDOINVERSE (MOORE-PENROSE) METHOD

The properties of this method were discussed in detail in Chapter 3, thus will not be repeated here. It has been shown [19] that this method can generate gimbal angle trajectories that pass arbitrarily close to singular points in gimbal angle space, therefore this method cannot be used by itself to avoid singular states.

From the simulation results given in Figure 5-1 this fact can be easily seen. The singularity measure m ($SQRT(DET(JJT))$) nears zero as the X component angular momentum (HX) approaches 1.15, indicating that the CMG system is singular. The singularity measure is non-zero as H_x passes 0.85, indicating that the Hyperbolic singularity analyzed in Chpater 4 is avoided. This is the method by which the degeneracy of the Hyperbolic singularity is currently determined. The inner product of the torque

solution (i.e. $\underline{\dot{\theta}}_P$) with the gradient of the singularity measure (*GRAD.TORK_SOL*) is also shown. Because the projection becomes negative, it is seen that the torque solution decreases the singularity measure as the singularity is approached. From the gimbal angle plots it is seen that gimbals #2 and #4 hardly move (the gimbal positions are shown with respect to the mounting configuration at $H_x = 0$, and $H_x = 1.15$ for easy visualization in Figure 5-2). It is seen from this figure that gimbal #2 always has minimum projection in the torque direction, while the other gimbals eventually reach maximum projection in this direction. In essence gimbal #2 is "hung-up" in an anti-parallel orientation; it has no projection along the requested torque direction, hence is not used. This serves to illustrate the general property of the pseudoinverse which tends not to move inefficiently oriented gimbals, and leave the system in a singular configuration well below the total momentum capacity (H_x will reach saturation at approximately 3.2 units).

It may still be possible, however, to pass through the singularity by switching to the rank 2 Moore-Penrose pseudoinverse algorithm described in [1] to maintain 2-axis control while the system is singular. As long as the singular direction does not lie along the desired torque direction, it is intuitively clear that the torque component in the plane spanned by the singular columns of the Jacobian can be generated. Unfortunately, this approach breaks down when the singular direction is colinear with the torque direction. This is easily seen from the formulation of the rank 2 pseudoinverse:

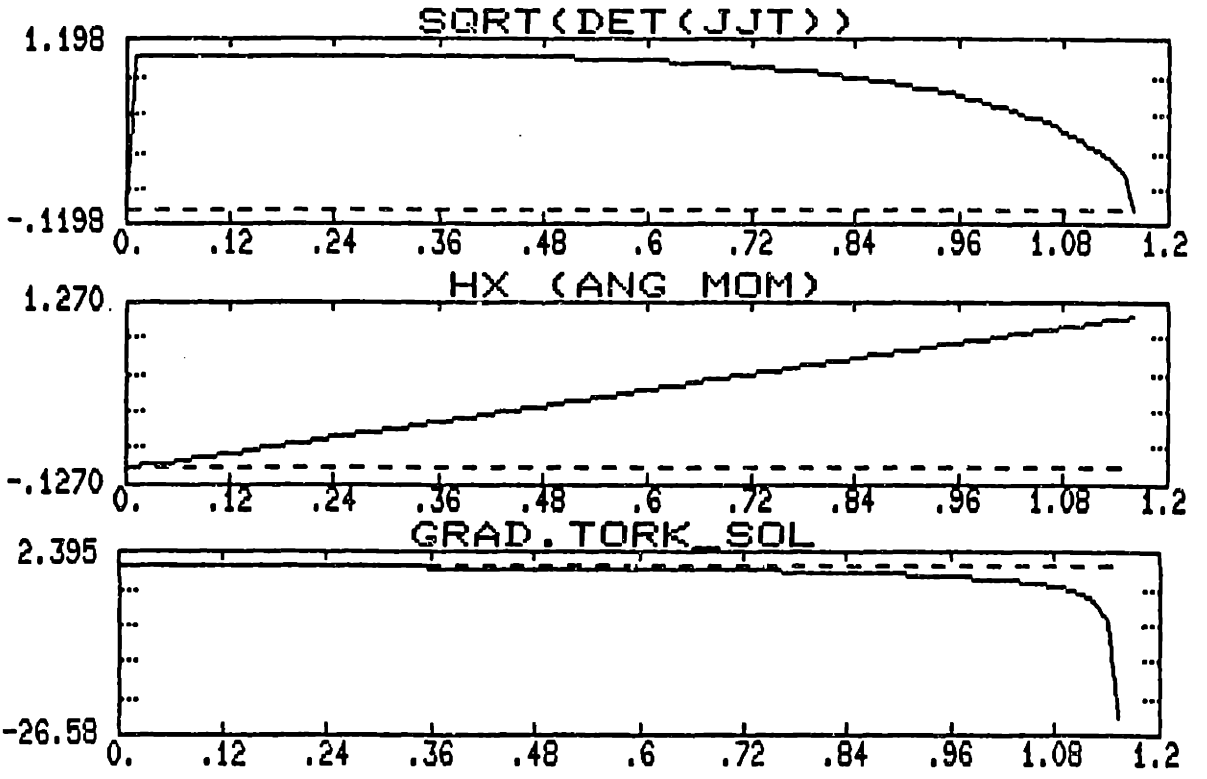

Figure 5-1. Simulation Results For Moore-Penrose Method (Part 1 of 2)

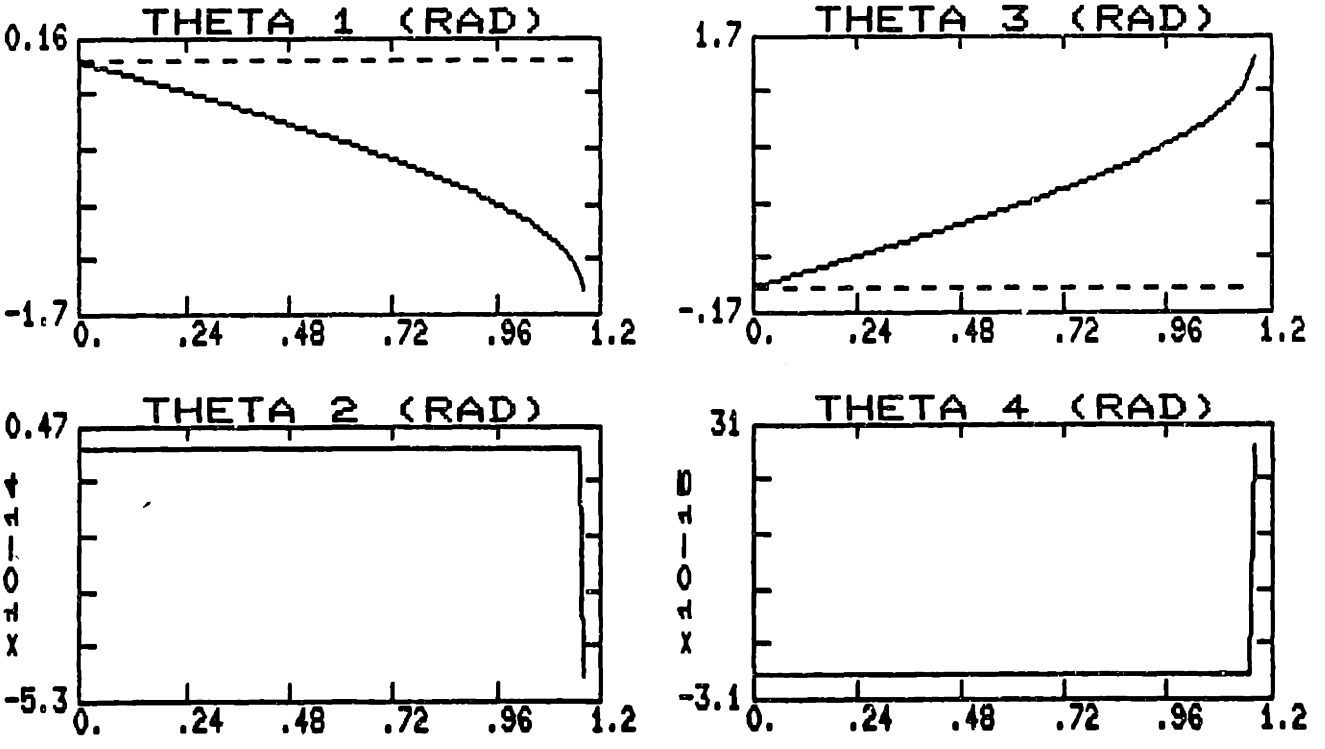

Figure 5-1. Gimbal Angles For Moore-Penrose Method (Part 2 of 2)

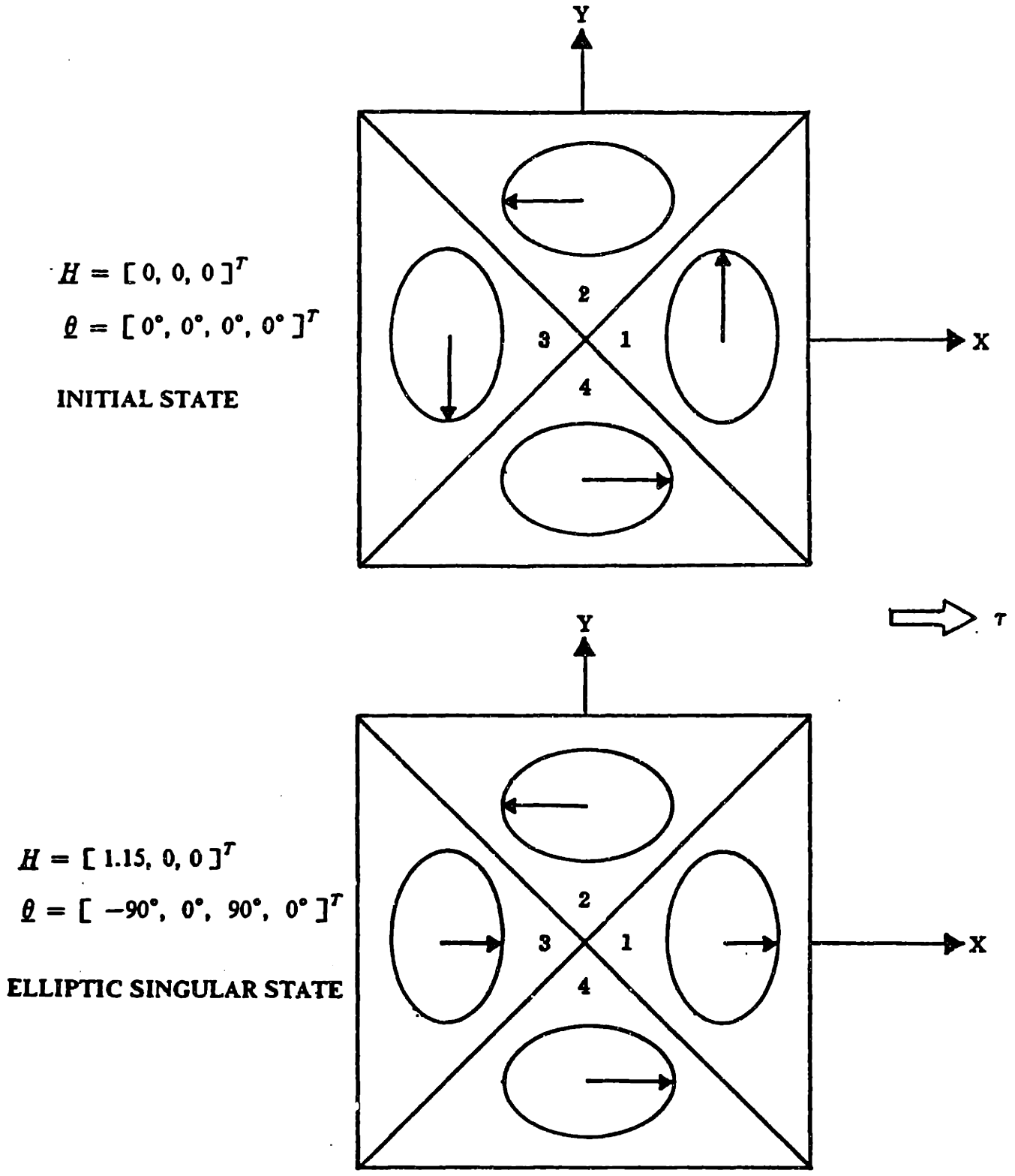

Figure 5-2. Visualization Of Gimbal Angle Motion For Moore-Penrose Simulation

$$\dot{\theta}_k^T = \frac{\sum_{i=1}^{4} \left| \underline{j}_i^s \ \underline{u} \ \underline{j}_k^s \right| \left| \underline{j}_i^s \ \underline{u} \ \underline{\tau} \right|}{\sum_{i<j}^{4} \left| \underline{j}_i^s \ \underline{j}_j^s \ \underline{u} \right|^2}$$

where $\dot{\theta}_k^T$ = *Torque producing gimbal rates*

$\underline{u}$ = *Singular direction* (*normal to plane spanned by* $\underline{j}_i^S$)

$\underline{j}_i^S$ = *Singular Jacobian column vectors*

It is seen that if $\underline{u}$ and $\underline{\tau}$ are colinear, the second determinant in the numerator is zero, thus no torque is possible in the requested direction. For the Elliptic singularity at $H_x = 1.15$, this is exactly the case; the singular direction and the torque direction are identical, therefore this approach can not always be used to produce torque in the desired direction.

5.3 WEIGHTED PSEUDOINVERSE

The pseudoinverse may also be weighted to provide additional mechanisms by which desired performance characteristics are achieved. This is accomplished by solving:

$$\min \quad \frac{1}{2} \dot{\underline{\theta}}^T W \dot{\underline{\theta}}$$

$$\textit{subject to} \quad J \dot{\underline{\theta}} = \underline{\tau}$$

The weighting matrix W must be positive definite. It is seen that the Moore-Penrose (M-P) method is obtained by setting the weighting equal to the identity matrix $\underline{1}$.

The properties of this method are essentially the same as those of the M-P method as long as $W = k\,\underline{1}$ For this case, the particular solution $\underline{\dot{\theta}}_P$ is orthogonal to the homogeneous solution $\underline{\dot{\theta}}_H$. Otherwise, this property is not preserved, and this new solution can be expressed as a combination of the M-P inverse and a homogeneous term. Assigning different values to the diagonal elements of W causes the participation of a particular gimbal with lower weighting to be favored more heavily in the solution; unequal weighting of gimbal rates thus enforces high-authority/ low-authority partitioning of gimbal activity. This method may be used to reflect the energetics of a system (thereby minimizing energy), which would make it a dynamic rather than a kinematic method. An example of this would be using the inertia matrix of a manipulator as the weighting matrix in order to minimize system kinetic energy. This approach has been used in robotic applications, however it did not offer any improvement over the M-P inverse as far as singularity avoidance is concerned [20].

From the previous pseudoinverse simulation results, it was noted that gimbal #2 was essentially not moved. To encourage the motion of gimbal #2, a time varying diagonal weighting matrix was attempted. The intent was to reduce the penalty of inefficiently placed gimbals, thereby hopefully encouraging their movement. Correspondingly, any maximally projected gimbals were weighted with a higher cost to attenuate their participation. The diagonal entries of the weighting matrix thus become:

$$w_i = w_0 + C_0 \left\{ \left| \underline{h}_i^T \bullet \underline{\tau} \right| + \underline{h}_i^T \bullet \underline{\tau} \right\} \qquad i = 1, \ldots, 4$$

$$\textit{where} \quad w_0 = \textit{Initial weighting}$$
$$C_0 = \textit{Multiplier}$$

The results of this approach are shown in Figure 5-3. The parameters that were used are $w_0 = 1$, $C_0 = 2$. The effect of the weighting matrix on the determinant of the square matrix $J W^{-1} J^T$ ($SQJ\ DET$), is seen not to prevent it from becoming singular. It is seen that the singularity at $H_x = 1.15$ was still not avoided. From the weighting plots it is seen (as expected) that gimbal #2 always has the smallest cost, while the cost on gimbals #1 and #3 continuously increased as they approached maximum projection on the torque direction. Comparing the gimbal angle plots of this approach with those of the M-P inverse, it seen that they are essentially identical. Although this method may hold promise in re-partitioning the use of different gimbals if off-diagonal terms were used in the weighting matrix, it has been shown to be ineffective in avoiding singular states. Since this solution can be written in terms of the M-P inverse and an appropriately chosen homogeneous solution, it will not be pursued further.

5.4 PSEUDOINVERSE WITH NULL MOTION

We have seen that the pseudoinverse solution by itself does not provide any singularity avoidance for Elliptic singularities. Since the homogeneous solution has no projection on the row space of (3-6), i.e. produces no torque, it can be used to shape the complete solution and hopefully provide a means of singularity avoidance. The steering problem then reduces to picking a vector in the null-space of the Jacobian such that all internal singularities are avoided. The addition of null motion thus is to steer the gimbal angle trajectory to an alternative non-singular configuration corresponding

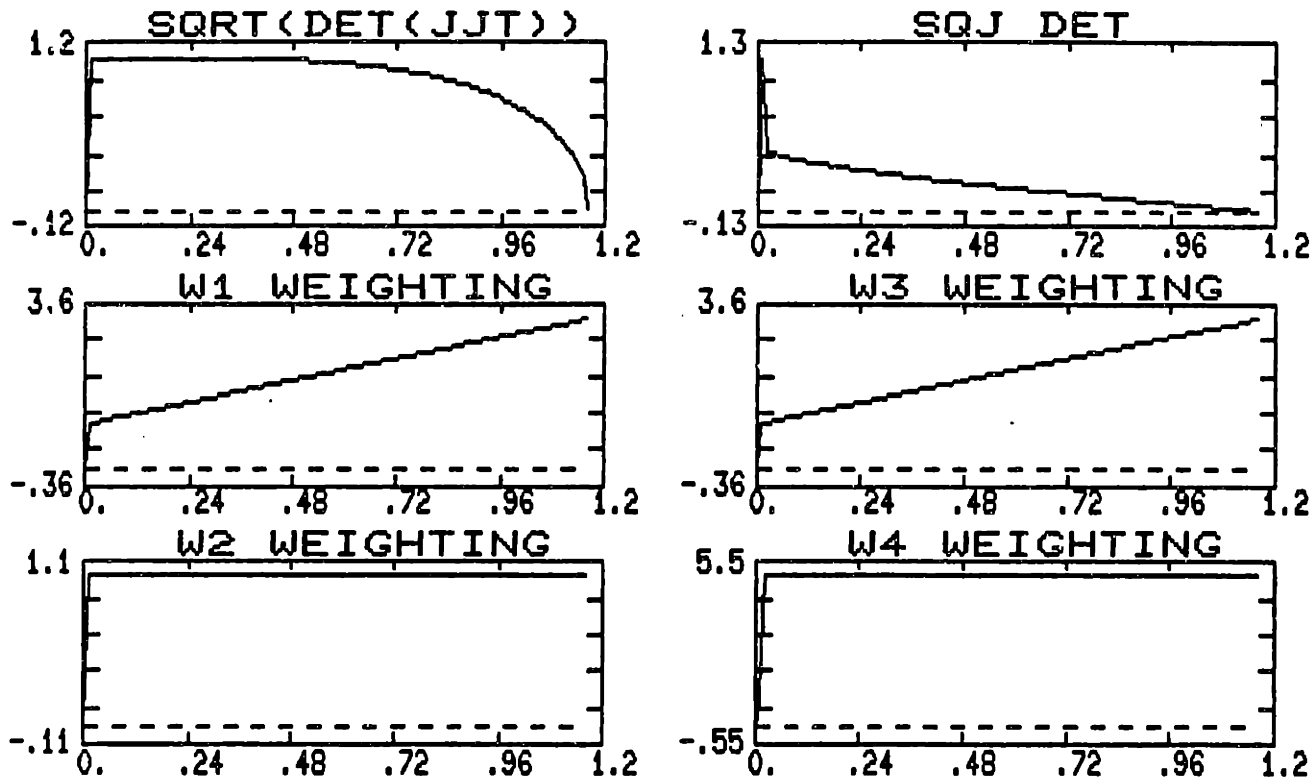

Figure 5-3. Simulation Results For Weighted-Pseudoinverse (Part 1 of 2)

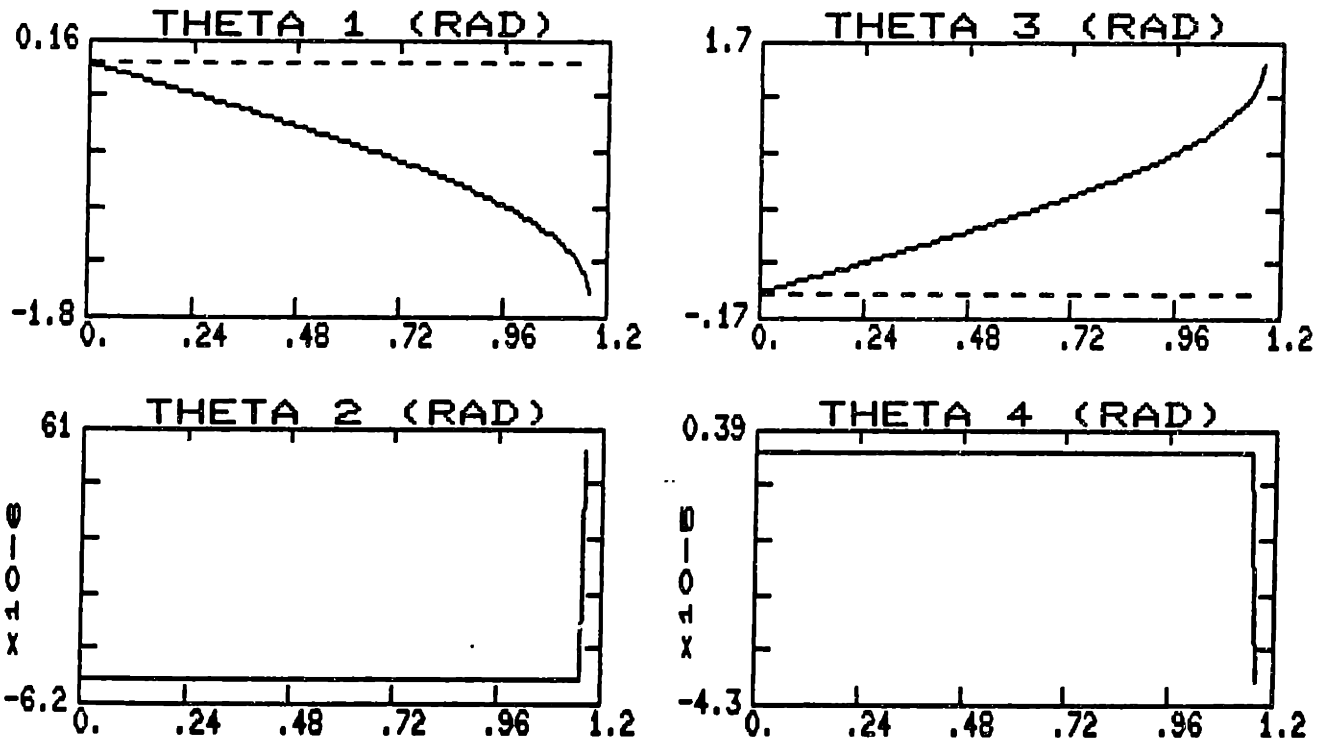

Figure 5-3. Gimbal Angles For Weighted-Pseudoinverse (Part 2 of 2)

to the singular momentum state. In Chapter 4, it was shown that not all neighborhoods of internal singularities can be escaped using null motion to reconfigure the momentum linkage; this method is effective only as long as the gimbal angle trajectory does not approach neighborhoods of Elliptic or degenerate Hyperbolic singularities. It will be demonstrated that the addition of any class of null motion does not completely address the singularity avoidance problem.

5.4.1 Projection Matrix

One way of obtaining a vector in the null-space of the Jacobian is by using an operator that projects an arbitrary n-vector into its null-space. One such operator, the Projection matrix, is given by:

$$P = \underline{1} - J^T(J J^T)^{-1} J$$

For a singularity avoidance control law, all that remains is to pick the projection vector $\gamma \underline{d}$ as in (5-4). In [19], it is shown that arbitrary gimbal angle trajectories which do not pass through a singular configuration may be generated using this method by an appropriate choice of $\gamma \underline{d}$. This result requires that one choose *a priori* a singularity free gimbal angle trajectory, and also select a projection vector that can recover or generate this trajectory. Normally, such a trajectory is not known beforehand; the generation of such a trajectory becomes the design objective.

The usual approach to singularity avoidance is to choose this projection vector such that a scalar performance index (such as the singularity measure), is "optimized".

One way of accomplishing this is to maximize a scalar performance criterion $p(\underline{\theta})$ by choosing $\underline{d}$ as in [16]:

$$\underline{d}^T = \frac{\partial p(\underline{\theta})}{\partial \underline{\theta}} \tag{5-6}$$

These types of procedures are usually refered to as gradient methods. Since, $\dot{p} = \underline{d}^T \dot{\underline{\theta}}$, we use (5-4) to obtain:

$$\dot{p} = \underline{d}^T J^T (J J^T)^{-1} \underline{\tau} + \gamma \underline{d}^T \left[\underline{1} - J^T (J J^T)^{-1} J \right] \underline{d} \tag{5-7}$$

The second term in the right-hand side is non-negative because the projection matrix is positive semidefinite [2], and contributes to an increase in the value of p. One way of choosing the scalar γ is to maximize $\dot{p}\,(\underline{u} = 0)$ subject to upper bounds on gimbal rates [16]. The singularity measure, m was chosen as the performance index. It should be noted, however, that the singularity measure is not a monotonic function of the gimbal angles, thus instantaneously maximizing this function can lead to local extrema of the measure. It is shown in [15] that this method does not avoid singular states because the system is controlled to stay at the local maximum, and there exist trajectories of local maxima which nearly extend to singular points. Another way of expressing this is that the right hand side of (5-7) can be negative and may dominate $\dot{p}$, thus resulting in a net decrease in the value of p. This phenomenon will be examined further in the next section.

It is also mentioned in [11] (without any particular references) that gradient methods using a performance index

$$p = \frac{1}{m^2}$$

have been tried unsuccessfully by several authors. It was suggested that the reason for this was that the determinant was not sufficiently sensitive to allow appropriate null motion be added in time to avoid close encounters with internal singularities.

5.4.1.1 Indirect Avoidance Control Law

Another way of choosing the projection vector can also be found in [11]. This method, called the indirect avoidance law, relies on the observation that internal singularities can be avoided in most cases by merely steering towards the Saturation singularity associated with the instantaneous torque request. This method was successfull in avoiding internal singularities for a 6-Pyramid CMG system. Since we have seen in our simulations that gimbal #2 was persistently "hanging-up" antiparallel to the torque request for the M-P inverse, this method seems to provide a means of encouraging this gimbal to move. The projection vector for this approach is defined as:

$$\underline{d} = \Delta\underline{\theta} = \underline{\theta}^{sat} - \underline{\theta}$$

$$\gamma = \left[\frac{\hat{z} \cdot \hat{y}}{\hat{x} \cdot \hat{y}} \right] \left| \dot{\underline{\theta}}_P \right|$$

$$where \quad \underline{\theta}_i^{sat} = \tan^{-1}\left[\frac{\hat{j}_i^{\,0} \cdot \hat{u}}{\hat{h}_i^{\,0} \cdot \hat{u}}\right]$$

$$\hat{u} = unit(\underline{\tau})$$
$$\hat{z} = unit(P\,\Delta\underline{\theta})$$
$$\hat{y} = unit(\Delta\underline{\theta})$$
$$\hat{x} = unit(\dot{\underline{\theta}}_P)$$
$$P = Projection\ matrix$$

The indirect avoidance law was implemented in simulations of the 4-CMG system without limiting the amount of null motion. The projection matrix was numerically calculated using the symbolic adjoint of $(J J^T)$. The simulation interval was 0.005 sec., with a final time of 1.18 sec. The results of the simulation are shown in Figure 5-4. It is seen that the Elliptic singularity is again not avoided since m still approaches zero at $H_x = 1.15$. The projection of the null vector, $\underline{z}$, on the gradient is seen to go to zero near the singularity, thereby rendering any null motion ineffective in avoiding it. From the gimbal angle plots, it is observed that both gimbals #2 and #4 move slightly, but not sufficiently to "un-lock" gimbal #2.

5.4.2 Null Vector

The Jacobian null-space basis vectors can also be used to form the null-vector. With this approach, only the scalar weighting factors remain to be determined. It should be noted that as the redundancy of the system increases, the dimension of the null-space also increases, which complicates the choice of these factors. For the case of four CMGs and a nonsingular Jacobian matrix, the null-space dimension is one, thus null motion is restricted to a line. All that remains in this case is to choose the magni-

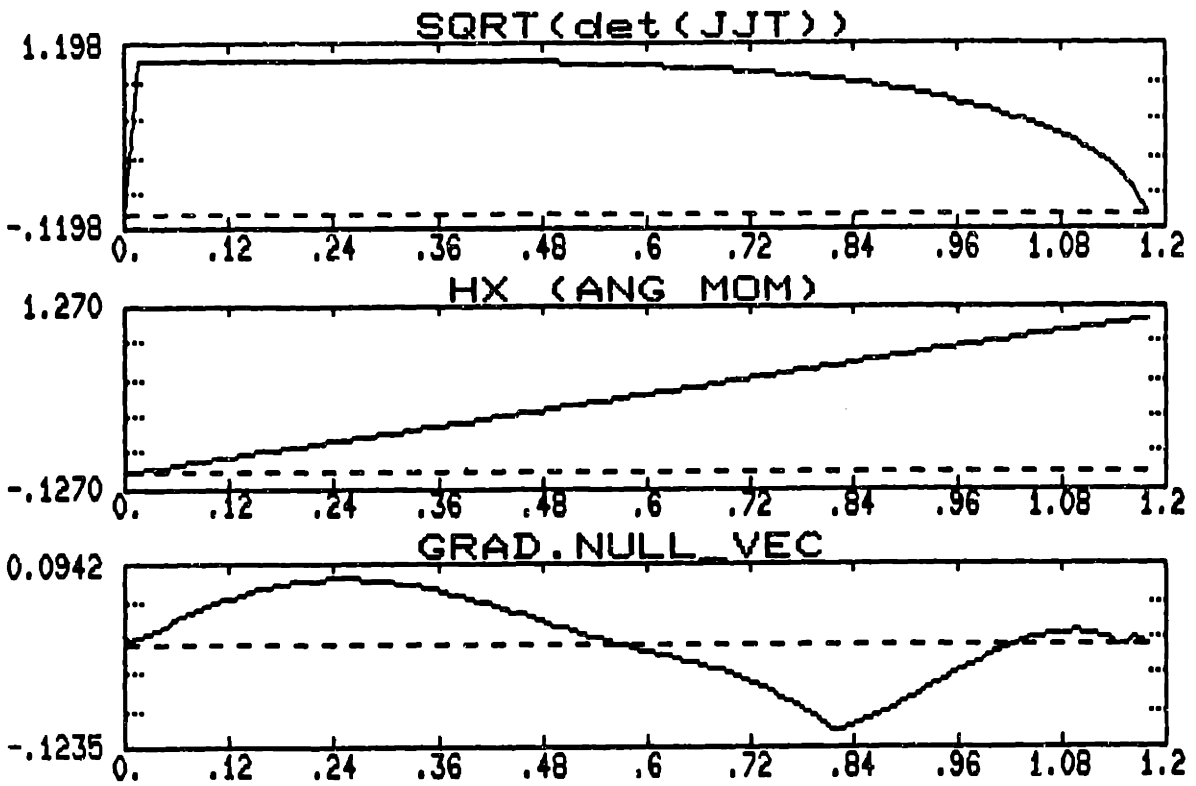

Figure 5-4. Simulation Results For Indirect Avoidance Law (Part 1 of 2)

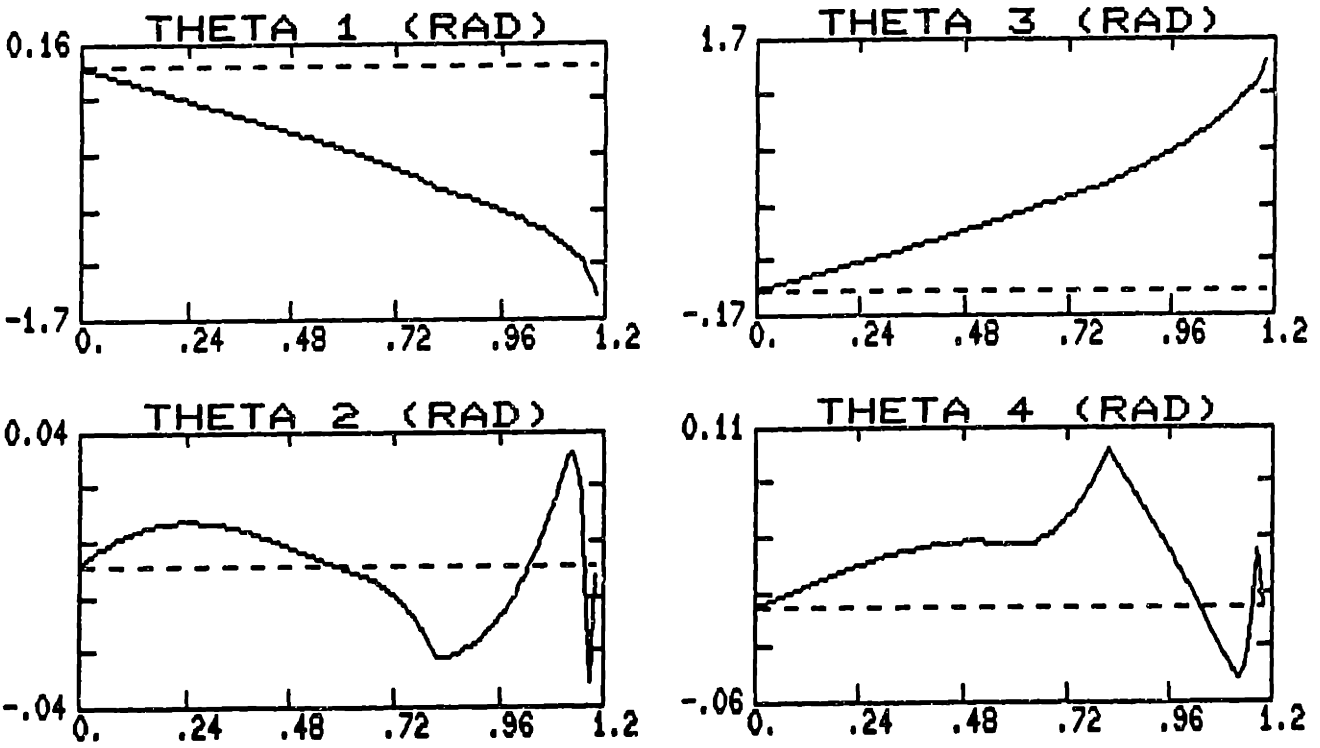

Figure 5-4. Gimbal Angles For Indirect Avoidance Law (Part 2 of 2)

tude and direction in which null motion is applied by using a single scale factor. The homogeneous solution can then be written as:

$$\underline{\dot{\theta}}_H = \lambda \underline{v}$$

One method of choosing the scale factor for a 4-Pyramid CMG system is given in [15]. This approach, called the maximum gain method, involves steering the null motion towards the point of maximum gain, m^2. This approach is global in the sense that the direction of null motion is oriented towards the point of global maximum gain in gimbal angle space, as obtained from a look-up table which is generated by off-line calculation and reduced to a small size by taking advantage of the symmetry of this particular configuration. This method also requires the location of *all* Elliptic type internal singularities to be determined in order that gimbal angle trajectories always avoid the neighborhoods of these singularities. This is accomplished by modifying the gimbal rates.

The null vector strategy was applied in two different singularity avoidance laws. Both of these methods exploit the relationship derived in Chapter 4 between the null-space of the Jacobian and the singularity measure (or gain). These methods are:

a) **Gradient Method**

b) **Inverse Gain Method**

5.4.2.1 Gradient Method

The singularity measure m, was chosen as the performance index to be maximized. Using (5-5), the time rate of change of the performance index becomes:

$$\dot{p} = \nabla_{\underline{\theta}} m \bullet J^T (J J^T)^{-1} \underline{\tau} + \lambda \nabla_{\underline{\theta}} m \bullet \underline{v} \tag{5-8}$$

The sign of λ is determined from the second term of (5-8). The gradient of the singularity measure was computed symbolically using MACSYMA (Macsyma Manual).

To complete the control law design, an appropriate weighting factor λ must be chosen. To do this, we must define the relevant parameters that may be advantageous to use in computing λ . Some useful parameters are:

- $\frac{1}{m}$. We know λ has to be at least proportional to $\frac{1}{m}$ to cancel the magnitude of the null-vector. Otherwise, the effectiveness of λ will be reduced as the system approaches a singularity.
- Power of singularity measure. The amount of null motion is related to distance from singularity. For example, we could set $\lambda = \frac{1}{m^2}$. This is the usual approach in other gradient methods.
- $\nabla_{\underline{\theta}} m \bullet \underline{\dot{\theta}}_p$. The amount of null motion is made proportional to the projection of the torque solution on the gradient of the performance index. It was observed earlier that this term can become negative, and thus reduce the value of p. By making the amount of null motion proportional to this term, this effect can potentially be taken into account and cancelled; for example, λ could be made

proportional to this term whenever it is negative. This scaling has not been utilized in other gradient methods.

- $\nabla_{\underline{\theta}} m \bullet \underline{v}$. The amount of null motion is made proportional to the projection of the null-vector on the gradient of the performance index. This term expresses the possibility of affecting the index through null motion; if this term is small, the effectiveness of null motion is reduced, regardless of how it is determined.

Taking into account all of the above criteria, the gradient method is formulated using a weighting factor that includes a a contribution from each parameter:

$$\lambda = \frac{\nabla_{\underline{\theta}} m \bullet \underline{v} \left| \nabla_{\underline{\theta}} m \bullet J^T (J J^T)^{-1} \underline{\tau} \right|}{m^2} \tag{5-9}$$

This approach is somewhat unique; of the gradient methods published in the literature [11], [15], all lack at least one of the four criteria mentioned above.

Simulation results for this method are shown in Figure 5-5. It is seen that the Elliptic singularity is still not avoided. The reason becomes evident if we look at the plots of the null-constant λ (*NULL CONSTNT*) , and the gradient projection on the null-vector (*GRAD.NULL_VEC*). It is seen that the null-constant remains essentially zero up to the singularity. This is because the null-vector has very small or no projection on the gradient at this period, thus no null motion was added. This simulation then is identical to using the M-P inverse by itself. Looking at the gimbal angle plots, we see that gimbal #2 does not move, just as in the M-P inverse method.

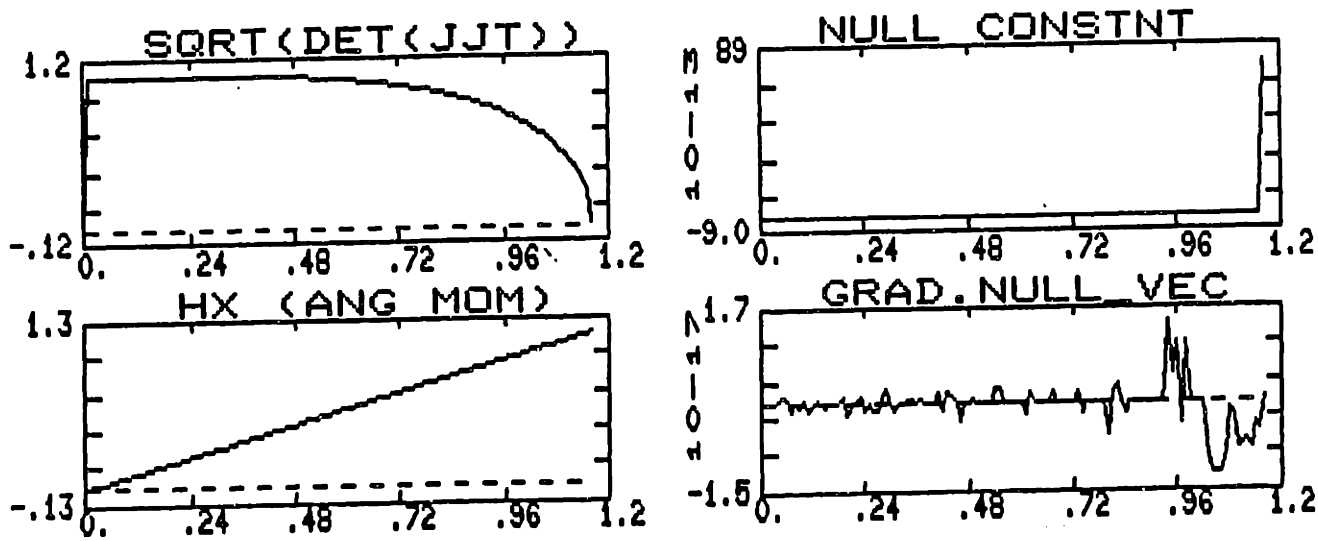

Figure 5-5. Simulation Results For Gradient Method (Part 1 of 2)

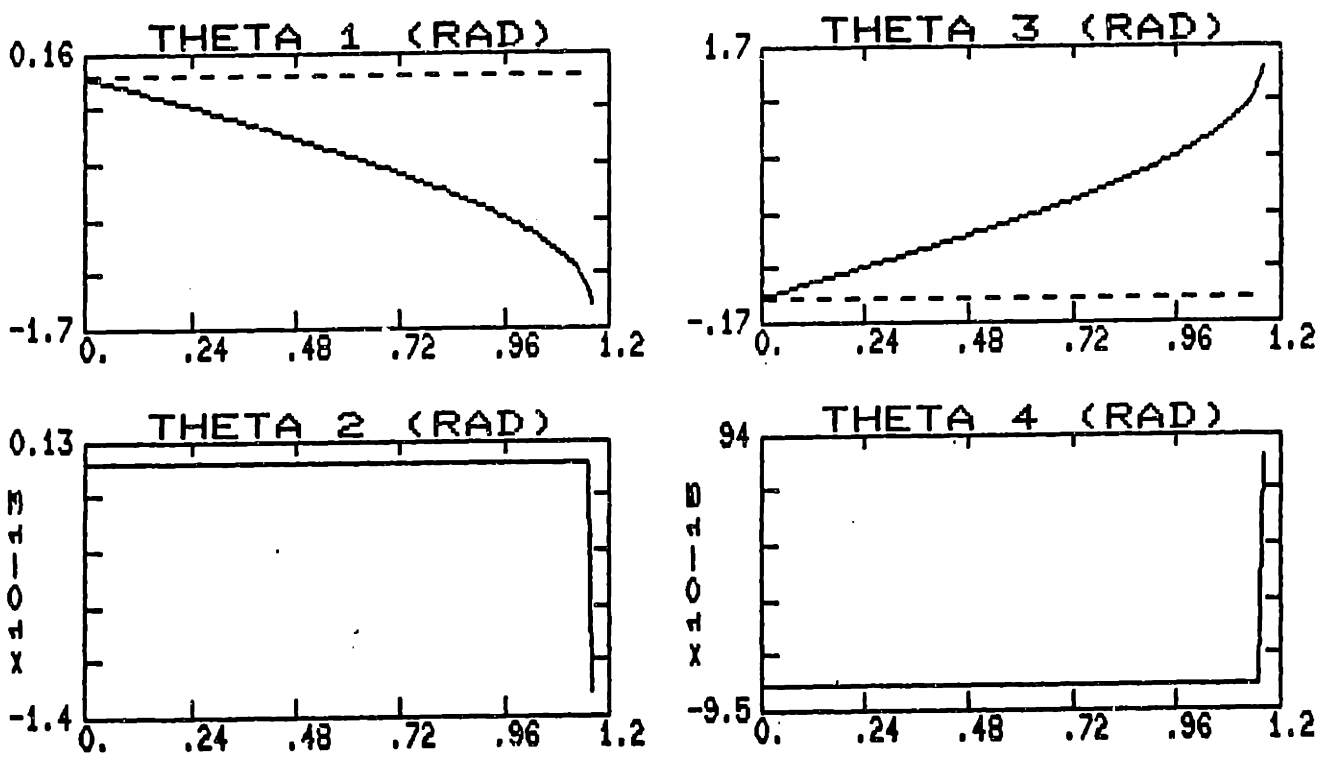

Figure 5-5. Gimbal Angles For Gradient Method (Part 2 of 2)

The Moore-Penrose pseudoinverse is actually seen in this case to directly generate a gimbal angle trajectory of locally extreme m when commanding momentum to increase from zero along the X-axis (as shown in this example). This illustrates a general defect of locally-optimal procedures which was mentioned previously; they tend to lock into trajectories of locally maximum gain which can actually lead into singular configurations.

To overcome this shortcoming, another form of the gradient was tried, where the null-on-gradient projection was replaced by its sign. This is given by:

$$\lambda = \frac{sign\left(\nabla_{\underline{\theta}} m \bullet \underline{v} \right) \left| \nabla_{\underline{\theta}} m \bullet J^T (J J^T)^{-1} \underline{\tau} \right|}{m^2} \qquad (5\text{-}10)$$

Simulation results for this approach are shown in Figure 5-6. It is seen that the singularity is still not avoided. At the end of the simulation, the system is actually trapped in a near-singular configuration about the Elliptic singularity; it does not attain the exact singular configuration, as seen from the very small (but still finite) value of m. The null-constant in this case is almost always non-zero and the null projection onto the gradient also becomes substantially non-zero, indicating that a different gimbal angle trajectory was generated here than the previous gradient method. In this case, the null motion (with magnitude now governed by the torque projection and singularity measure) is added increasingly to the solution as the torque request pushes the system toward the singular state. Looking at the gimbal angle trajectories, it is seen that gimbal #2 moves about 15° during the period when the null-projection is non-zero; however this is not sufficient to avoid the singular state, and it is pulled back again again by the torque request. The gimbal angle plots for this example also illustrate how gimbal

#4 has to correspondingly move in order to balance off-axis torques and "unlock" gimbal #2.

5.4.2.2 Inverse Gain Method

The previous examples indicated that dynamically manipulating the direction of null motion to instantaneously maximize controllability has been ineffective in avoiding singularities. This is due to the tendency of tangent-based methods to lock onto locally optimal gimbal angle trajectories that can lead toward singularities, as stated earlier. Based on this observation, a non-directional approach to singularity avoidance was tried, where the direction of added null motion was not specified. null motion was introduced in whatever direction the positive null-vector pointed; no sign factor was imposed. This was accomplished by choosing the weighting factor to include only a contribution inversely proportional to the sixth power of the singularity measure:

$$\lambda = \frac{1}{m^6}$$

The reason for this choice is detailed in the following argument. It was shown in Chapter 4 that the null-vector, $\underline{v}$ can be written as:

$$\underline{v} = m\hat{v}$$

where $\hat{v}$ is the unit vector in the direction of the null-vector. As discussed for the gradient method, the magnitude of the null vector is cancelled by dividing it with m . null motion is thus added in the positive null direction, and the amount is proportional to $\frac{1}{m^5}$. Although this approach has the advantage that it does not constrain null motion to always increase the singularity measure (this can avoid local optimum lockup, as

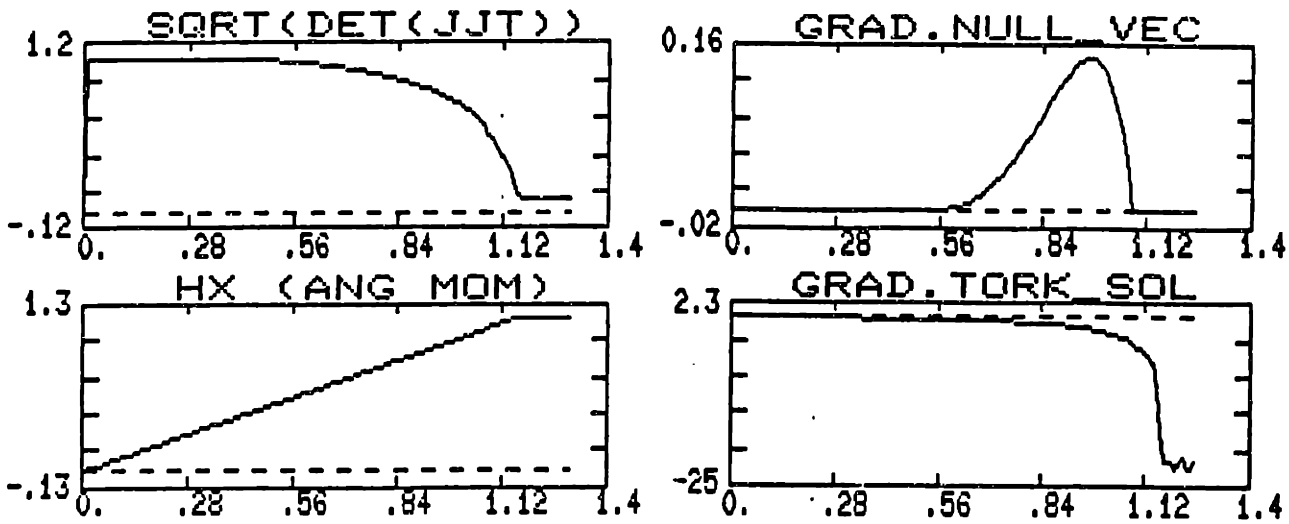

Figure 5-6. Simulation Results For Second Gradient Method (Part 1 of 2)

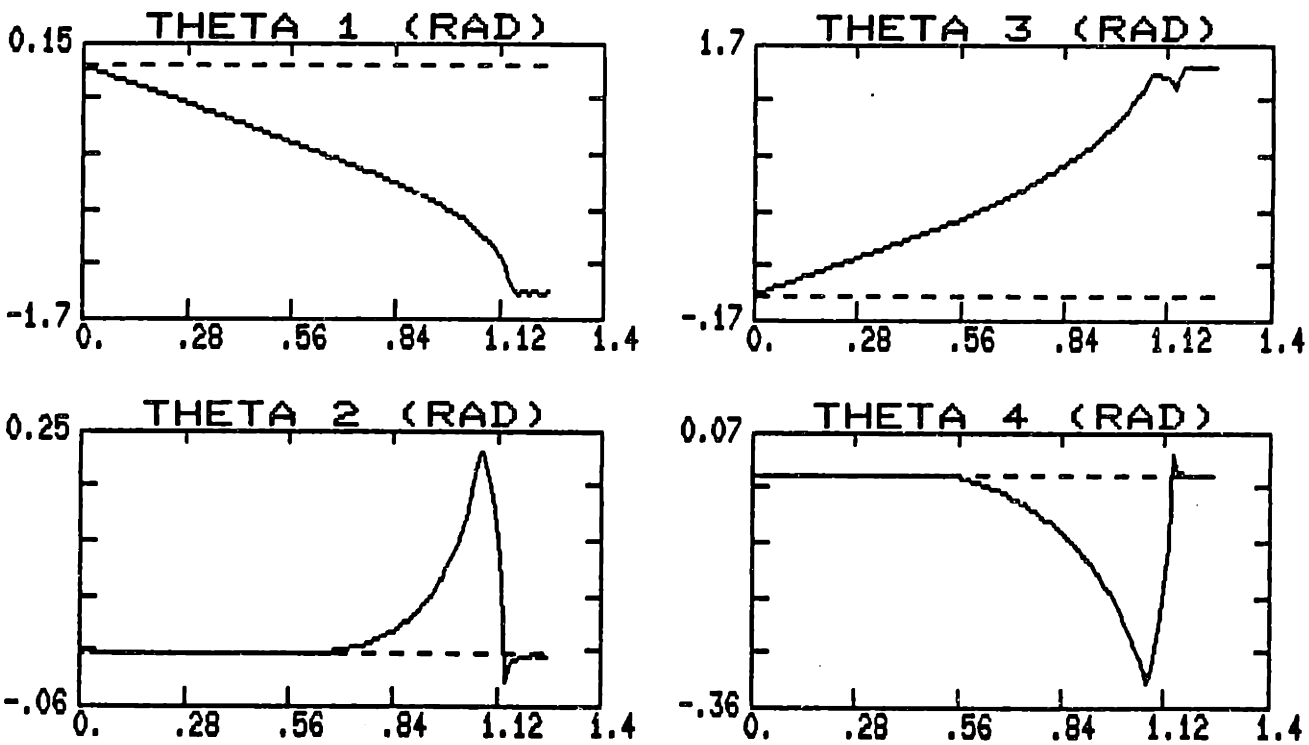

Figure 5-6. Gimbal Angles For Second Gradient Method (Part 2 of 2)

encountered in the gradient method), this approach has two potential shortcomings. These are:

a) null motion is added without regard to whether the performance index can be instantaneously affected by null motion. The indicator for this situation is:

$$\nabla_\theta m \cdot \underline{v} = 0$$

Even though null motion may not instantaneously increase the singularity measure (as dictated by the above situation), null rates of arbitrary magnitude may still be calculated and added to the solution.

b) Since the direction of null motion is not prescribed, it may actually decrease the magnitude of the singularity measure; thus inadvertantly steering towards a singularity.

From simulations using different exponents on m, it was noticed that increasing the exponent in the control law tended to increase the minimum value of m encountered during the simulation, thus reducing peak torque producing gimbal rates. This can be explained by the fact that increasing the exponent "flattens out" the m trajectory when $m < 1$. The effect is to anticipate the singularity earlier than with the control laws using smaller exponents; the net amount of null motion is thus also greater and begins to be introduced at an earlier time.

Simulation results applying the inverse gain method are shown in Figures 5-7 through 5-9. The magnitude of the null-constant was limited to 15. Looking at the plots of H_x and m in Figure 5-7, this method is evidently seen to avoid the singularity.

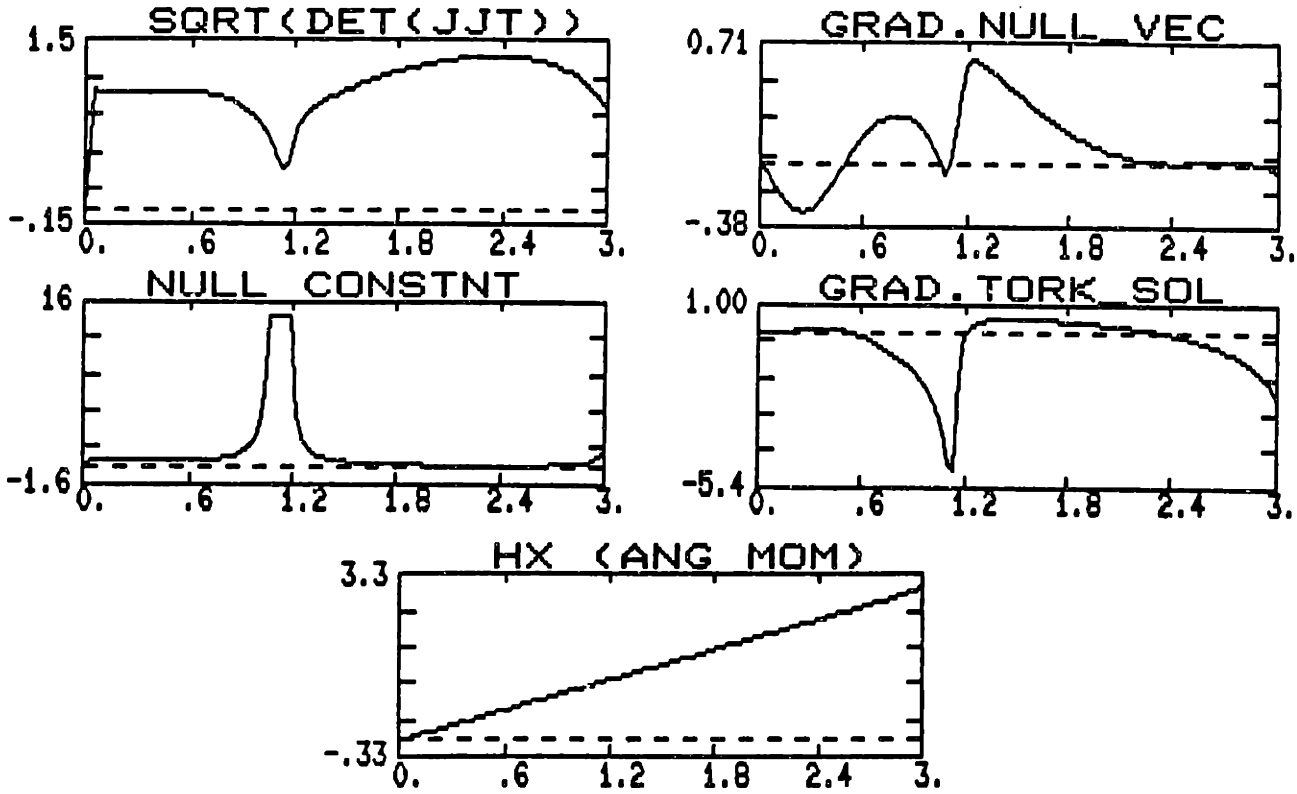

Figure 5-7. Simulation Results For Inverse Gain Method (Part 1 of 2)

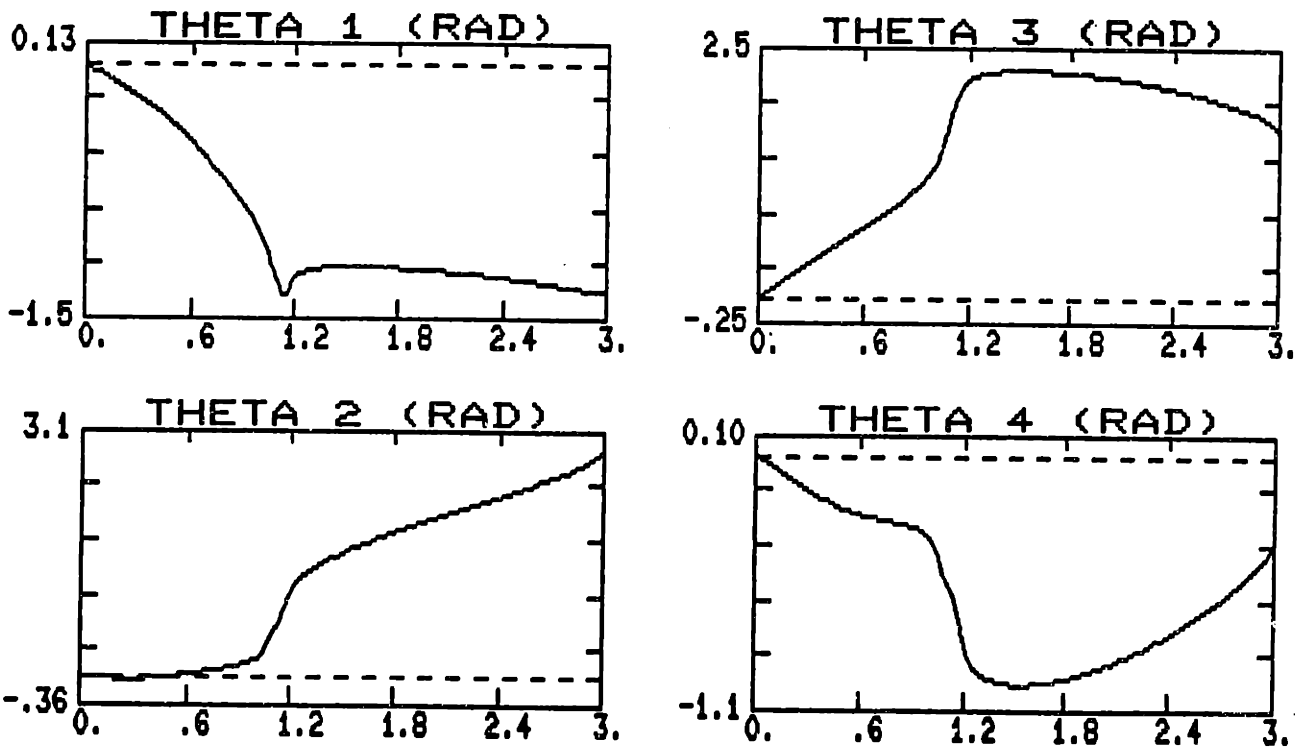

Figure 5-7. Gimbal Angles For Inverse Gain Method (Part 2 of 2)

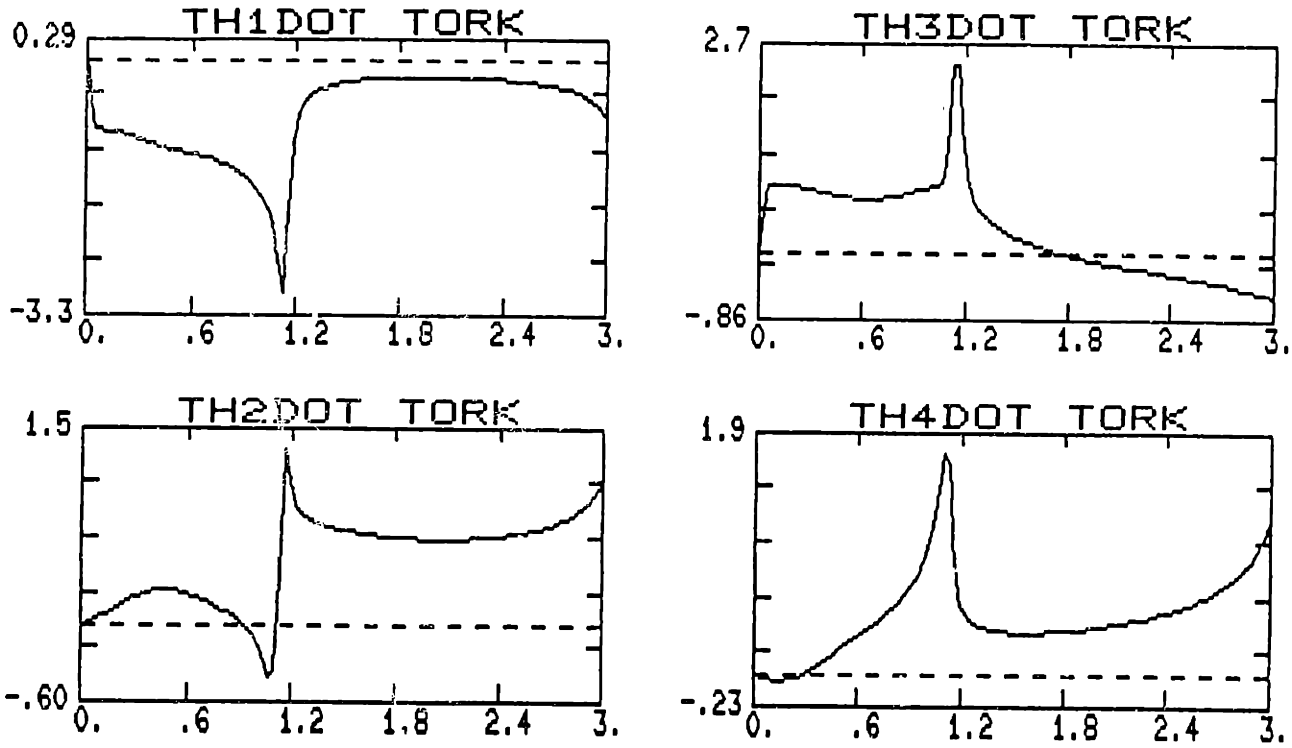

Figure 5-8. Torque Producing Gimbal Rates For Inverse Gain Method (Rad/Sec) (Part 1 of 2)

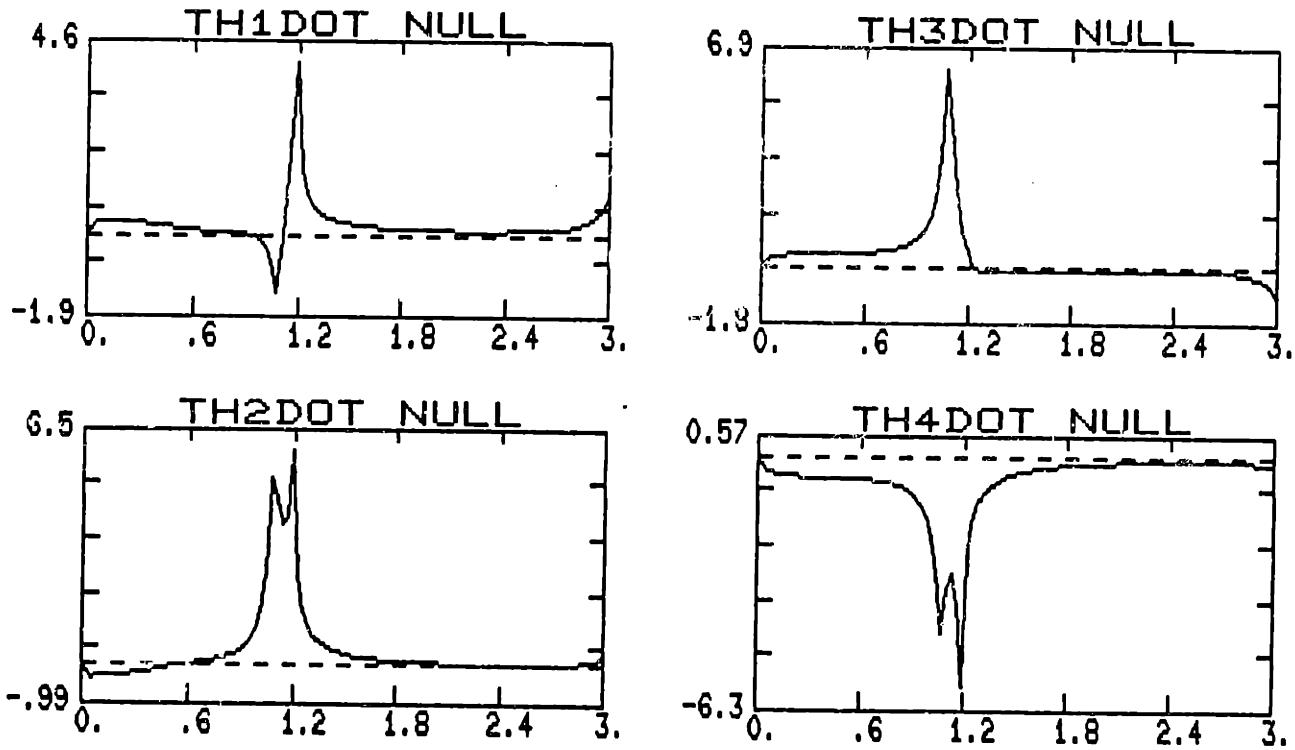

Figure 5-8. Null Gimbal Rates For Inverse Gain Method (Rad/Sec) (Part 2 of 2)

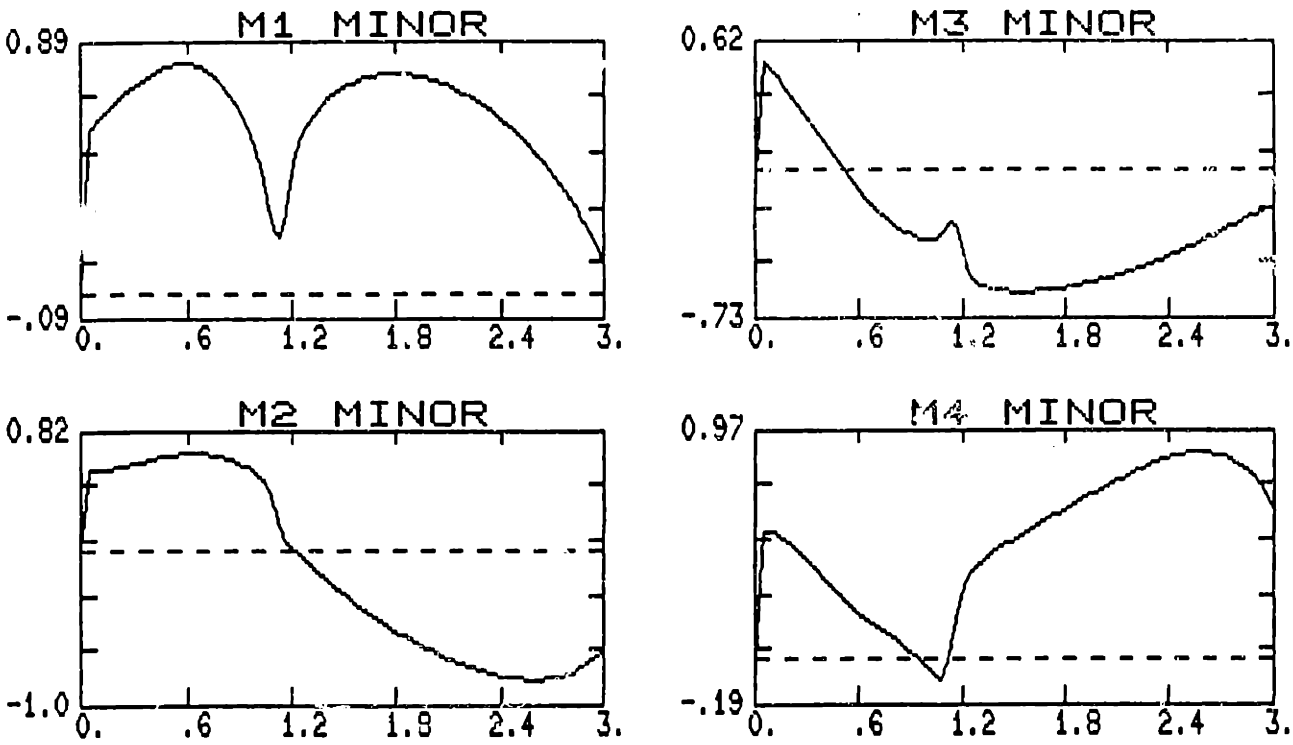

Figure 5-9. Jacobian Minors For Inverse Gain Method

The measure m is seen to dip somewhat as the singularity is approached, but definitely remains non-zero; H_x is seen to continuously increase until the end of the simulation. The reason for singularity avoidance may indeed be that this method does not constrain null motion to always increase the singularity measure, thereby allowing the gimbal angle trajectory to depart from local m-extrema, as seen from the non-zero values of the null projection encountered during the simulation. The effect of the torque and null projections on the singularity measure is clearly seen in the corresponding plots; for $t < 0.6$ *sec.* , the torque solution increases the system gain, whereas the null projection decreases it. This is clearly evident in the slight dip in the plot of singularity measure over this time period. It is also seen that the null projection is very small near the singularity, and actually remains at zero near the end of the run (after about 2.4 *sec.*), when m has reached its maximum. A physical interpretation of this maximum m, in terms of the mechanical analog, suggests that the linkage may not be instantaneously

reconfigured by null motion to a locally larger value of m; this determines the local extrema of the singularity measure (in the absence of a torque request), hence yields a zero gradient projection on the null-vector From the gimbal angle plots, it is seen that gimbal #2 is eventually rotated completely towards the the torque direction. Gimbal #4 also moves to compensate for the off-axis torque errors introduced by the motion of gimbal #2 while it is being reconfigured from the "hung-up" negative projection orientation.

In Figure 5-8, both the torque and non-torque producing gimbal rates are shown. Large spikes are evident in both rates near the singularity. The largest magnitude of the applied null motion occurs at these spikes, where the null-projection is very small, thus rendering these motions ineffective in affecting the singularity measure. These large null-rates are due to the correspondingly large value of the null constant and small (but non-zero) valued minors that generate these motions. From the minor plots presented in Figure 5-9, it is clearly seen that the singularity is avoided, since only minors #2 and #4 approach zero near $t = 1.15\ sec.$ Due to the large gimbal rates, this method cannot be considered a viable candidate for a Steering law.

Because of the substantial null motion projection onto the m-gradient seen in Figure 5-7, it is seen that the gimbal angle trajectory generated by this approach is not locally m-extreme. In addition, as noted above, this method added most of the null motion when the system was already nearly singular. In order to properly avoid the singular state, it would have probably been desirable to add null motion earlier in the trajectory, when $m > 1$ and the system was far-removed from problematic orientations. A second form of the inverse gain was thus formulated to accomplish this

strategy. The weighting factor is now chosen to also provide substantial null motion at high-m configurations:

$$\lambda = \begin{cases} m^6 & \text{if } m > 1 \\ \dfrac{1}{m^6} & \text{if } m < 1 \end{cases} \tag{5-11}$$

Simulation results using this "second inverse gain method" are shown in Figures 5-10 through 5-12. The magnitude of the null-constant was limited to $\lambda_{max} = 3$. From Figure 5-10, it is seen that this method is able to avoid the singularity. Comparing Figure 5-10 to Figure 5-7 , it is seen that the singularity measure has a larger magnitude throughout the simulation for this updated method, implying a wider margin of singularity avoidance, hence smaller torque producing gimbal rates. The null projection appears very different for this method, which indicates that a different gimbal trajectory was generated. This is evident by looking at the corresponding gimbal angle plots, where it is obvious that gimbals #1 and #3 followed markedly different trajectories than encountered in the previous test (Figure 5-7). Because the singularity was better avoided, gimbal #2 is seen to have a much smoother trajectory.

Both the torque and non-torque producing gimbal rates are shown in Figure 5-11. Comparing these plots with those in Figure 5-8, it is clearly evident that the gimbal rates generated by the second form are much smaller than those from the first form. Most importantly, no spikes are apparent in the gimbal rates calculated using the second method. Looking at the null rates, it is seen that they no longer peak at large values near the singularity. These rates are less than half as large as the corresponding null rates calculated by the first form. From the minor plots presented in Figure 5-12,

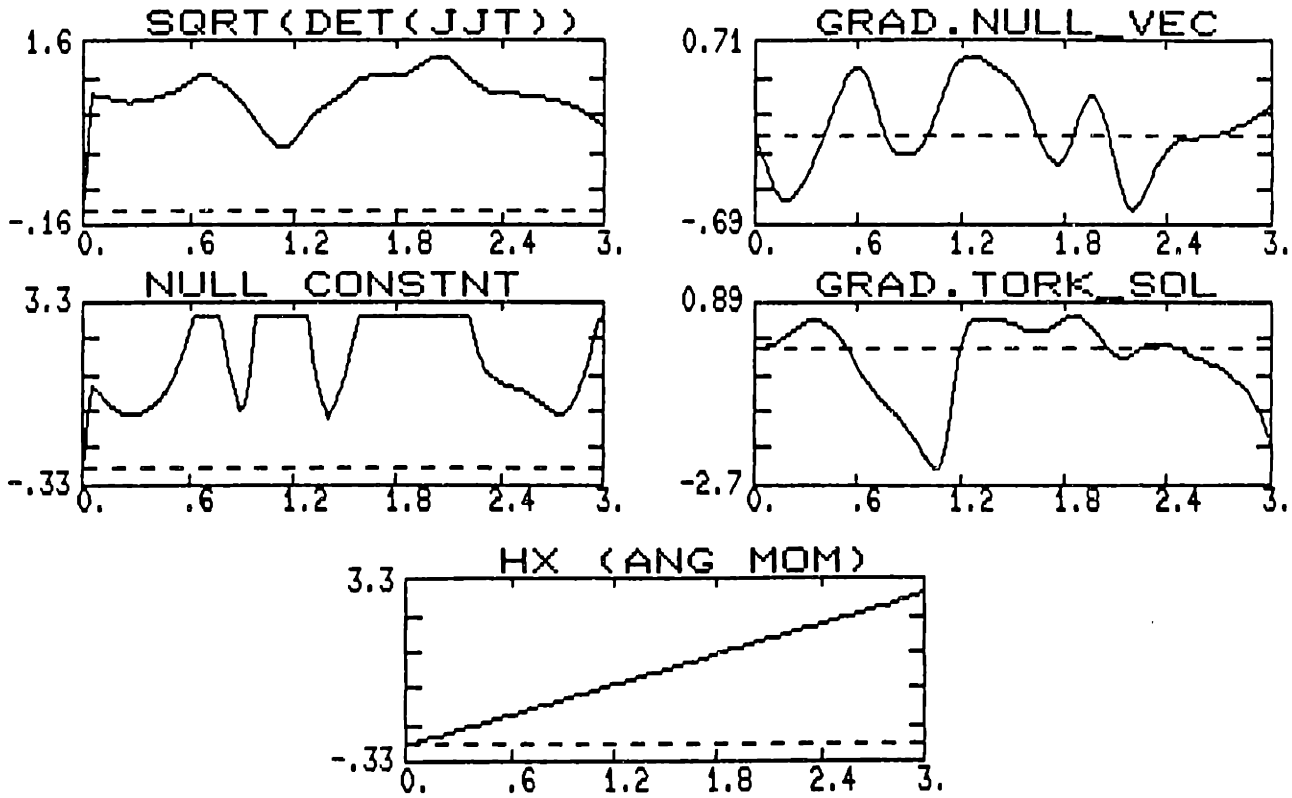

Figure 5-10. Simulation Results For Second Inverse Gain Method (Part 1 of 2)

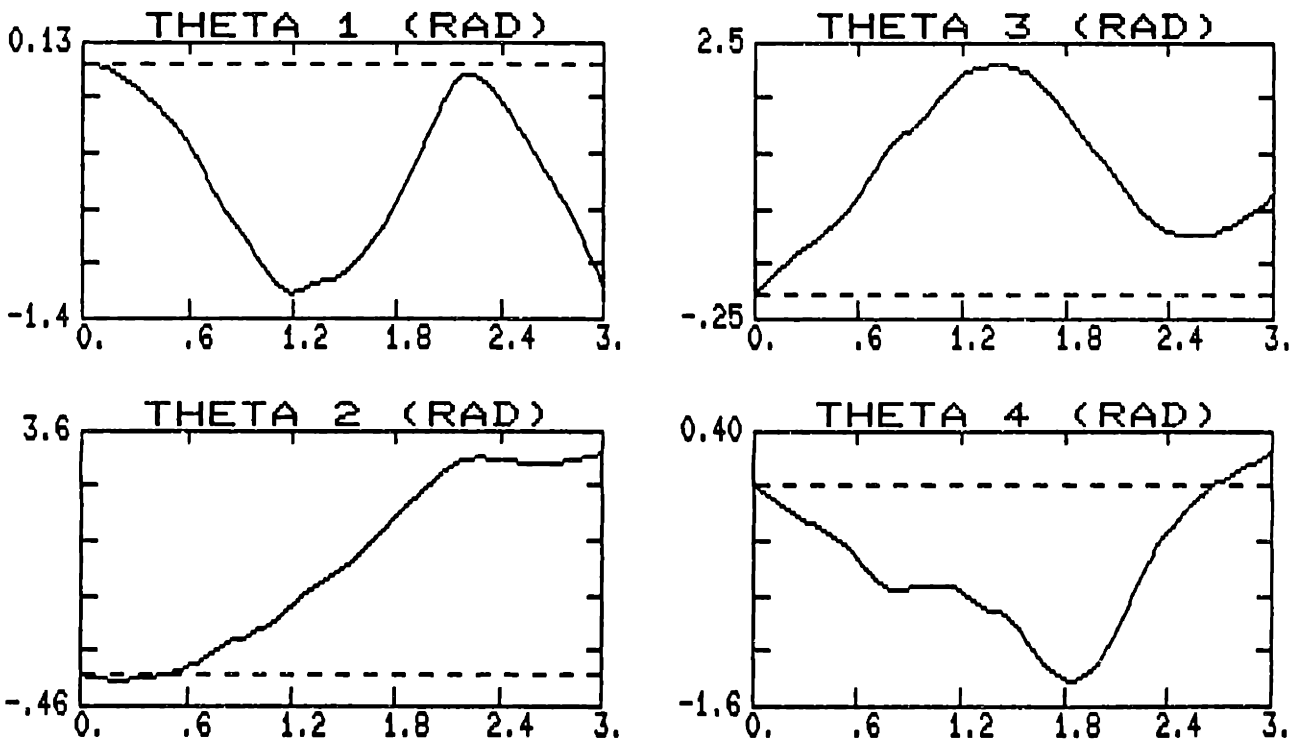

Figure 5-10, Gimbal Angles For Second Inverse Gain Method (Part 2 of 2)

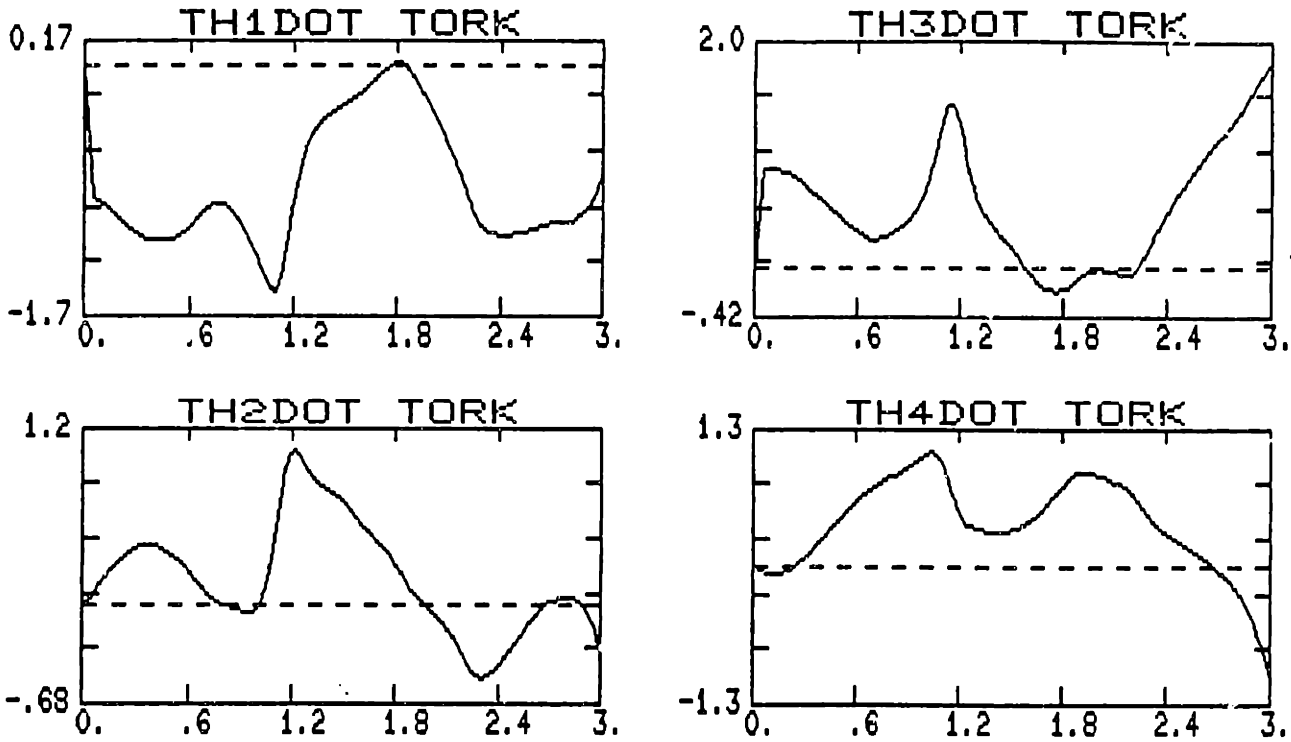

Figure 5-11. Torque Producing Gimbal Rates For Second Inverse Gain Method (Rad/Sec) (Part 1 of 2)

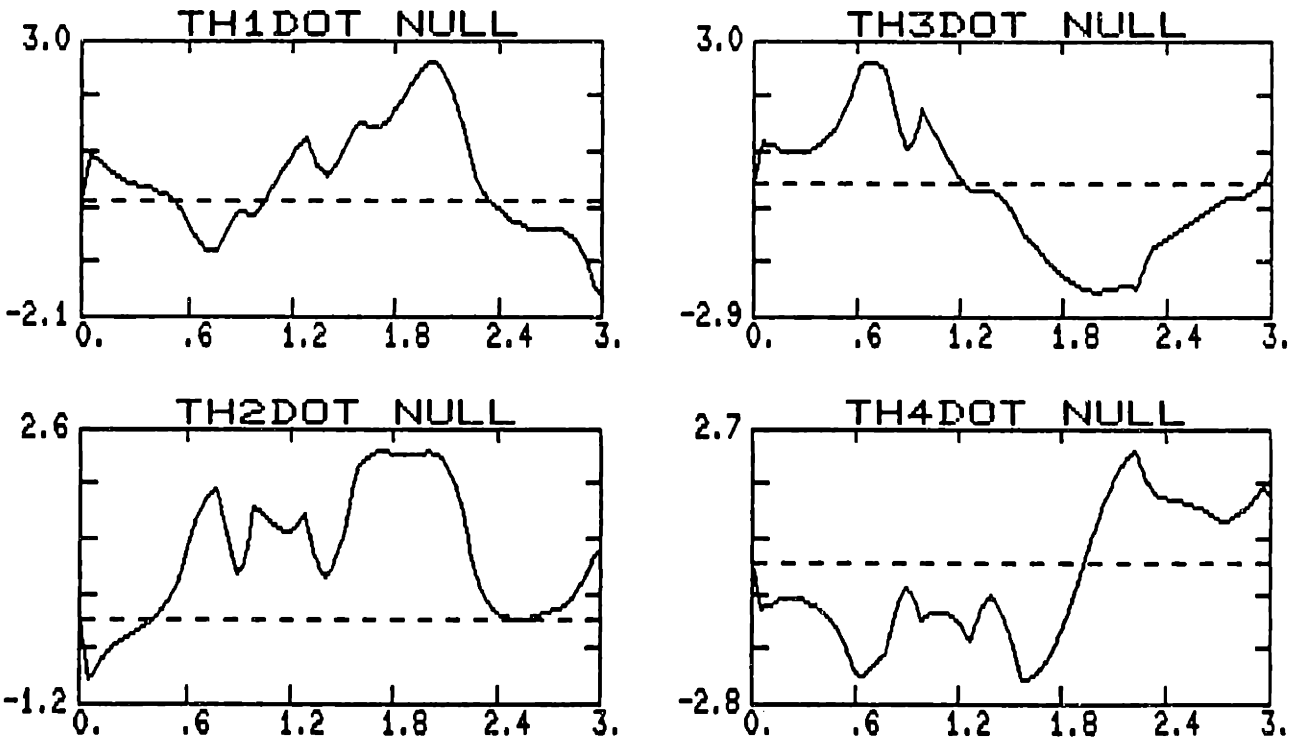

Figure 5-11. Null Gimbal Rates For Second Inverse Gain Method (Rad/Sec) (Part 2 of 2)

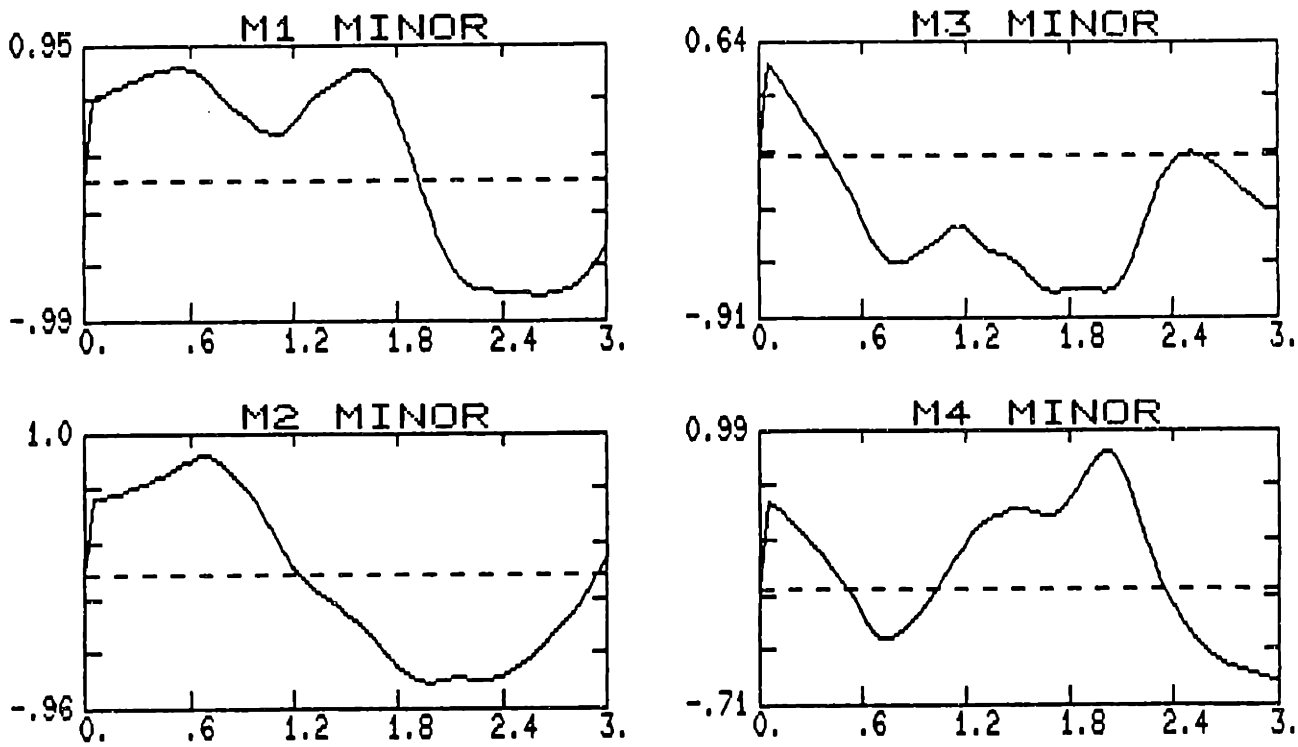

Figure 5-12. Jacobian Minors For Second Inverse Gain Method

it seen that only minor #2 is zero at $t = 1.15$ *sec.* Comparing this figure to Figure 5-9, the differences in the two plots are clearly seen. It is readily noted that two minors were zero near the sigularity for the first form, whereas only one minor was zero for the second form, again implying a much wider avoidance of the singularity.

5.4.3 Non-Constant Torque Request With Second Inverse Gain Method

To illustrate the adverse property of the inverse gain method (i.e. the arbitrary direction of null motion may actually steer the system toward a singularity), a non-constant torque request was used. The torque trajectory was defined such that the momentum trajectory shown in Figure 5-13 was followed with unit torque magnitude. In terms of the mechanical analog, the end effector moved along the prescribed path with unit velocity.

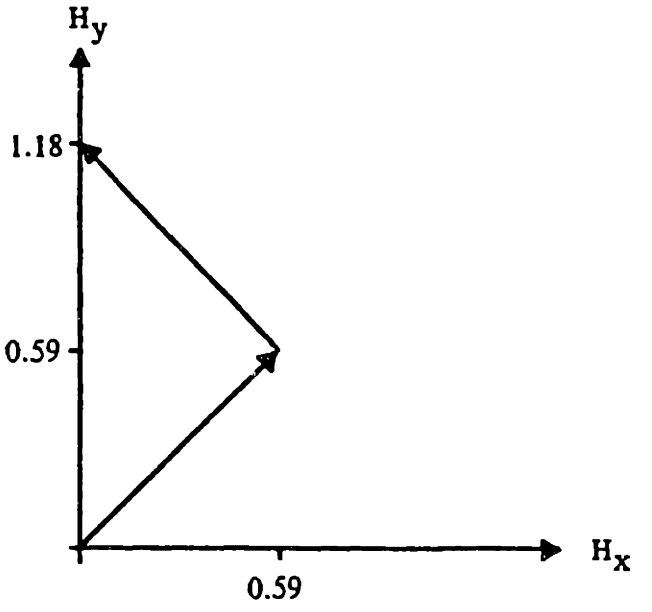

Figure 5-13. Momentum Trajectory For Non-Constant Torque Simulation

To simulate this maneuver, the torque request was defined in the following manner:

$$\underline{\tau} = \begin{bmatrix} 0.7071 \\ 0.7071 \\ 0 \end{bmatrix} \quad \textit{for } t < 0.83 \textit{ sec.}$$

$$\underline{\tau} = \begin{bmatrix} -0.7071 \\ 0.7071 \\ 0 \end{bmatrix} \quad \textit{for } 0.83 \textit{ sec.} < t < 1.626 \textit{ sec.}$$

Simulation results for this maneuver are shown in Figures 5-14 through 5-16. The magnitude of the null-constant was limited to 3. From Figure 5-14, it is clearly seen that the system becomes singular just before the torque direction is switched (at $t = 0.83$ *sec.*). From this figure, it is observed that the null projection remained negative until the switch time was reached, thus the effect of adding null motion was to reduce the singularity measure. From the torque projection plot, we see that torque produc-

ing gimbal motion does not contribute appreciably to the singularity measure. A large spike at the switch time is also observed in the torque projection plot, indicating a loss of control along the commanded torque direction. The reduction in m now is almost entirely due to the addition of of null motion.

Gimbal angles are given in Figure 5-14, and both torque and non-torque producing gimbal rates are shown in Figure 5-15. Large spikes are evident in the torque producing rates at the switch time, as would be expected, since the system is nearly singular in the direction commanded after the switch. From the null motion plots, it is seen that the magnitude of the null motion is zero at the switch point, since all Jacobian minors are singular. This is clearly seen in Figure 5-16.

5.5 CONCLUSION

We have shown that the inverse gain method is able to avoid the Elliptic singularity. It has also been shown that the performance results of the second form of this method (which applies substantial null motion at high m states) are superior to the first form (which applies most null motion when the magnitude of m drops significantly). The calculated null-rates, however, are still high for the second form. This feature, when combined with the property that the non-directional applied null motion may actually steer the system to a singularity (as was demonstrated in the non-constant requested torque simulation), make this approach inappropriate for application as a generic Steering law.

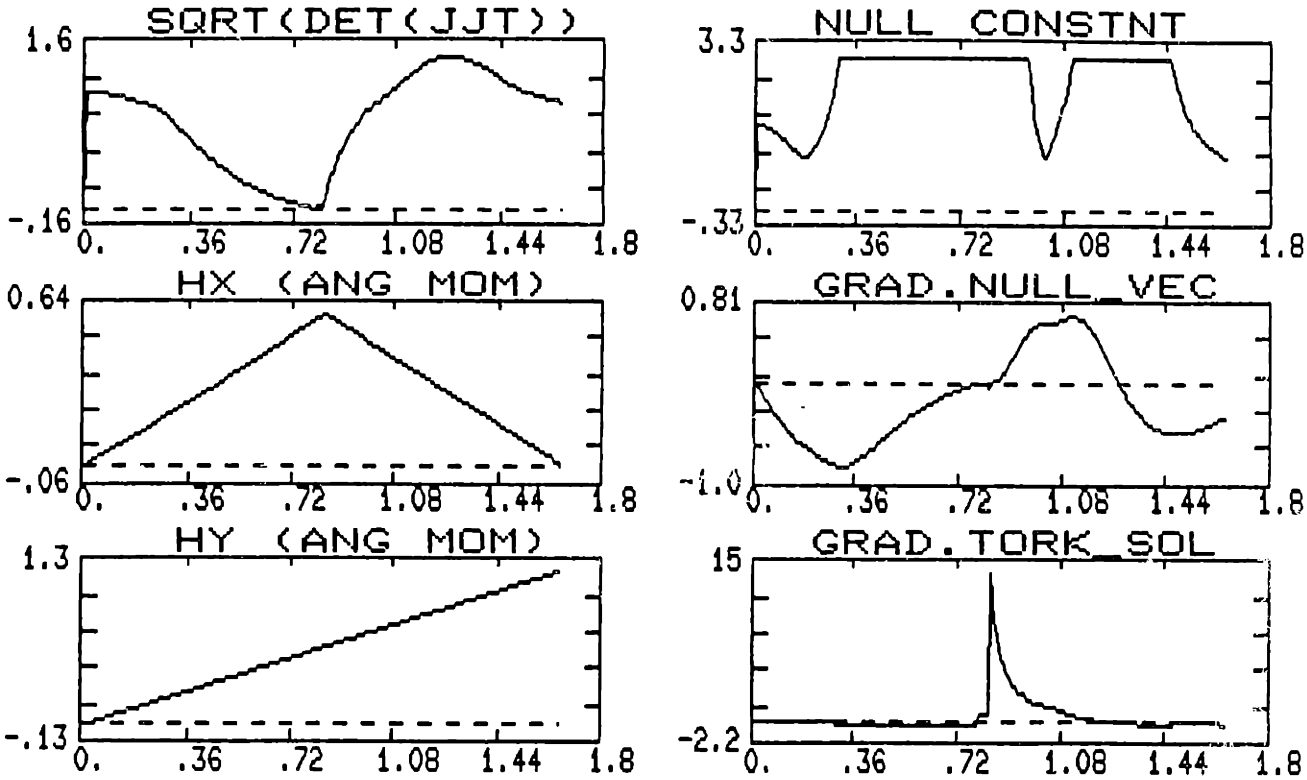

Figure 5-14. Non-Constant Torque Results For Second Inverse Gain Method (Part 1 of 2)

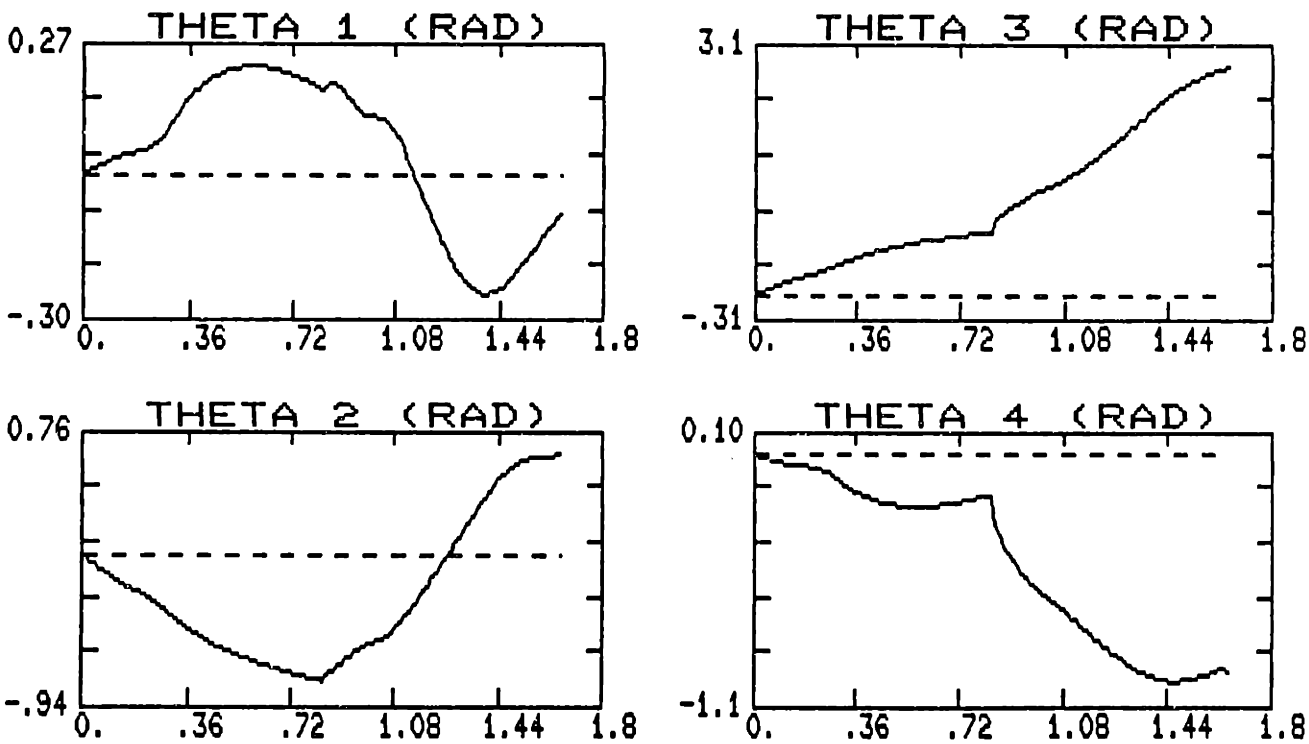

Figure 5-14. Gimbal Angles For Non-Constant Torque Request (Part 2 of 2)

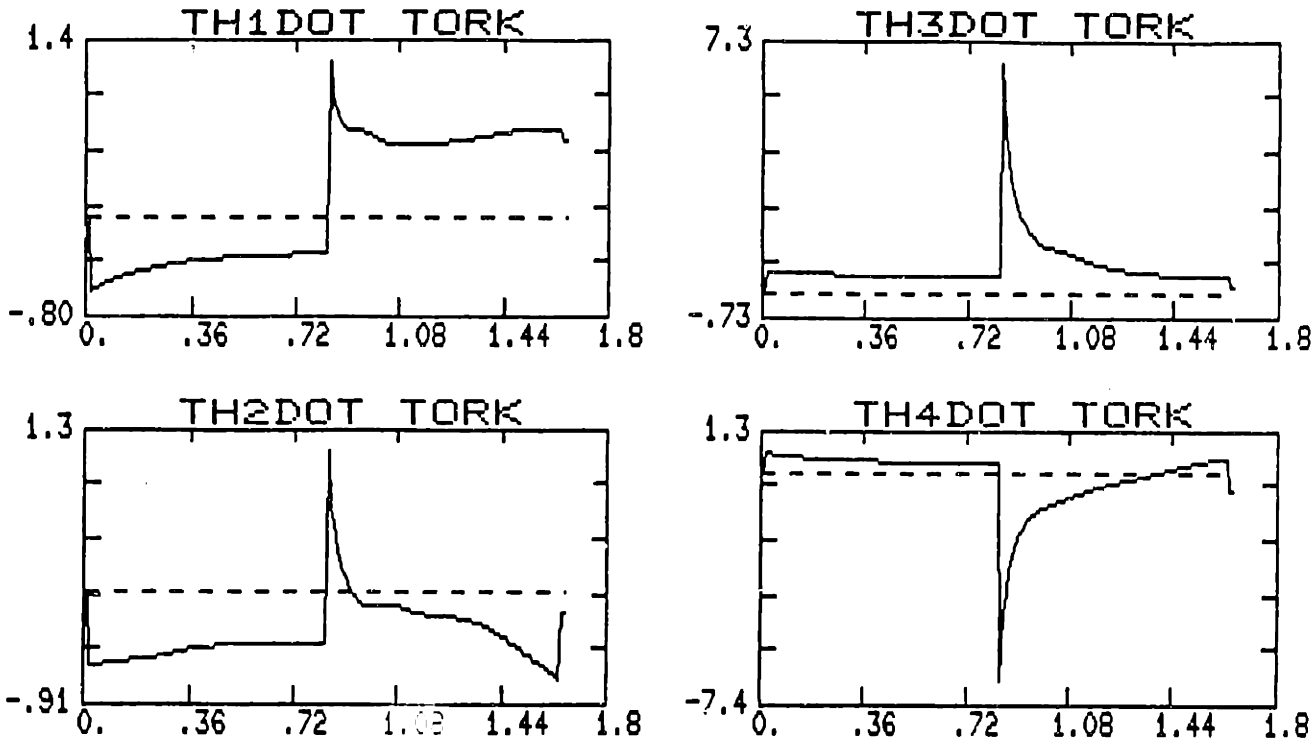

Figure 5-15. Torque Producing Gimbal Rates For Non-Constant Torque Request (Rad/Sec) (Part 1 of 2)

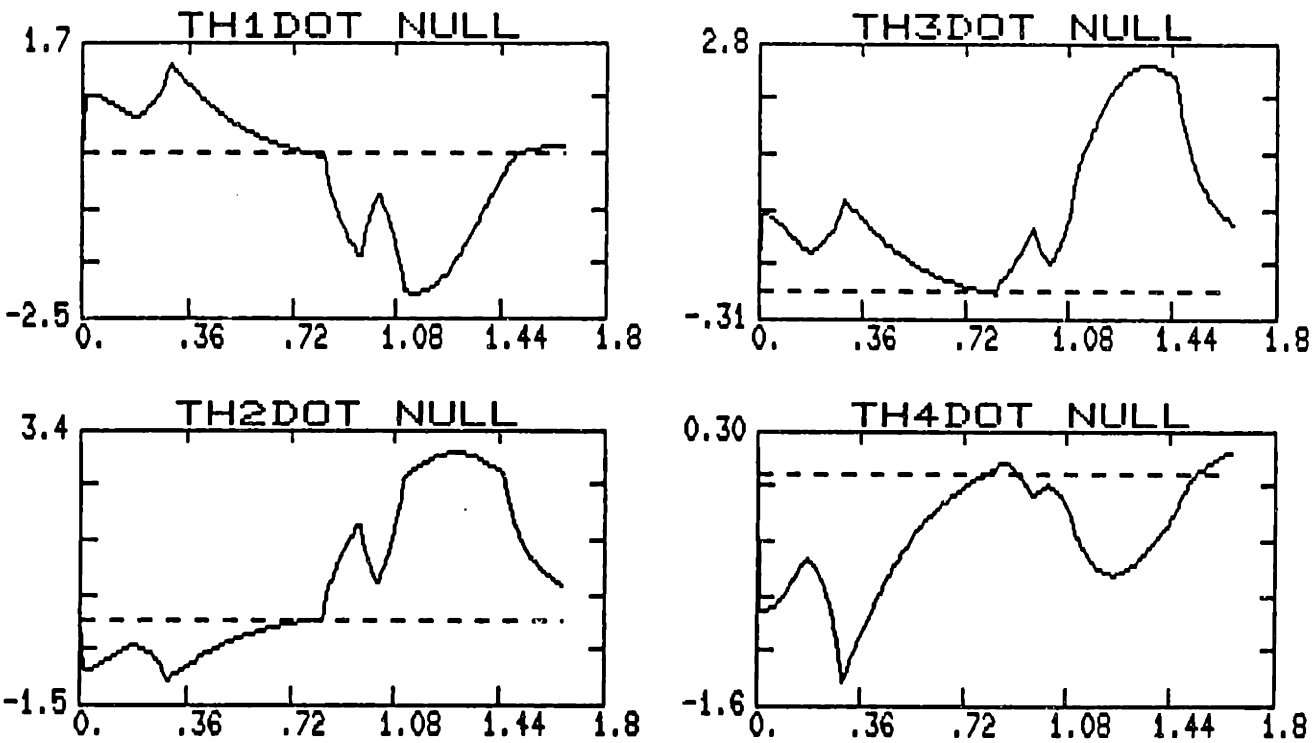

Figure 5-15. Null Gimbal Rates For Non-Constant Torque Request (Rad/Sec) (Part 2 of 2)

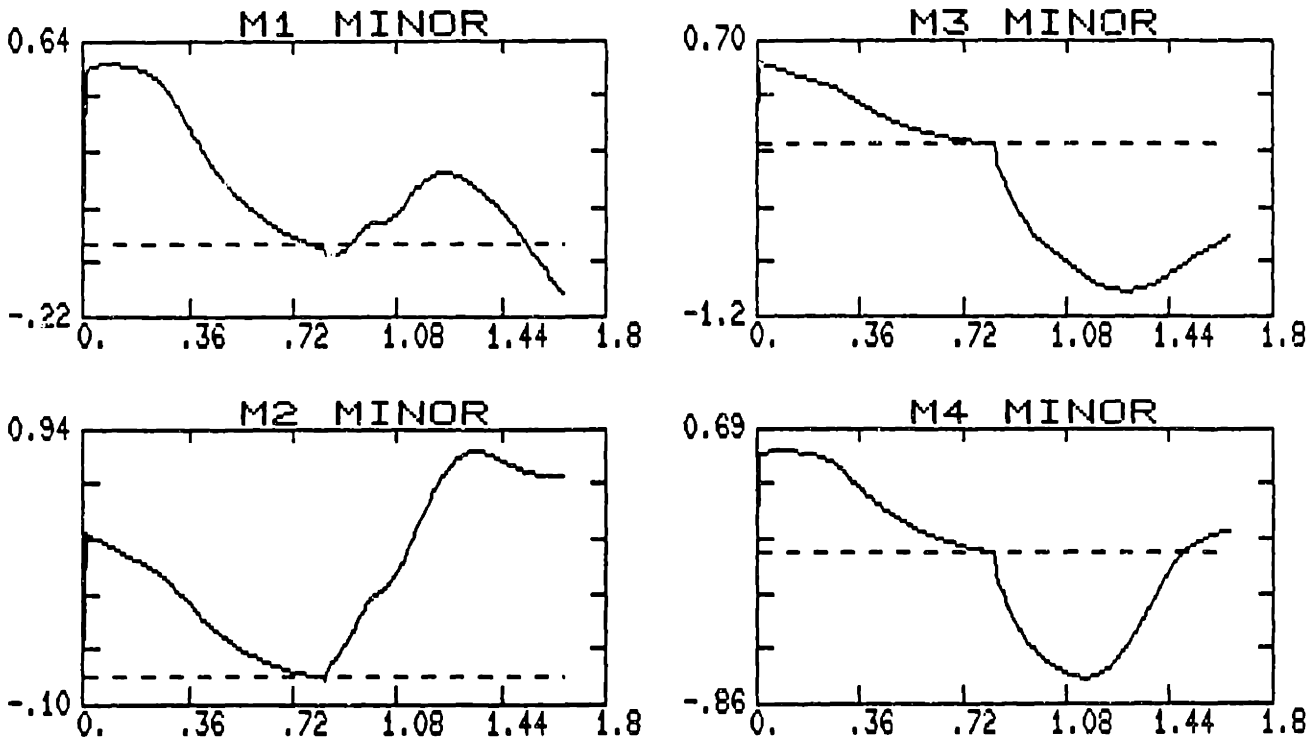

Figure 5-16. Jacobian Minors For Non-Constant Torque Request

CHAPTER 6

REDUNDANCY RESOLUTION VIA THE SINGULARITY ROBUST INVERSE (SR-INVERSE)

6.1 INTRODUCTION TO THE SR-INVERSE

The results of Chapter 5 indicated that real-time avoidance of internal Elliptic type singularities cannot be adequately accomplished using any of the available Steering laws or any of the proposed methods. It was seen that the torque solution produced by the Moore-Penrose pseudoinverse eventually drives or restricts the system to a singular configuration. Since solving the torque equation exactly was demonstrated to drive the system directly to a singularity, one might surmize that if small torque errors are allowed, it may become possible to avoid these types of singularities. This strategy presumes that the Outer controller (see Chapter 3) is structured to accomodate errors in requested torque during attitude maneuvers. These errors can be considered to be disturbance torques, and compensated through appropriate feedback.

One method of accomplishing this is provided by the Singularity Robust inverse (SR-inverse), proposed for manipulators in [21] as an alternative to the Moore-Penrose pseudoinverse. Using this method, an approximate output torque close to the desired torque can be generated, even when the Jacobian matrix is singular. Accuracy of solving the torque equation is traded with feasibility of the solution (i.e. gimbal rates remain finite and bounded in exchange for the build up of torque error near a singular configuration).

The SR-inverse is obtained by solving the following minimization problem:

$$\min \quad \frac{1}{2} \underline{e}^T W \underline{e}$$

$$\textit{where} \quad \underline{e} = \begin{bmatrix} \underline{\tau} - J\dot{\underline{\theta}} \\ \dot{\underline{\theta}} \end{bmatrix}$$

$$W = \begin{bmatrix} W_1 & [0] \\ [0] & W_2 \end{bmatrix}$$

Setting W_1 equal to the identity matrix, ($W_1 = \underline{1}$), and $W_2 = \kappa \underline{1}$, the SR-inverse is obtained:

$$J^{=} = J^T (J J^T + \kappa \underline{1})^{-1} \tag{6-1}$$

The particular solution can be written in terms of the SR-inverse as:

$$\dot{\underline{\theta}}_P = J^T (J J^T + \kappa \underline{1})^{-1} \underline{\tau} \tag{6-2}$$

6.2 PROPERTIES OF SR-INVERSE

The particular solution obtained using this method is still orthogonal to the homogeneous solution. This is easily shown by evaluating the inner product of the two solutions:

$$< \dot{\underline{\theta}}_P, \dot{\underline{\theta}}_H > \; = \dot{\underline{\theta}}_P^T \cdot \dot{\underline{\theta}}_H = \lambda (J J^T + \kappa \underline{1})^{-1} J \underline{v} = 0$$

The above relation holds, since $J \underline{v} = 0$ by definition of the null-vector. The robustness property of this method generates feasible solutions to the torque equation even at

or in the neighborhood of singular points. At singular points, the pseudoinverse becomes singular, (i.e. results in infinite rate solution), whereas the SR-inverse still returns a finite rate solution. It is seen that the pseudoinverse is identical to the SR-inverse with $\kappa = 0$. The scalar weighting factor κ expresses the tradeoff between exactness and feasibility of solution. For small values of κ, a small error is introduced in the torque solution. Small values of κ also yield large rate magnitudes in the neighborhood of singular states. As κ grows, however, the torque error calculated near a singular state increases and the calculated gimbal rates decline.

The SR-inverse approach, however, is not without shortcomings. The most crucial problem is that if the system does become singular using this method, and a torque is requested along the singular direction, the SR-inverse is unable to generate non-zero torque producing gimbal rates. The system could then be trapped in the singular state. This property is shown by the Singular Value Decomomposition of the SR-inverse, which for the 4-CMG system is:

$$J^{\#} = V \Sigma^{\#} U^T \tag{6-2}$$

where $\Sigma^{\#} = \begin{bmatrix} \frac{\sigma_1}{\sigma_1^2 + \kappa} & 0 & 0 \\ 0 & \frac{\sigma_2}{\sigma_2^2 + \kappa} & 0 \\ 0 & 0 & \frac{\sigma_3}{\sigma_3^2 + \kappa} \\ 0 & 0 & 0 \end{bmatrix}$

U = *Matrix* (3×3) *of left singular vectors* (*span range space of* J)

V = *Matrix* (4×4) *of right singular vectors* (*span domain space of* J)

Using (6-3), the particular solution (6-2) can be written as:

$$\dot{\underline{\theta}}_P = V \Sigma^{\#} U^T \underline{\tau} \tag{6-4}$$

If the torque request $\underline{\tau}$ lies along one of the column vectors of U, the gimbal rates computed by the SR-inverse are given by:

$$\dot{\underline{\theta}}_P = \frac{\sigma_i}{\sigma_i^2 + \kappa} \underline{v}_i \tag{6-5}$$

From (6-5), it is seen that if one of the singular values, σ_i, is zero (i.e. system is singular) and the torque request is along the left singular vector, $\underline{u}_i$, corresponding to this singular value, the output becomes zero. In this case, the gimbals will not move, thus trapping the system in the singular configuration. Unless this singularity allows escape by null motion (as discussed in Chapter 4), there is no possibility of removing the system from the singular configuration.

6.3 DETERMINATION OF WEIGHTING FACTOR

To overcome the problem of conflicting requirements on the value of the weighting factor, it is made to vary with the nearness to singularities. In this way, κ will have a large value near singularities, and small or zero value away from singularities. The weighting factor is thus chosen in the following manner:

$$
\begin{aligned}
&IF \quad m > m_{CR} \quad THEN \\
&\kappa = 0 \\
&ELSE \\
&\qquad IF \quad \frac{\kappa_0}{m} < \kappa_{max} \quad THEN \\
&\qquad \kappa = \frac{\kappa_0}{m} \\
&\qquad ELSE \\
&\qquad \kappa = \kappa_{max}
\end{aligned}
$$

$$
\begin{aligned}
where \quad m_{CR} &= Critical\ value\ of\ m \\
\kappa_0 &= Constant \\
\kappa_{max} &= Maximum\ value\ of\ weighting\ factor
\end{aligned}
$$

In this fashion, the weighting factor is adjusted according to distance from singularity by inversely scaling with the singularity measure. The reason for the applied maximum value is to prevent the determinant of the square Jacobian matrix ($J J^T + \kappa \underline{1}$) from becoming too large; in this case, the torque producing rates would correspondingly grow very small, which would require an extended period of time for the gimbal angles to change. By imposing an upper limit, the response of the system is essentially speeded-up.

6.4 SINGULARITY AVOIDANCE PROPERTIES OF SR-INVERSE

In order to examine the singularity avoidance properties of the SR-inverse, simulations similar to those in Chapter 5 have been carried out. The SR-inverse is computed numerically, using the symbolic inverse of the square Jacobian matrix. Results from four different simulations are presented in this section; these are:

a) **SR-Inverse**

b) **SR-Inverse With First Gradient Method**

c) **SR-Inverse With Second Gradient Method**

d) **SR-Inverse With Second Inverse Gain Method**

All simulations used the same parameters as given in Chpater 5. The critical value of the singularity measure was chosen as $m_{CR} = 1.0$, with constant $\kappa_0 = 0.1$. The plotted percent torque error is determined from the difference between requested input and CMG output torque, i.e.:

$$\%\ Torque\ Error\ = 100\,(\underline{\tau} - J\dot{\theta}_P)$$

where $\underline{\dot{\theta}}_P$ is determined from (6-2).

6.4.1 SR-Inverse

The results of this simulation are shown in Figure 6-2. The maximum allowed value of the weighting constant was $\kappa_{max} = 0.2$. The plots clearly show that the Elliptic singularity is not avoided. It is evident that even though $m \rightarrow 0$, the determinant of the square Jacobian matrix ($SQJ\ DET$) remains nonzero. This illustrates a fundamental property of the SR-inverse; gimbal rates can still be computed when the Jacobian matrix is singular. The value of κ ($SR\_INV\ GAIN$) is noted to increase as the singularity is approached in order to allow the square Jacobian matrix to be inverted (see (6-2)). From the gimbal angle plots, it is seen that gimbals #2 and #4 remain stationary, as was also the case for the Moore-Penrose pseudoinverse method. This result indicates that the SR-inverse similarly cannot avoid Elliptic type singularities without

assistance, essentially because the primary difference between the SR and the M-P inverse is in the magnitude of the particular solution. The "direction" is still the same (i.e. orthogonal to null-space), as illustrated in Figure 6-1, for a one-dimensional row and null space.

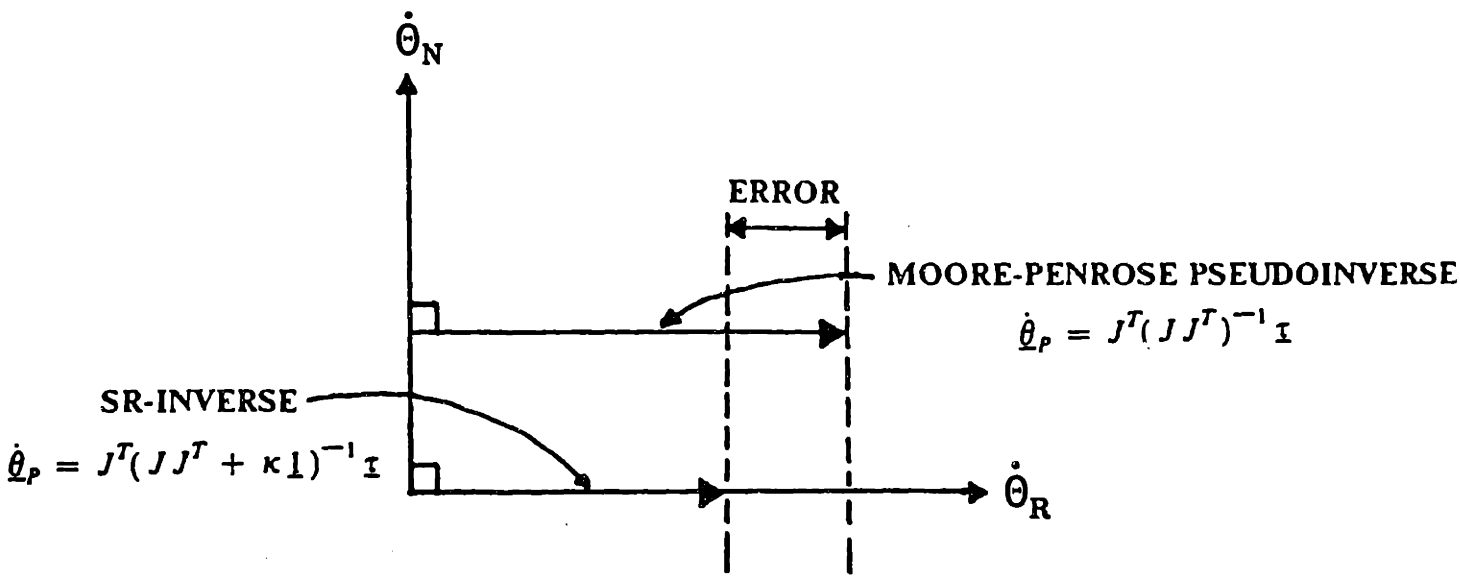

Figure 6-1. Solution Space Visualization

The complete torque equation solution is spanned by the row and null space. The SR-inverse as well as the M-P inverse solutions lie in the row space. From Figure 6-1, it is seen that the only difference between the two is the length (or magnitude) of the torque producing gimbal rates. Because the SR-inverse tends to produce smaller gimbal rates near singular regions, it allows more time for the application of null motion, thus introduction of null motion may prove more effective, as will be demonstrated below. Since the primary effect of the SR-inverse is along the direction of commanded torque,

the SR-inverse applied without null motion is indeed expected to have analogous singularity avoidance properties to the M-P inverse, as was demonstrated in Figure 6-2.

6.4.2 SR-Inverse With First Gradient Method

The simulation results for this method are shown in Figure 6-3. The weighting constant was limited at $\kappa_{max} = 0.2$. From Figure 6-3, it is seen that the singularity is again not avoided. The reason for this is the same as that given in Chapter 5 for the M-P inverse with this gradient method; essentially no null motion was added because the gimbal angle trajectory remained at a local *m*-extremum. From Figure 6-3 it is seen that gimbals #2 and #4 do not move, allowing the system to become singular at $H_x = 1.15$.

6.4.3 SR-Inverse With Second Gradient Method

Simulation results for this approach are shown in Figures 6-4 through 6-6 . The weighting factor was limited at $\kappa_{max} = 5$, although this limit was not neccessary in this case, since κ remained under 0.28, as can be seen from Figure 6-4. Since the singularity measure remains well above zero in this test, the singularity has been avoided. From the momentum component plots (*HX, HY, HZ*), it is seen that the momentum trajectory is diverted about the singularity, causing about 70% torque error in the *X*-direction, and considerably smaller errors about the *Y* and *Z* axes. The effect of null motion was to alter the Jacobian matrix, thus enabling the SR-inverse to generate finite off-axis torque errors that aided in skirting the singularity. Singularity avoidance is accomplished by not forcing the system to go directly through the singular momentum state.

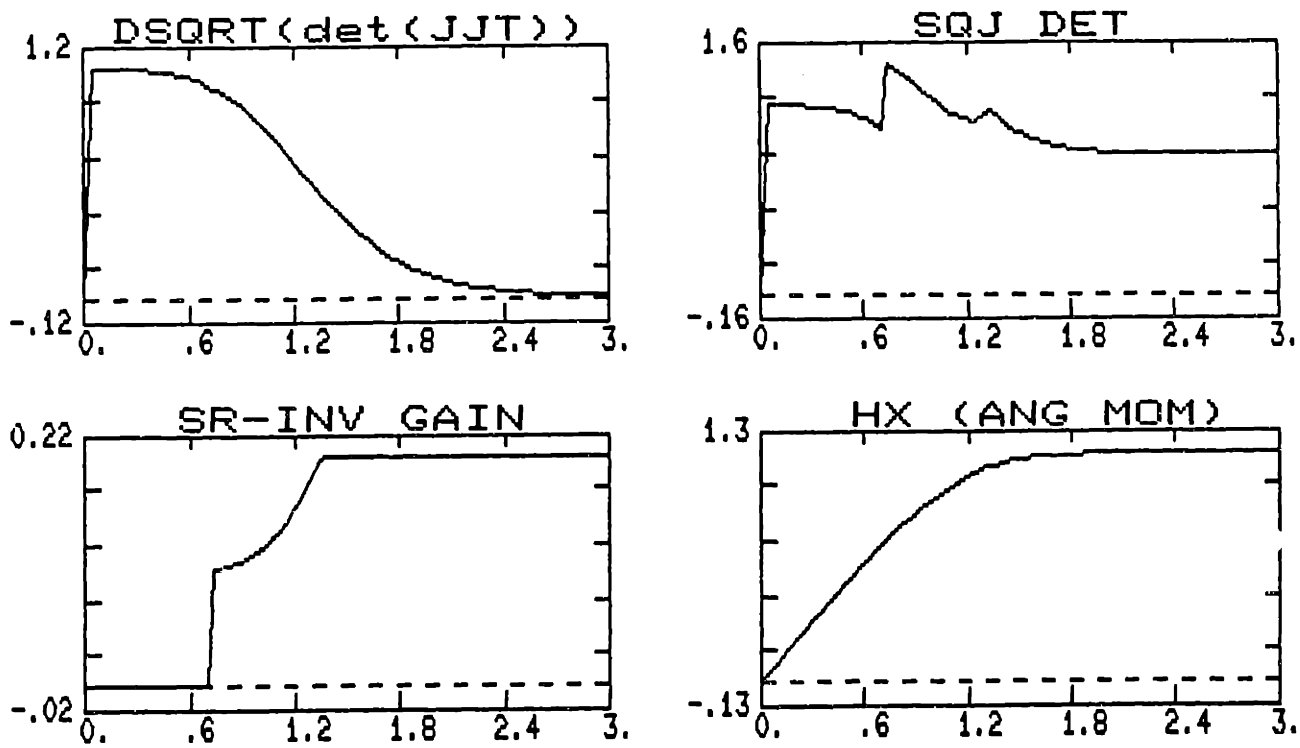

Figure 6-2. Simulation Results For SR-Inverse (Part 1 of 2)

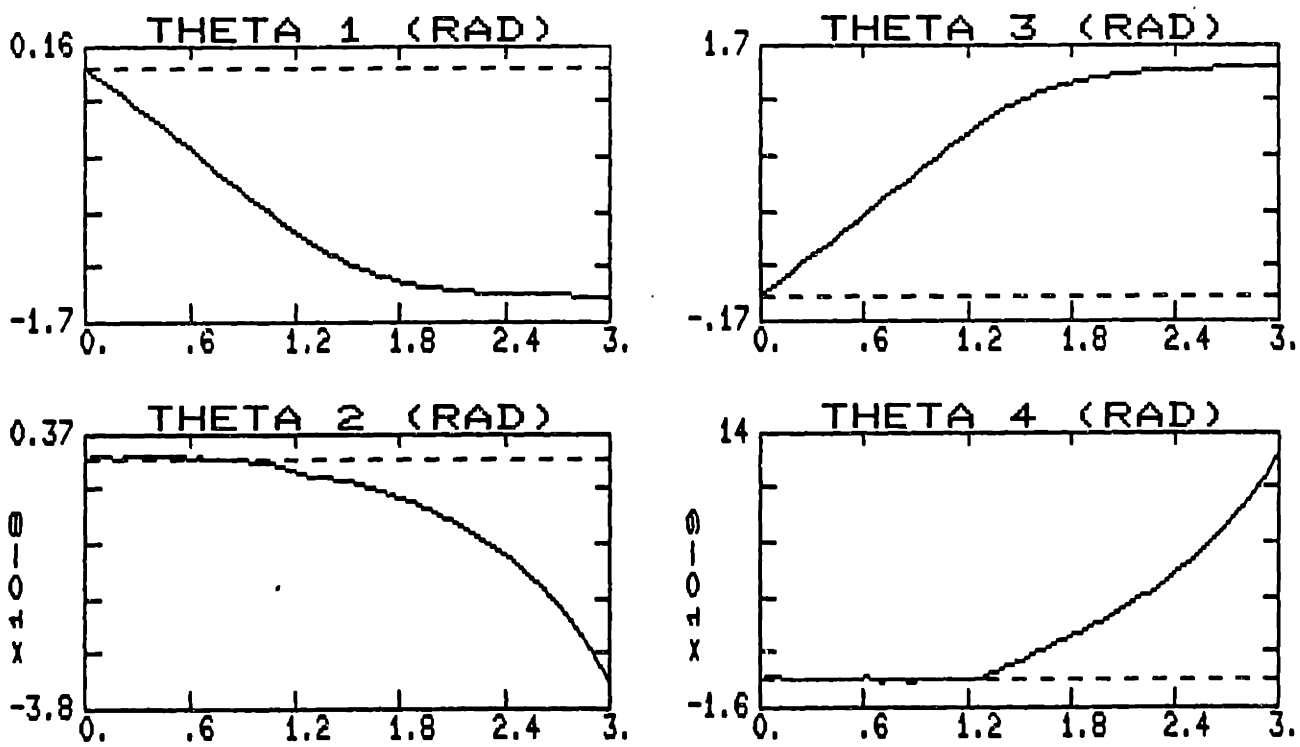

Figure 6-2. Gimbal Angles For SR-Inverse (Part 2 of 2)

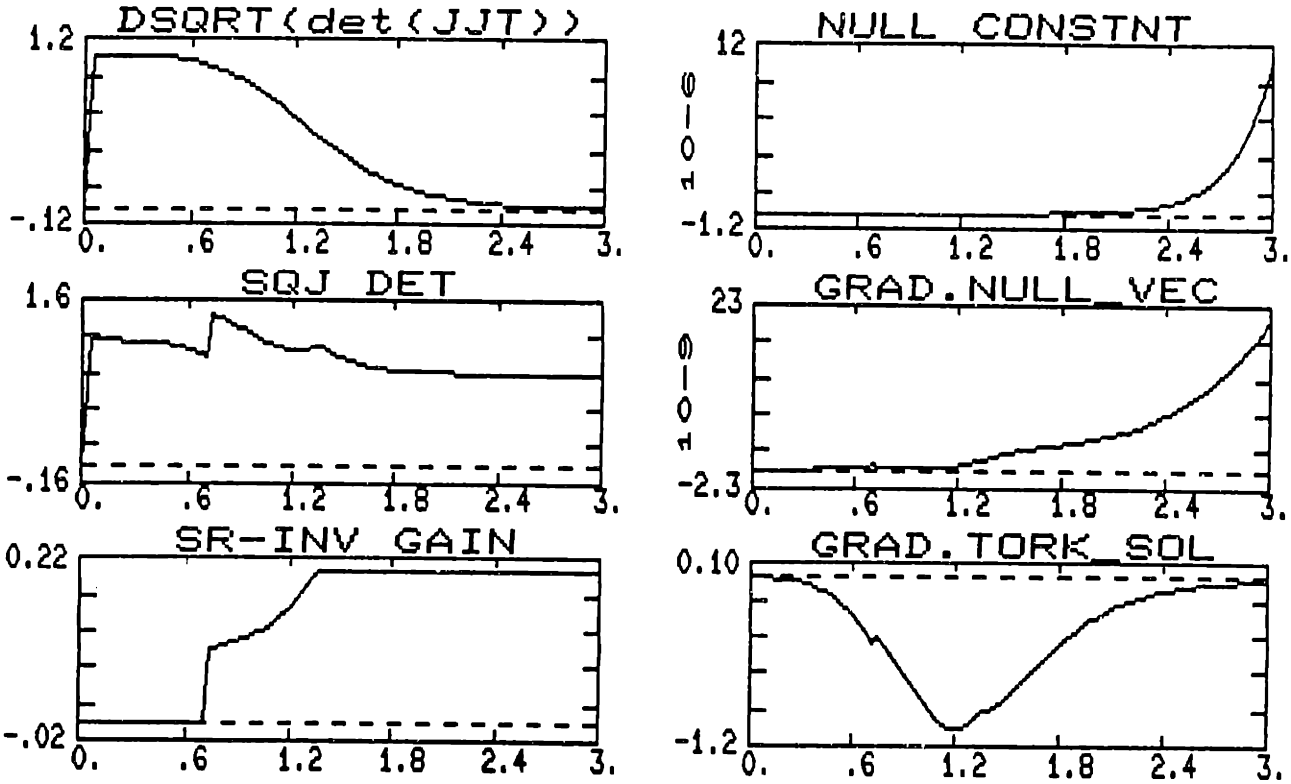

Figure 6-3. Simulation Results For SR-Inverse With First Gradient Method (Part 1 of 2)

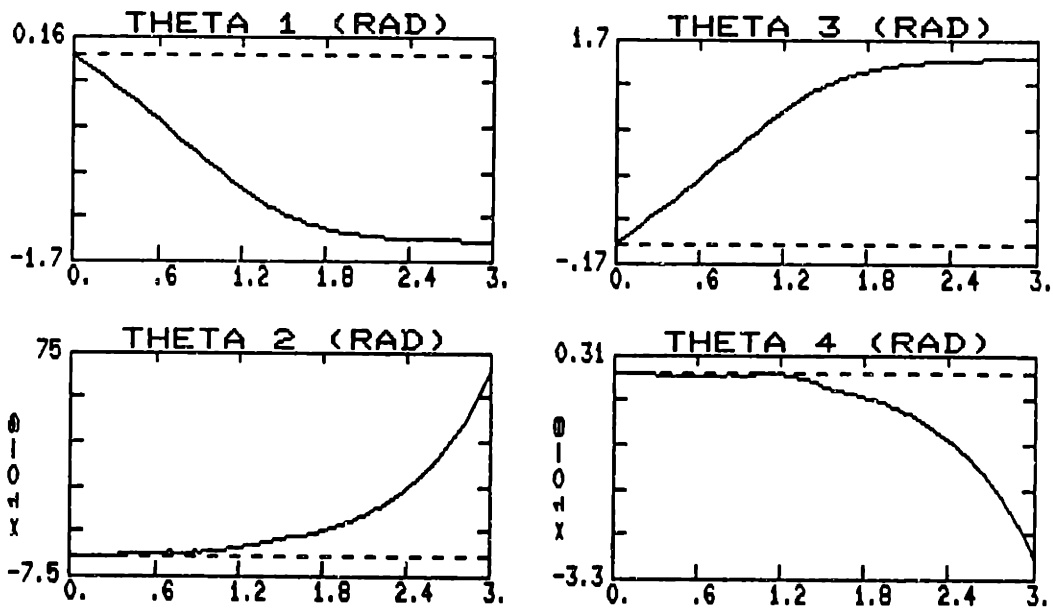

Figure 6-3. Gimbal Angles For SR-Inverse With First Gradient Method (Part 2 of 2)

A complimentary reason for the avoidance is clear if we compare the X-momentum plots of this approach with those of the inverse gain method in Chapter 5 (Figure 5-10), where one can see that the SR-inverse solution lags the inverse gain solution. At $t = 3\ sec.$, the difference in momentum between the two methods is approximately 0.6 units. This illustrates the explanation given earlier; i.e. the response is slowed down sufficiently to allow more time for null motion to act. Given enough time for reconfiguration by null motion at each simulation interval, the singularity measure could approach its global maximum. In this way, the gimbal angles are free to follow a globally maximum singularity measure trajectory, as opposed to a locally maximum trajectory that is generated by gradient methods. Following a globally maximum trajectory provides a superior means of accomplishing singularity avoidance.

From Figure 6-5, it is seen that both gimbals #2 and #4 are moved in this case, allowing gimbal #2 to be "unlocked" from its anti-parallel orientation. From the minor plots, it is seen that only one minor (M_2) becomes singular at $t = 1.15\ sec.$ Looking at Figure 6-6, it is seen that both torque and non-torque producing rates have reasonable magnitudes (not exceeding 1.8 rad/sec); by avoiding the singularity, the requirement for small gimbal rates is implicitly met.

6.4.4 SR-Inverse With Second Inverse Gain Method

Simulation results for this method are shown in Figures 6-7 through 6-9 . The null-constant (*NULL CONSTANT*) was limited to $\lambda_{max} = 3$, in order to limit the magnitude of null-gimbal rates. The maximum allowed SR weighting factor was $\kappa_{max} = 1$. Enforcing this maximum value was again not necessary in this case, as can be seen from the SR-inverse gain plot in Figure 6-7. The singularity measure plot, also on this

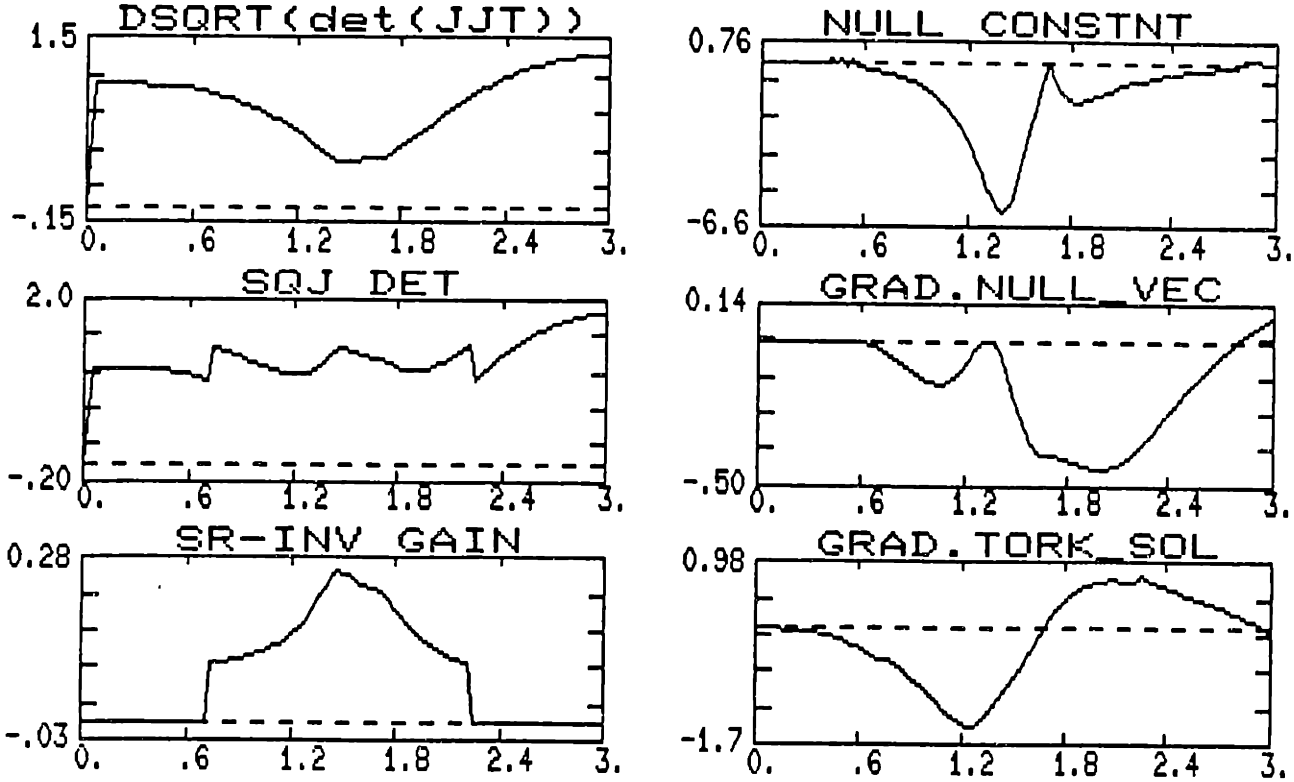

Figure 6-4. Simulation Results For SR-Inverse With Second Gradient Method (Part 1 of 2)

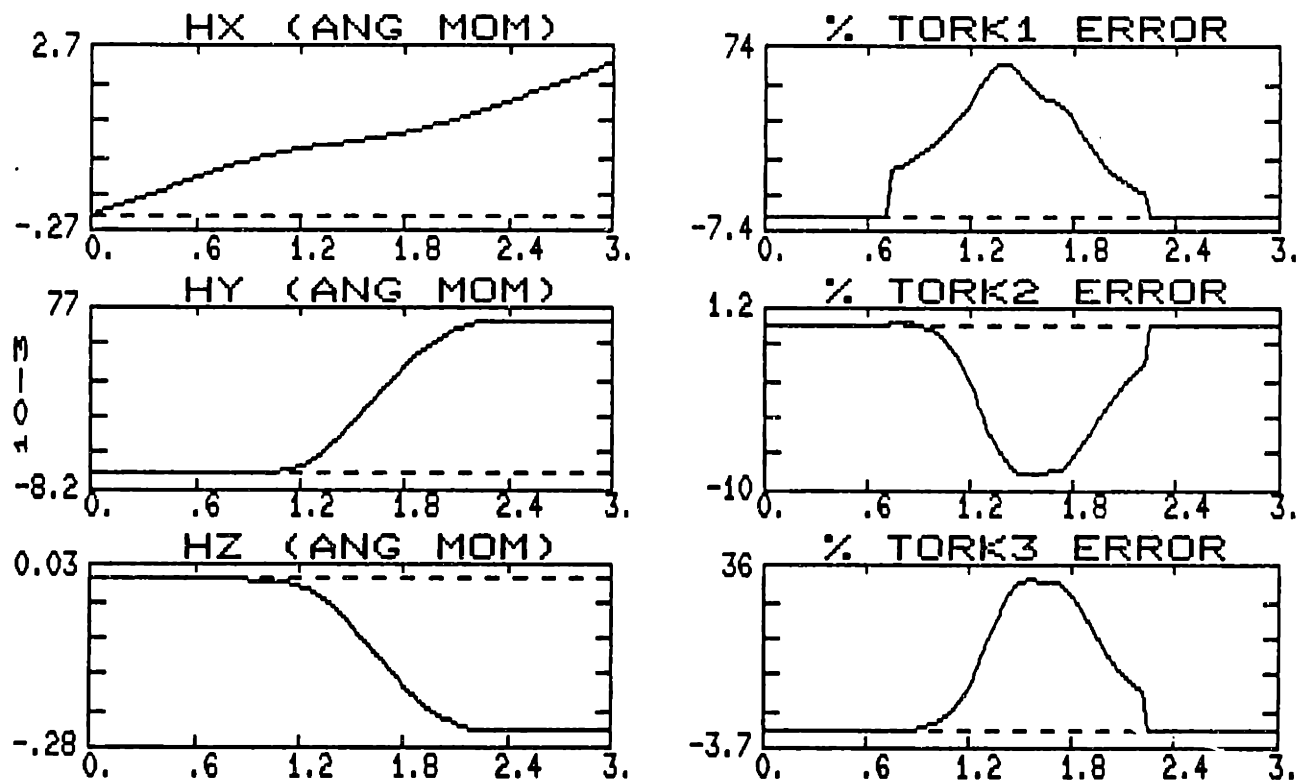

Figure 6-4. Momentum Trajectory And Torque Errors For SR-Inverse With Second Gradient Method (Part 2 of 2)

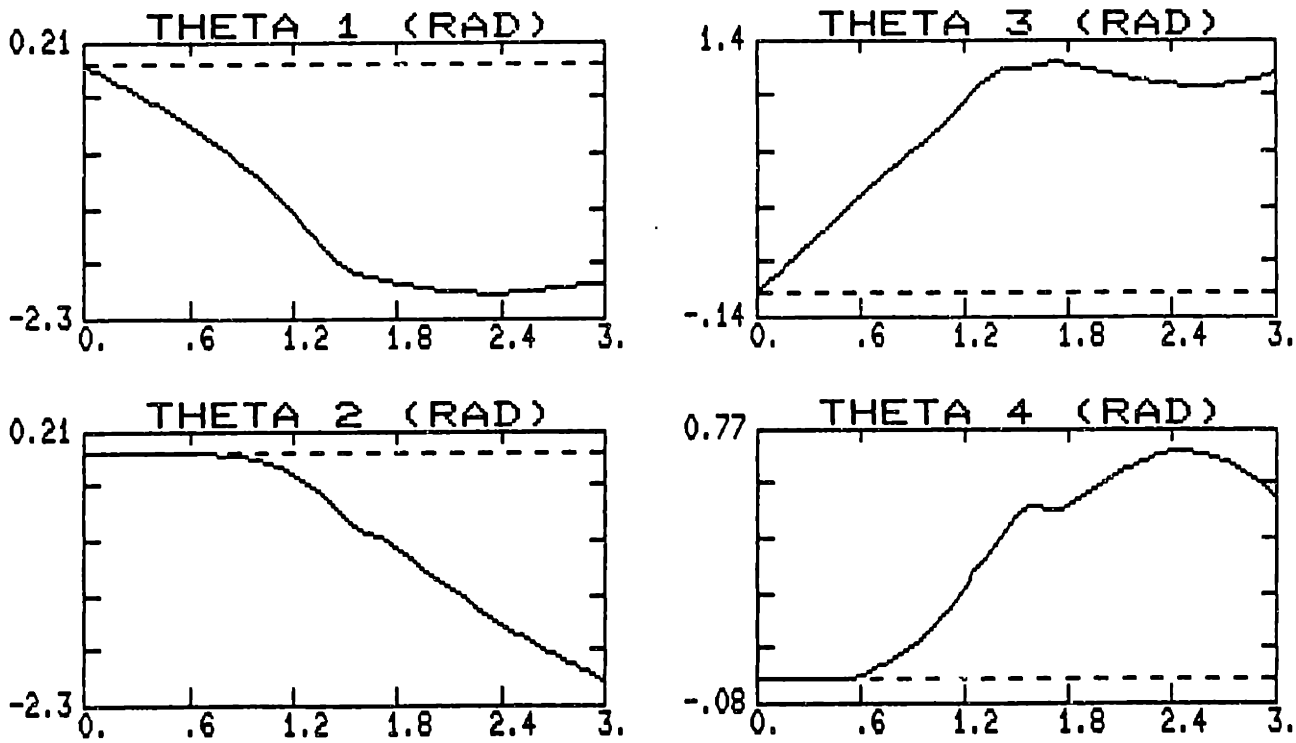

Figure 6-5. Gimbal Angles For SR-Inverse With Second Gradient Method (Part 1 of 2)

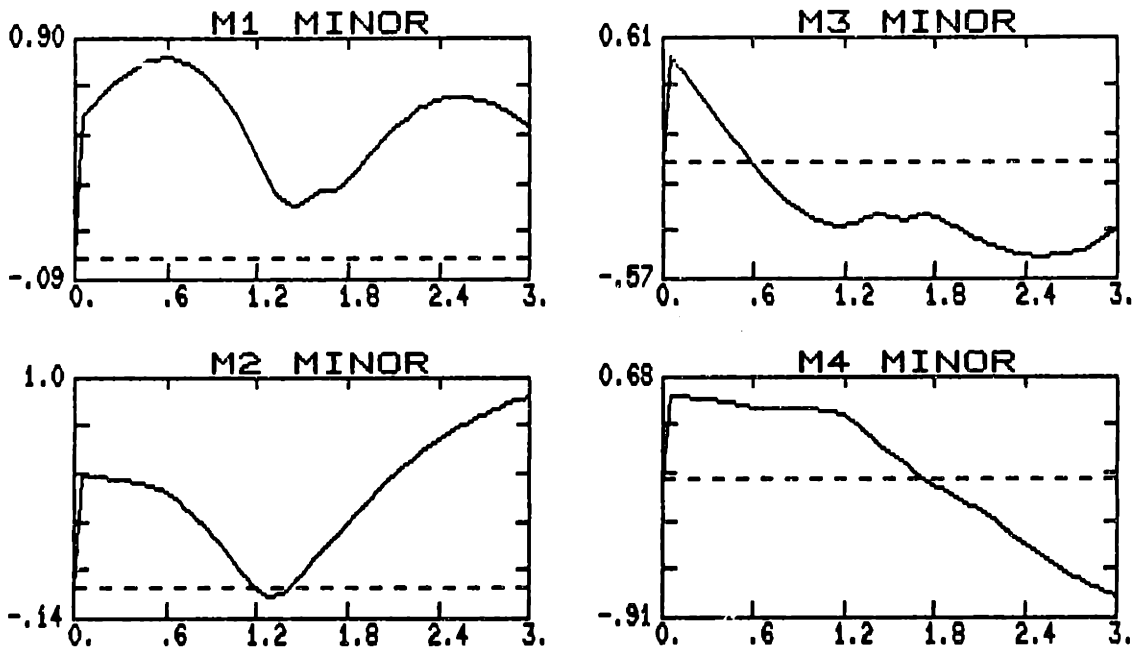

Figure 6-5. Jacobian Minors For SR-Inverse With Second Gradient Method (Part 2 of 2)

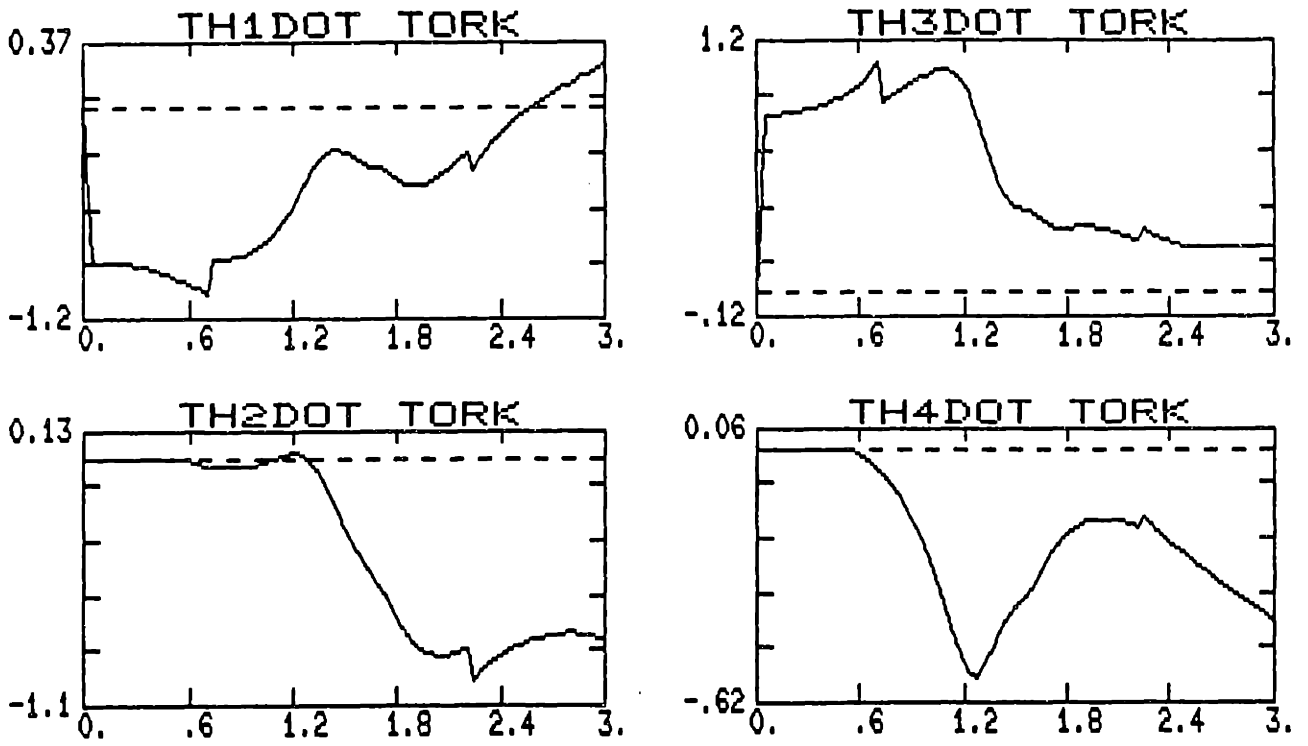

Figure 6-6. Torque Producing Rates For SR-Inverse With Second Gradient Method (Rad/Sec) (Part 1 of 2)

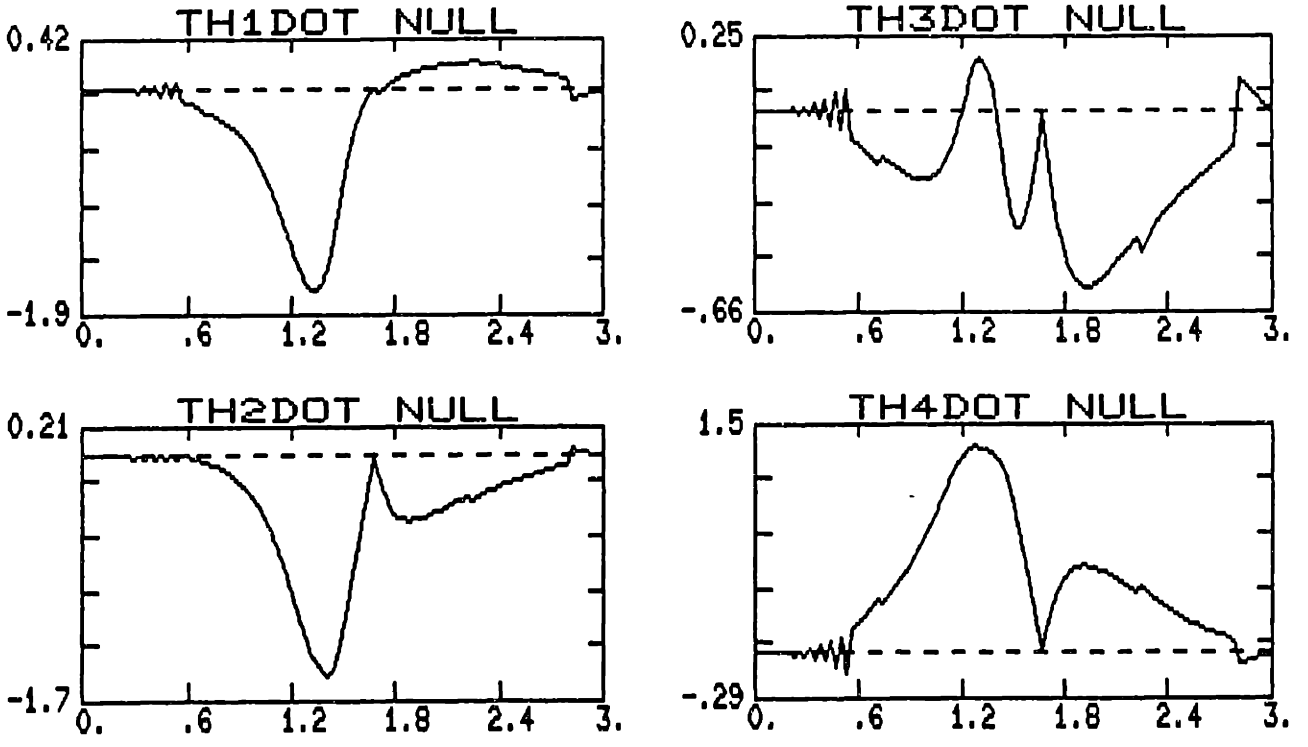

Figure 6-6. Null Rates For SR-Inverse With Second Gradient Method (Rad/Sec) (Part 2 of 2)

page, indicates that the singularity is again avoided. The maximum torque error introduced via the SR-inverse is approximately 25% in the X-direction, when the system is near the singularity. Comparing results obtained in Chapter 5 with the second inverse gain method using the M-P inverse (Figure 5-10), it is observed that both the null-constant and torque solution projection are smaller for the SR-inverse approach. Because of the torque errors introduced by the SR-inverse in the singular region, however, a lag of 0.2 units is evident in the X-momentum plot for the SR-inverse. The gimbal angles and minors are shown in Figure 6-8. Near the singular momentum state ($H_X = 1.15$, $t \cong 1.15$ *sec.*), it is seen that none of the minors are singular, i.e. are zero.

Comparing the gimbal rates from this approach, shown in Figure 6-9, to those analogously obtained from the M-P inverse, the peak torque producing gimbal rates calculated by the SR method are seen to be approximately 0.4 rad/sec smaller. The null rates, however, are essentially the same.

6.5 NON CONSTANT TORQUE REQUEST SIMULATION

In this simulation, the same non-constant torque request used in Chapter 5 for the M-P inverse with the second inverse gain method is applied to the SR-inverse equipped with the same null algorithm. Simulation results are shown in Figures 6-10 through 6-12 . The maximum allowed SR weighting factor was $\kappa_{max} = 0.2$, while the maximum value of the null-constant was $\lambda_{max} = 3$. From Figure 6-10, it is seen that the system is driven to a singular state, even though the SR-inverse is used. It is also observed that at the singularity any null motion is ineffective since the null projection there is zero. The reason for this is that the null vector is identically zero at this singularity,

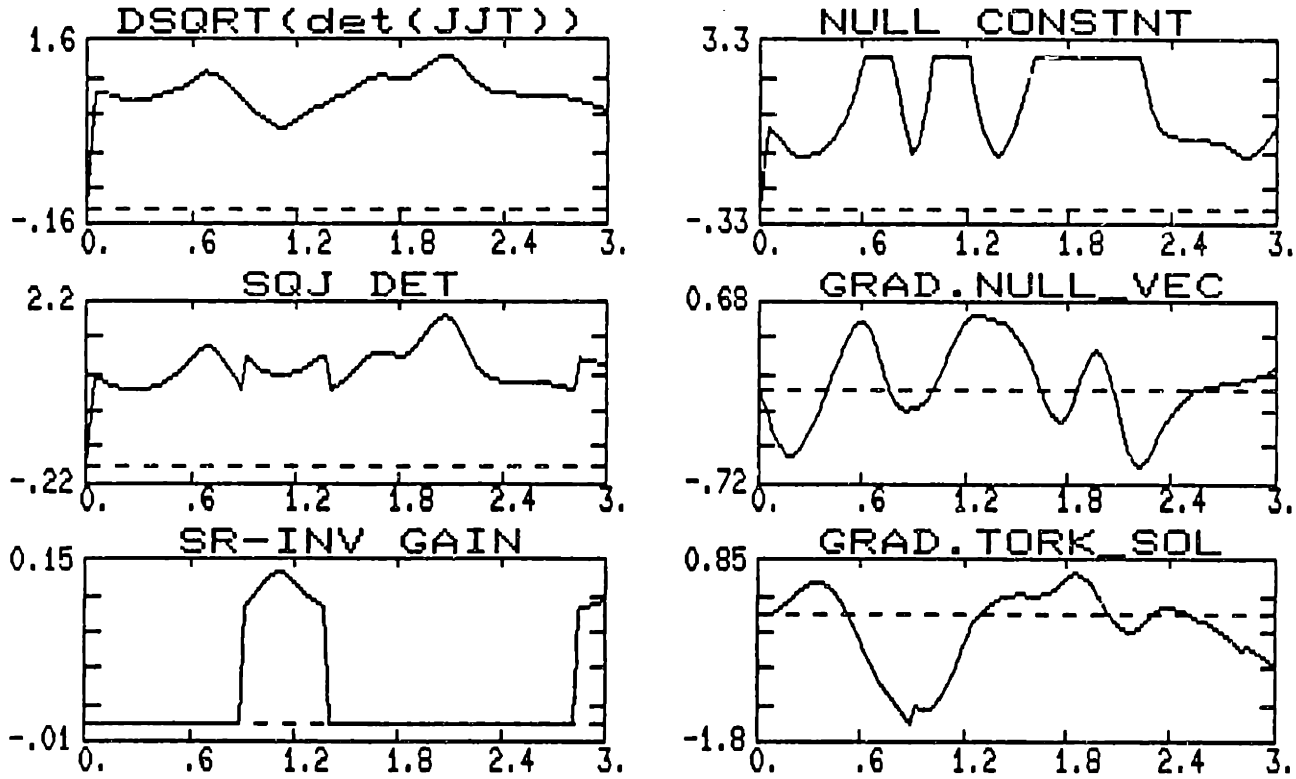

Figure 6-7. Simulation Results For SR With Second Inverse Gain Method (Part 1 of 2)

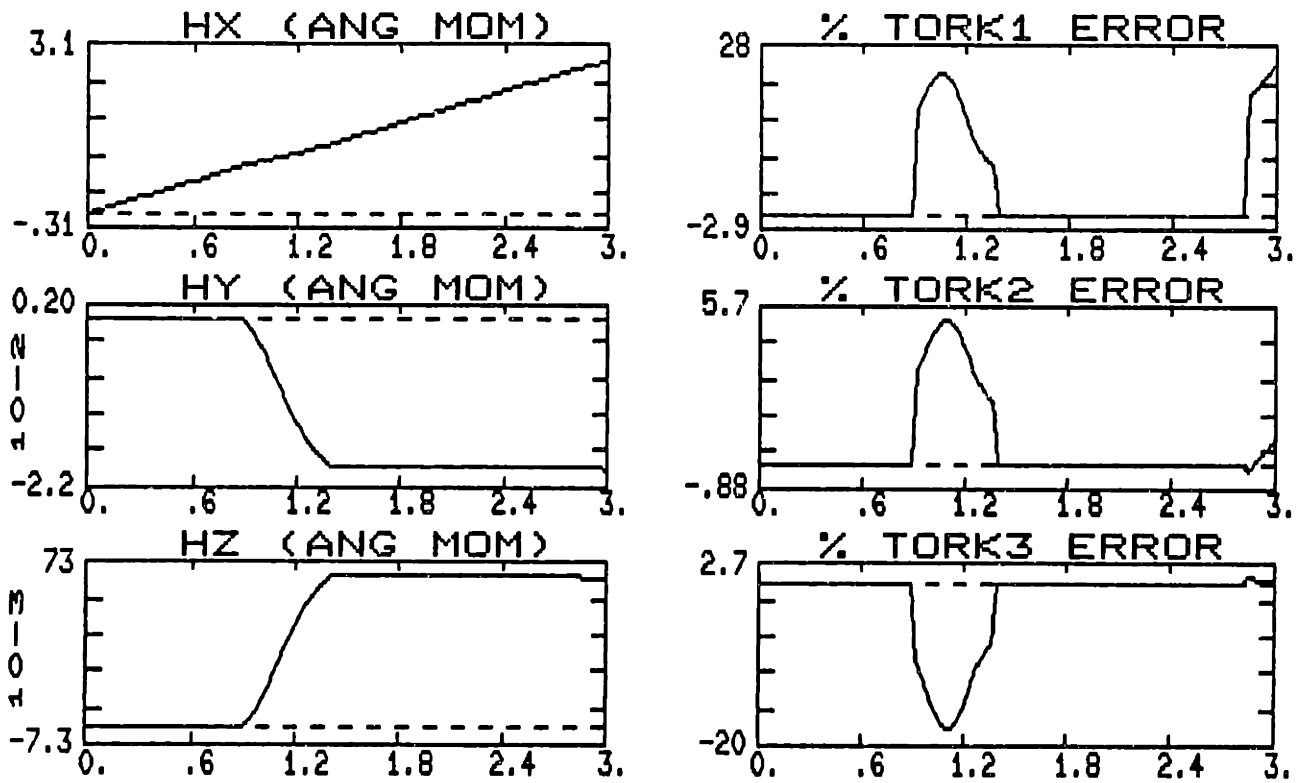

Figure 6-7. Momentum Trajectory And Torque Error For SR With Second Inverse Gain Method (Part 2 of 2)

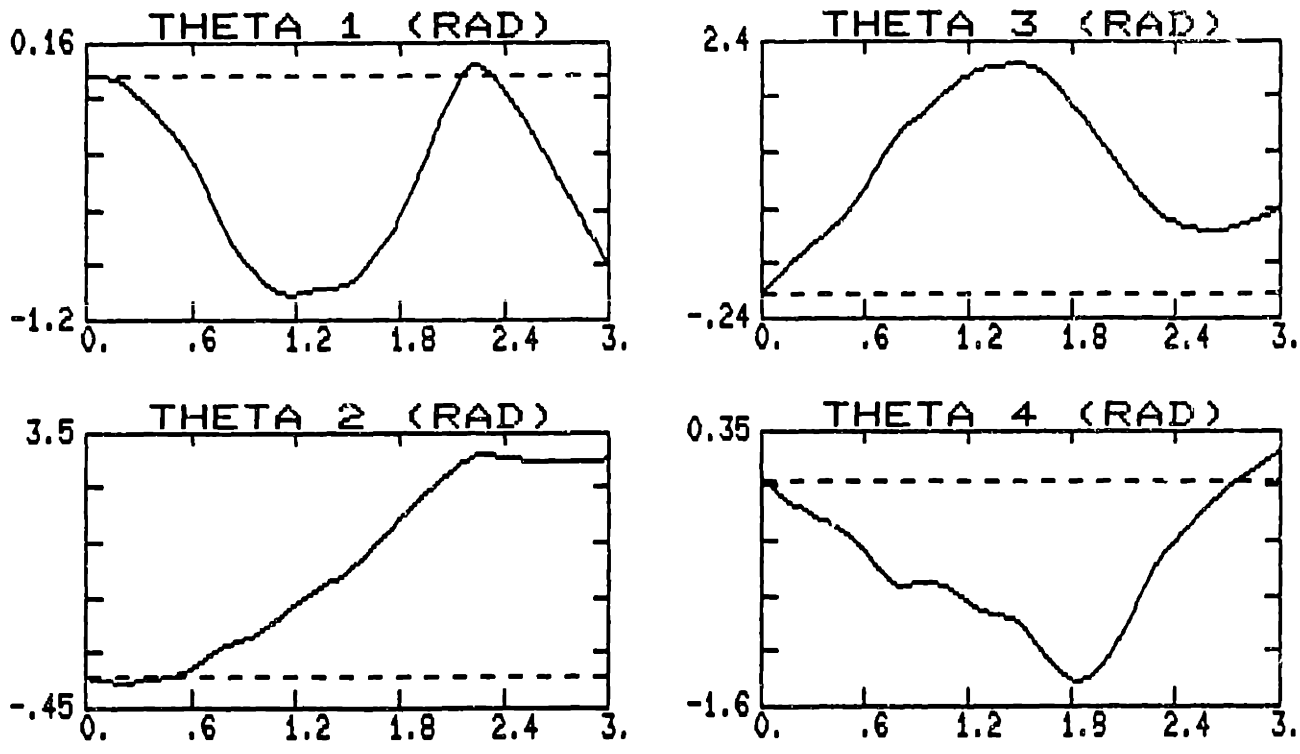

Figure 6-8. Gimbal Angles For SR With Second Inverse Gain Method (Part 1 of 2)

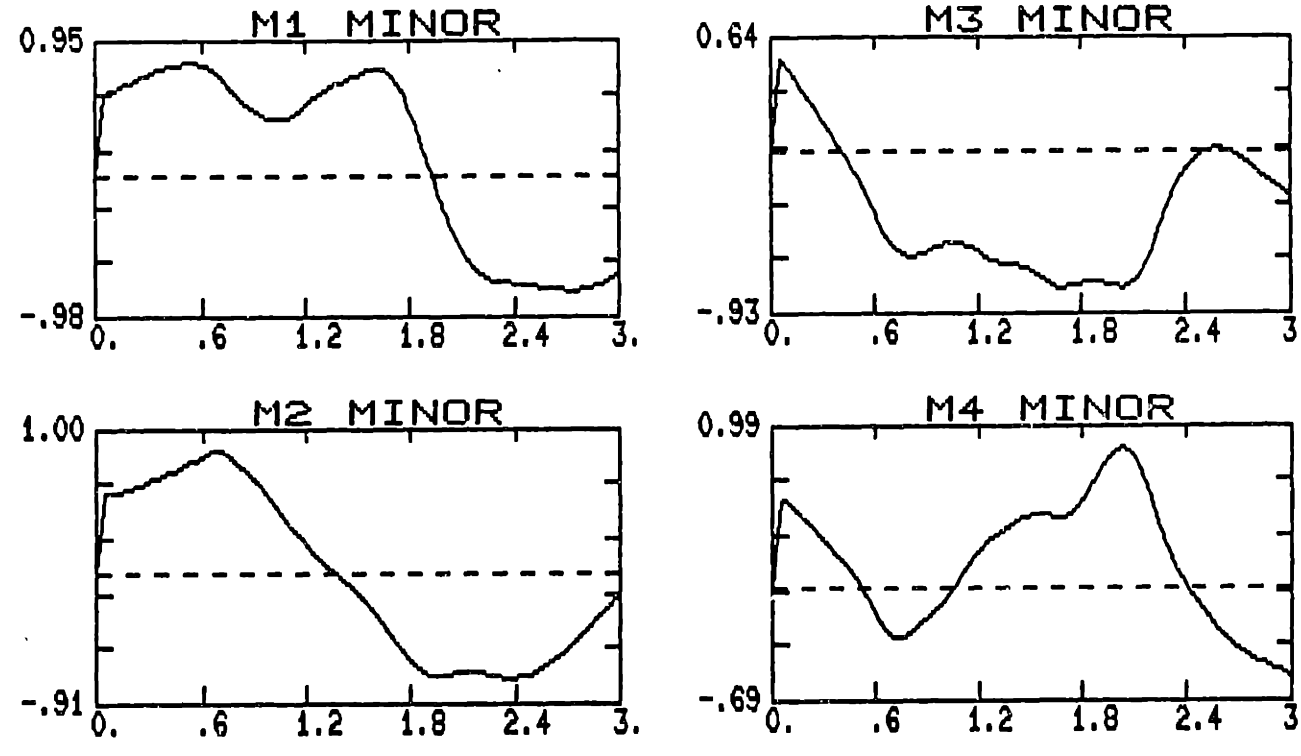

Figure 6-8. Jacobian Minors For SR With Second Inverse Gain Method (Part 2 of 2)

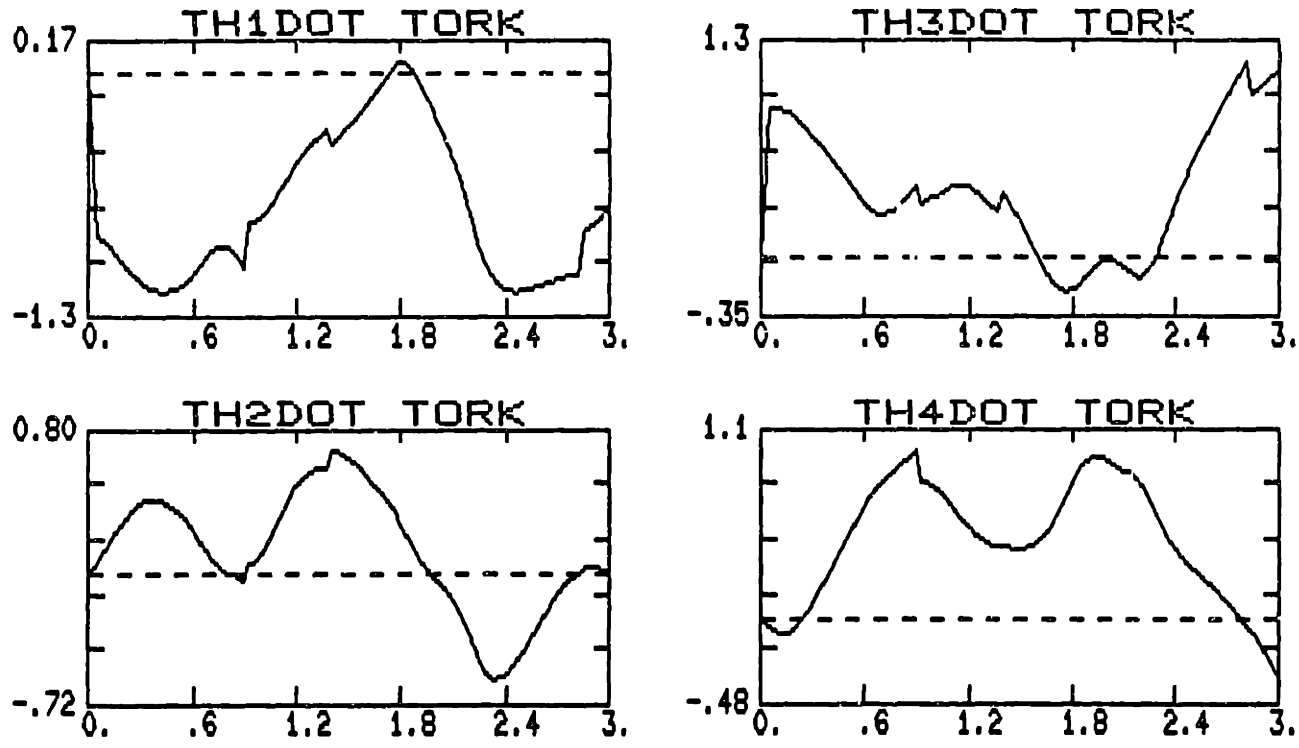

Figure 6-9. Torque Producing Gimbal Rates For SR With Second Inverse Gain Method (Rad/Sec) (Part 1 of 2)

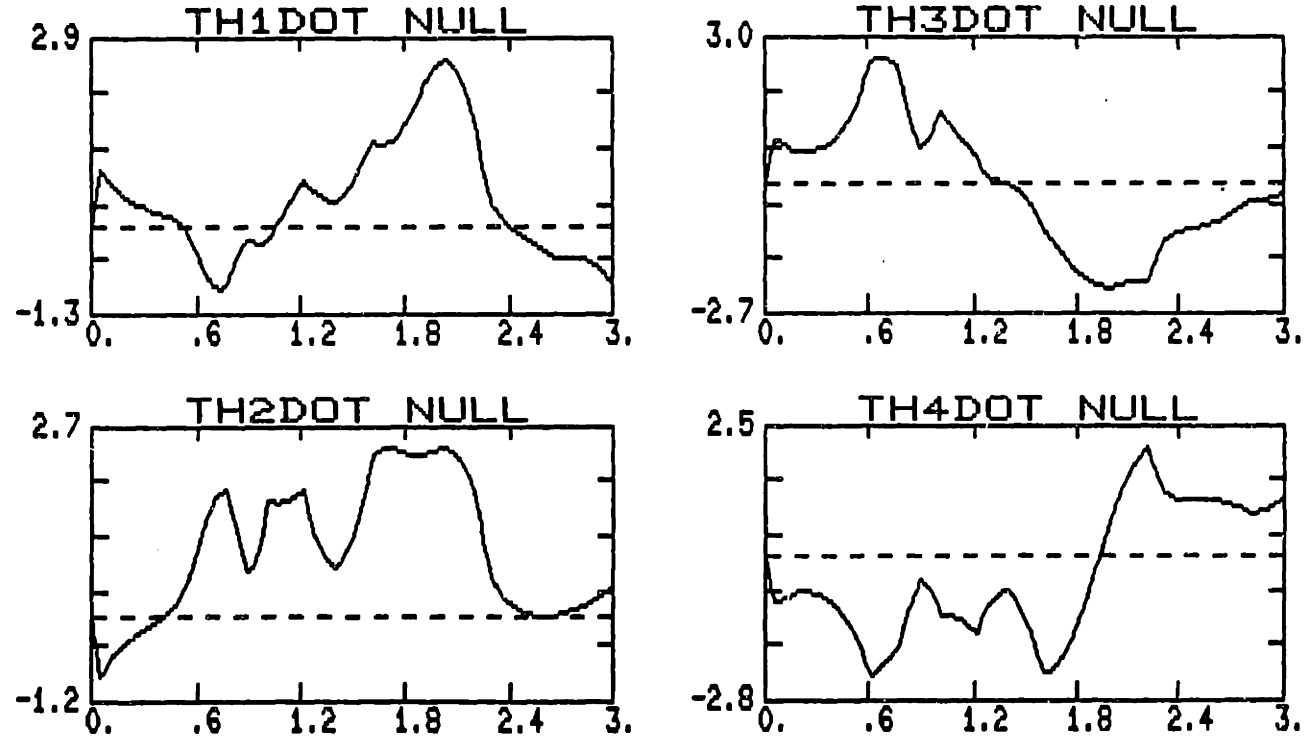

Figure 6-9. Null Gimbal Rates For SR With Second Inverse Gain Method (Rad/Sec) (Part 2 of 2)

since all Jacobian minors are zero (see Figure 6-11). The momentum trajectory and torque errors are shown in Figure 6-10, from which it is seen that substantial torque errors are generated by the SR approach. Comparing Figures 6-10 and 5-14, we observe that the system remains singular for a longer period using the SR method, whereas the torque projection spike in Figure 5-14 is at least an order magnitude larger than the corresponding spike for the SR method, creating proportionally larger torque producing gimbal rates. The difference in momentum trajectory followed by both methods is clearly evident from this comparison.

From Figure 6-11, we observe that all minors are simultaneously zero for a substantial period of time. Comparing the minor plots in this figure to those in Figure 5-16, it is seen that the minor trajectories for both methods are essentially the same up to the switch time (0.83 sec.), and very different afterwards. A similar effect is seen when comparing gimbal angle trajectories in Figures 6-11, 5-14.

The superior performance of the SR approach is evident from the results in Figure 6-12. From this figure, it is seen that the peak torque producing gimbal rates do not exceed 1.4 rad/sec, as compared to 7.4 rad/sec for the M-P based method in Figure 5-15. In addition, the SR-inverse is not seen to generate large spikes in gimbal rates that were noted in the M-P results. The null-rates for the SR method are significantly smaller, as also seen in these plots. This is due to the different gimbal angle trajectory that the M-P method followed after the switch time, which resulted in a higher singularity measure state, as well as higher values for the minors. In conclusion, the superior performance of the SR based method over the corresponding M-P based approach is clearly evident from this simulation. As discussed before, however, if the

requested torque direction at the switch time was along the singular direction corresponding to the singular momentum state, the SR approach would not have been able to extract the system from the singular configuration, since zero torque producing rates are generated.

6.6 CONCLUSION

It has been shown that the SR-inverse is able to avoid the Elliptic singularity at $H_x = 1.15$ only when equipped with an appropriate null motion algorithm. The superior performance of this method has also been shown for a case requiring a non-constant torque. The general singularity avoidance property of the SR-inverse has also been discussed, and it has been shown that the prime mechanism by which this method avoids singularities is by slowing the system response to an input torque request in the neighborhood of a singularity, allowing more time for null motion to be applied. In terms of the mechanical analog, the end-effector velocity is reduced before reaching the singularity, allowing a longer interval over which null motion can be performed. The SR-inverse can also introduce finite torque errors orthogonal to the requested torque direction; although these errors aid in skirting the singular region, the slow-down along the commanded axis, coupled with null motion, provides the most significant effect.

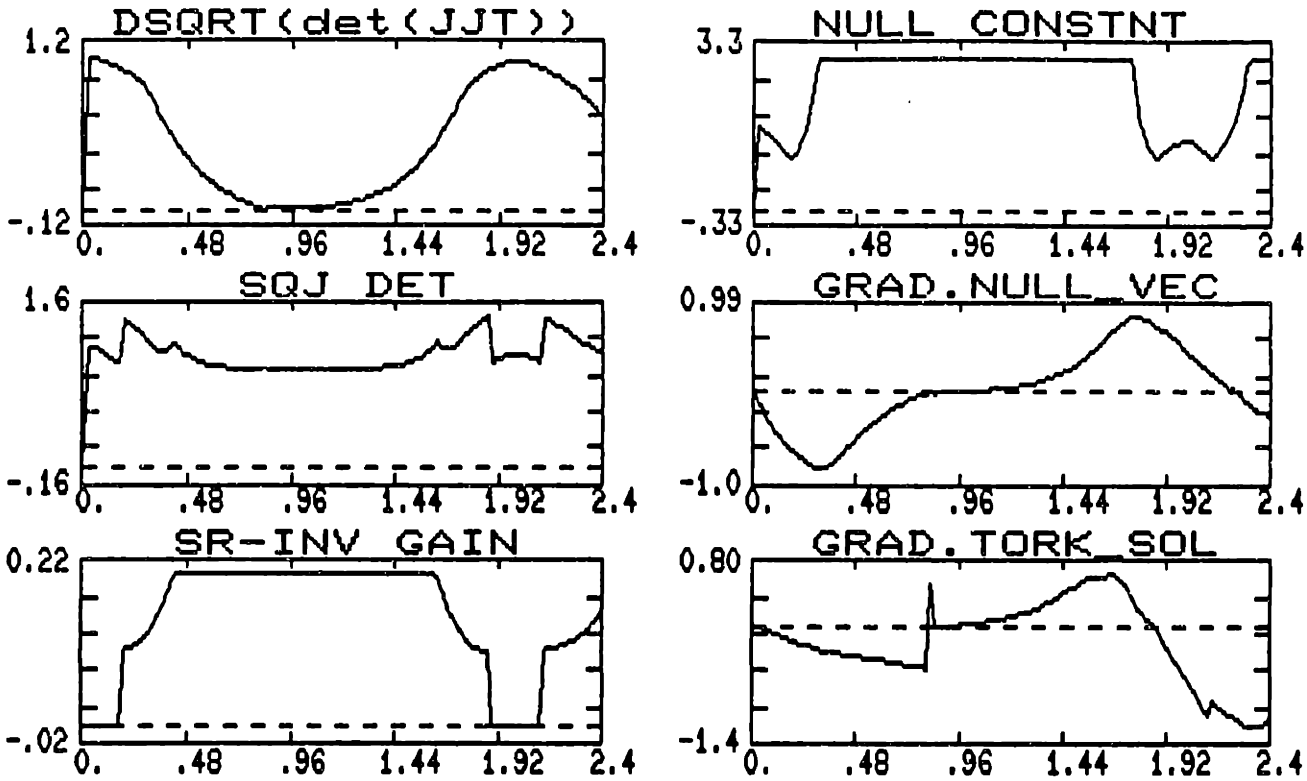

Figure 6-10. Simulation Results For Non-Constant Torque Request (Part 1 of 2)

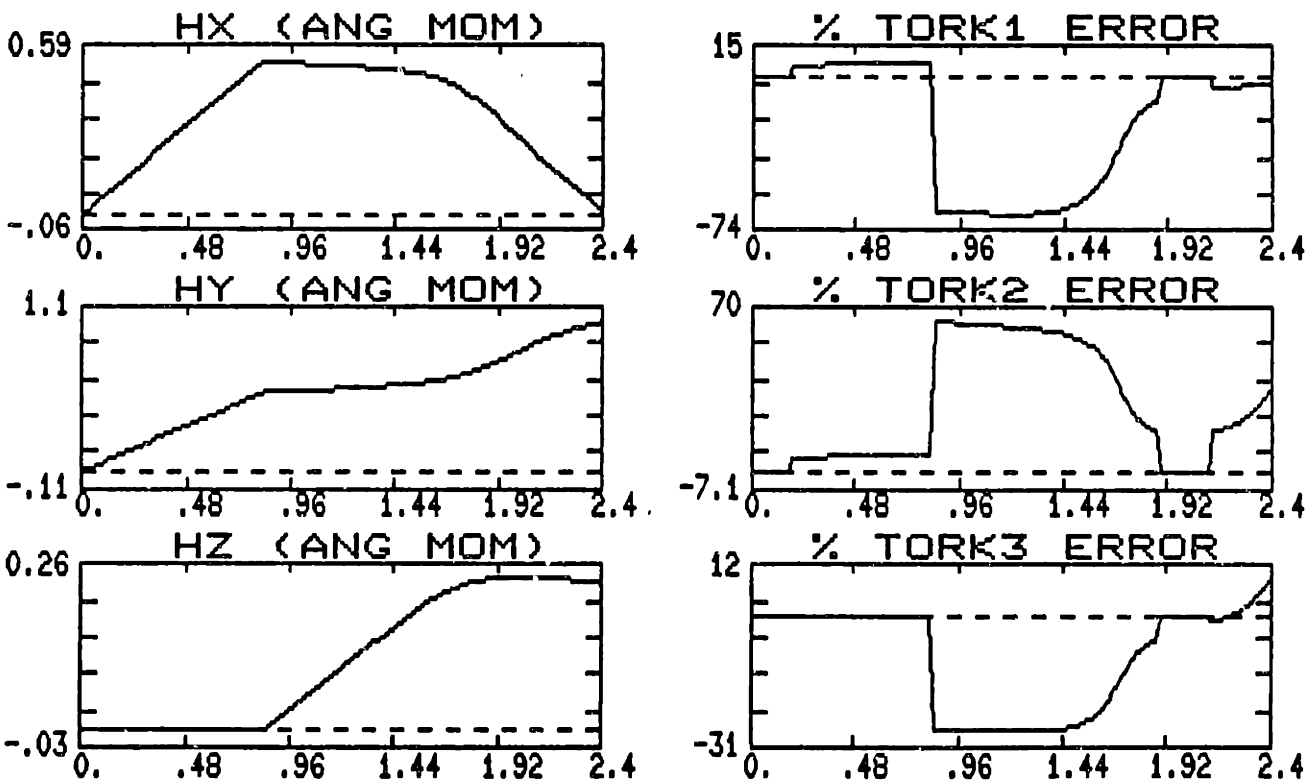

Figure 6-10. Momentum Trajectories And Torque Errors For Non-Constant Torque Request (Part 2 of 2)

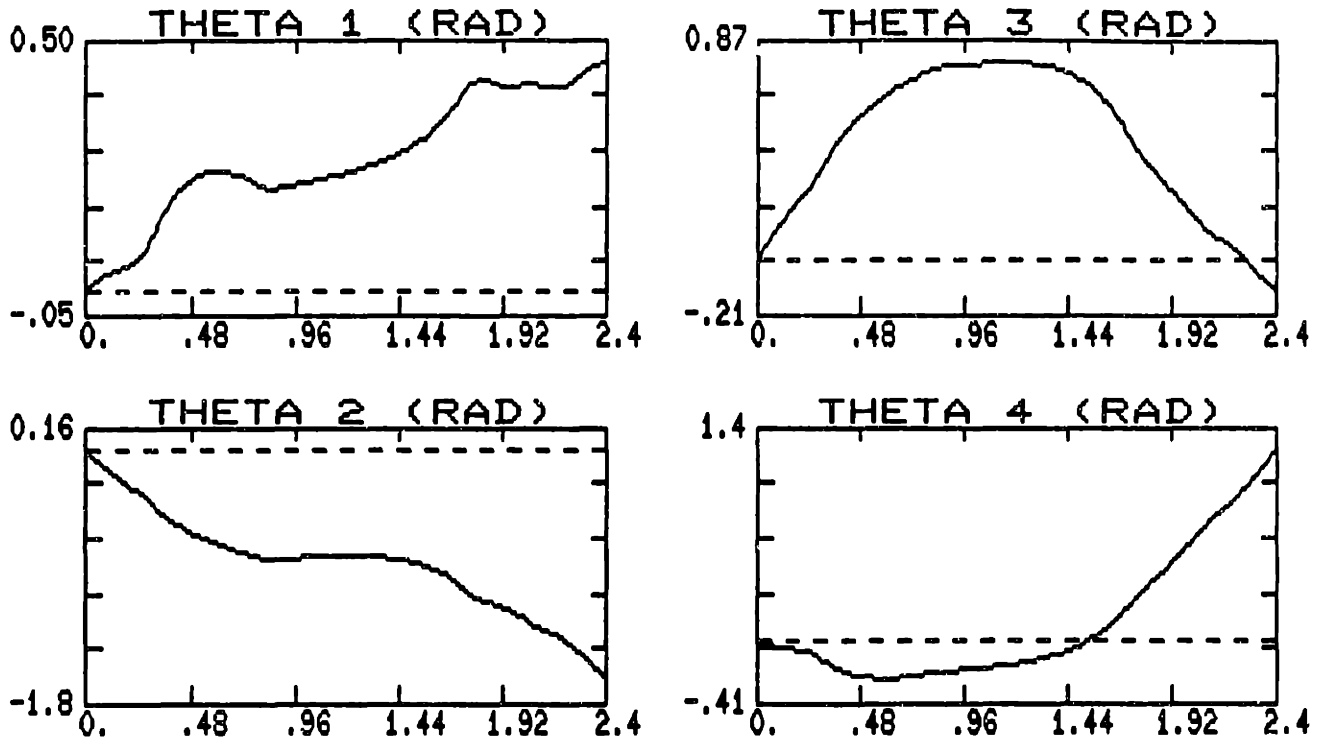

Figure 6-11. Gimbal Angles For Non-Constant Torque Request (Part 1 of 2)

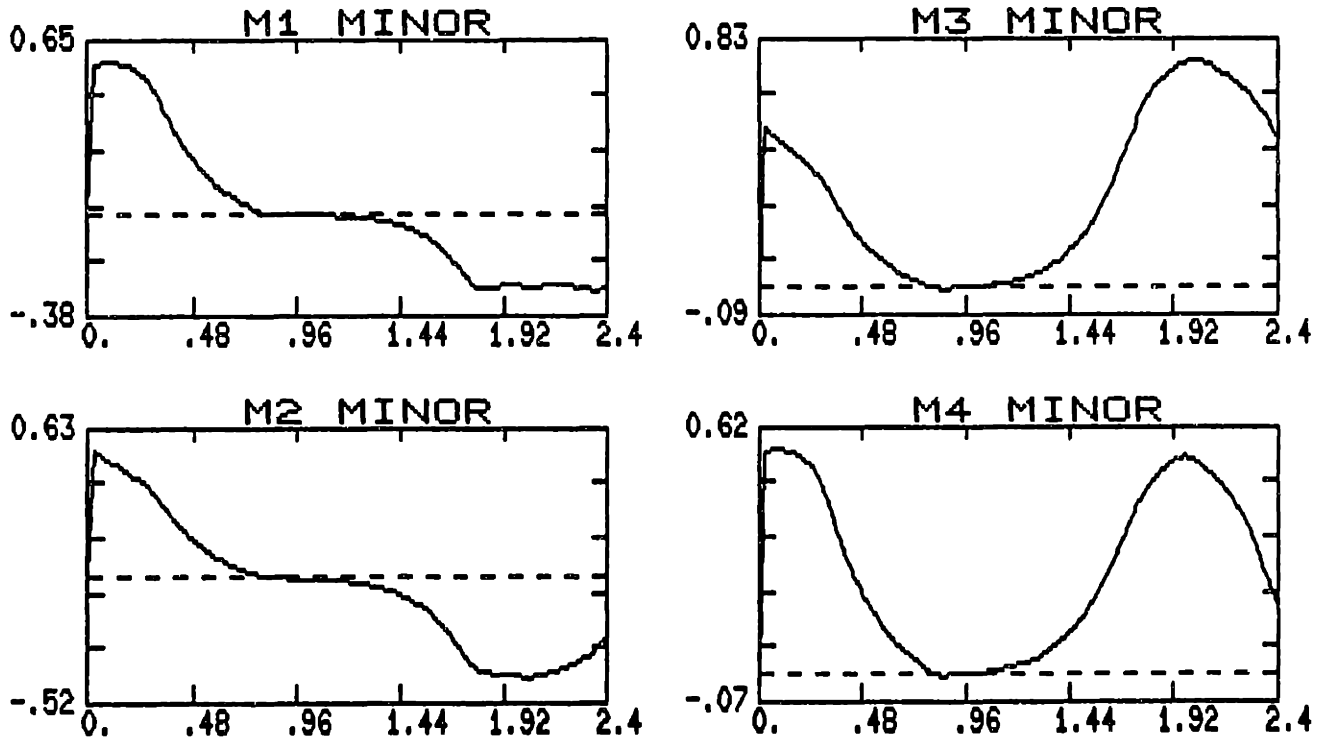

Figure 6-11. Jacobian Minors For Non-Constant Torque Request (Part 2 of 2)

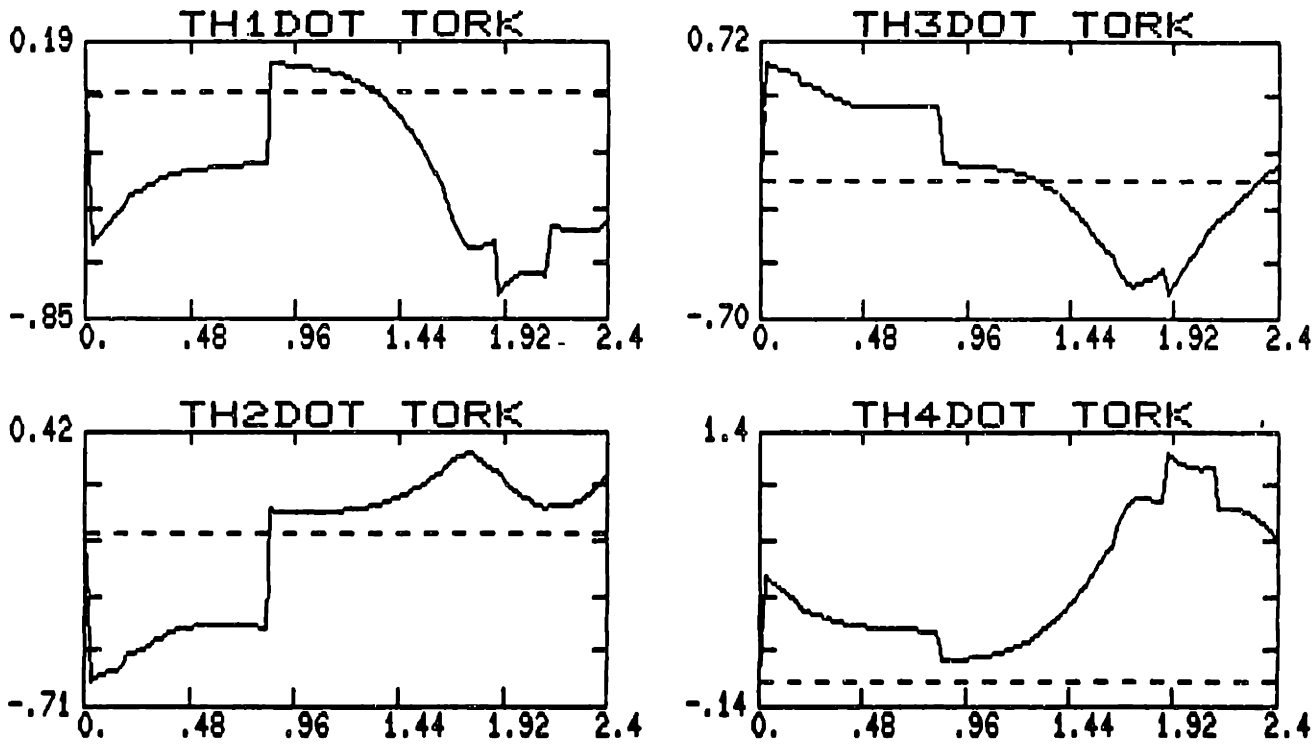

Figure 6-12. Torque Producing Gimbal Rates For Non-Constant Torque Request (Rad/Sec) (Part 1 of 2)

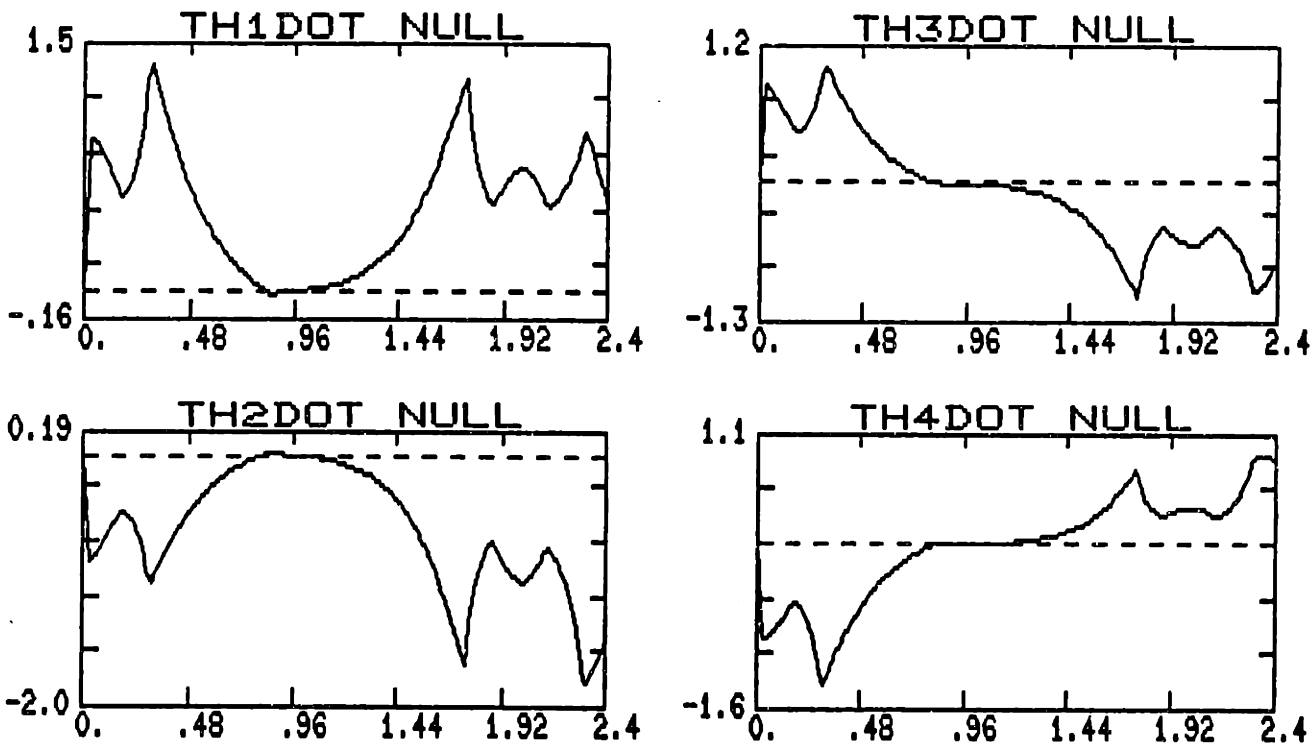

Figure 6-12. Null Gimbal Rates For Non-Constant Torque Request (Rad/Sec) (Part 2 of 2)

CHAPTER 7

CONCLUSIONS AND RECOMMENDATIONS

In this thesis, the problem of spacecraft attitude control using redundant single gimbal CMGs has been investigated. Specifically, the singularity problems associated with a 4-CMG system has been examined, in addition to the formulation of a general torque based Steering law for redundancy resolution. A Steering law using the SR-inverse with appropriate null motion has been shown to provide a promising approach to singularity avoidance; by not restricting the system to produce the exact torque request, singular CMG configurations are avoided.

In Chapter 2, single gimbal CMG fundamentals were reviewed, and the mechanical analog to the CMG system, the robotic manipulator, was proposed. It was shown that both systems possess similar difficulties with singular configurations, and that results from one area may be applicable to the other. A simple method of generating an orthogonal null-space basis to the Jacobian matrix was also presented.

In Chapter 3, the control architecture for spacecraft equipped with single gimbal CMGs was reviewed. A dual-level control structure using an Outer and Inner Control loop was discussed, as well as the desirability of the Outer control loop to accomodate occasional errors in torque delivered by the CMG system.

In Chapter 4, the singular states of single gimbal CMGs were classified, and a test for null motion near a singularity was presented. Examples of the different types of singularities were presented for both the CMG system and a planar manipulator. The singularity measure and its relationship to the null-space of the Jacobian was exam-

ined. It was shown that the magnitude of the non-singular Jacobian null-space vector is identical to the singularity measure.

In Chapter 5, various torque-input Steering laws were reviewed, and alternative singularity avoidance methods based on the Moore-Penrose pseudoinverse were presented. It was shown that existing singularity avoidance methods do not avoid Elliptic-type internal singularities. Although the inverse gain method was shown to generally avoid this type of singularity, it may nonetheless still drive the system toward a singular configuration due to its nondirectional nature, as was demonstrated. The results of this chapter indicated that reliable real-time avoidance of internal Elliptic-type singularities cannot be accomplished using any of the available Steering laws or any of the proposed methods.

In Chapter 6, the SR-inverse was introduced as an alternative to the Moore-Penrose pseudoinverse. It was shown that this inverse can avoid Elliptic-type internal singularities when equipped with an appropriate null motion algorithm. The superior performance of this method was demonstrated for a non-constant torque request; its singularity avoidance characteristics surpassed those presented in Chapter 5, and gimbal rates calculated using this method were generally smaller. It was noted, however, that if the system was driven to a singular state using this approach, and a torque is requested along the singular direction, the SR-inverse can only generate zero torque producing gimbal rates, thus trapping the system in the singular state unless the singularity is escapable by null motion.

For a completely general SR-inverse based Steering law, the form of the null-algorithm needs to be investigated further, since the performance of this approach is directly related to the specific form of null-algorithm used in conjunction with the SR-inverse. To overcome the problem of being trapped in a singular state when a torque along the singular direction is requested, momentary torque errors could be introduced such that the SR-inverse is able to drive the system out of the singular state. The projection of the null-vector onto the gradient of the singularity measure may prove useful in resolving the nature (i.e. escapable/non-degenerate or unescapable/degenerate) of Hyperbolic singularities.

LIST OF REFERENCES

1. Margulies G., Aubrun N., "Geometric Theory of Single-Gimbal Control Moment Gyro Systems", AIAA Guidance and Control Conference, San Diego, California, August 16-18, 1976 (Paper No. 76-1945, pp. 255-267).

2. Noble B., Daniel J. W., *Applied Linear Algebra*, Prentice-Hall, Inc. New Jersey, 1977.

3. "Space Shuttle Orbiter Operational Level C Functional Subsystem Software Requirements
   Guidance, Navigation, and Control, Part C, Flight Control Orbit DAP", Rockwell International, STS 83-0009A, June 30, 1985.

4. Redding D. C., Adams N. J., "Optimized Rotation-Axis Attitude Maneuver Controller For The Space Shuttle Orbiter", J. of Guidance, Control, and Dynamics, Vol. 10, No. 1, January-February 1987, pp. 4-13.

5. Bedrossian N., "Review of Redundant Single Gimbal CMG Control Law Design", CSDL Intralab Memorandum, August 1987.

6. Hughes P. C., *Spacecraft Attitude Dynamics*, John Wiley & Sons, Inc. New York, 1986.

7. Bedrossian N., "Robust Controller Design for Torque Free Spacecraft Maneuvers", M.I.T. course 2.153 term project, December 1984.

8. Schiehlen W. O., "Two Different Approaches for a Control Law of Single Gimbal Control Moment Gyro Systems", NASA TM X-64693, August 1972.

9. Strang G., *Introduction To Applied Mathematics*, Wellesly-Cambridge Press, Wellesly, MA, 1986.

10. Paradiso J., "A Highly Adaptable Steering/Selection Procedure For Combined CMG/RCS Spacecraft Control", C.S. Draper Lab. Report CSDL-R-1835, March 1986.

11. Cornick D.E., "Singularity Avoidance Control Laws for Single Gimbal Control Moment Gyros", AIAA Guidance and Control Conference, Boulder, Colorado, August 1979, (Paper No. 79-1968, pp. 20-23).

12. Matusky M. P., "Systems of Single-Gimbal Control Moment Gyros", C.S. Draper Lab. Space Guidance And Navigation Memo No. 10E-87-07, May 18, 1987.

13. Hattis P., "Predictive Momentum Management for the Space Station", J. of Guidance, Control, and Dynamics, Vol. 9, No. 4, July-August 1986, pp. 454-461.

14. Kennel H. F., "Angular Momentum Desaturation for ATM/LM/CSM Configuration Using Gravity Gradient Torques", NASA TM X-53764, August 9, 1968.

15. Kurokawa H., Yajima S., Usui S., "A New Steering Law of a Single-Gimbal CMG System of Pyramid Configuration", Proc. X'th IFAC Symposium on Automatic Control in Space, Toulouse, France, June 25-28, 1985, pp. 249.

16. Yoshikawa T., "A Steering Law for Three Double-Gimbal Control Moment Gyro Systems", NASA TM X-64926, March 1975.

17. Yoshikawa T., "Manipulability of Robotic Mechanisms", Second International Symposium on Robotics Research, Kyoto, Japan, August 20-23, 1984.

18. Chang P. H., "Analysis And Control Of Robot Manipulators With Kinematic Redundancy", Ph.D. Thesis, Massachusetts Institute of Technology, Mechanical Engineering, May 1987.

19. Baillieul J., Hollerbach J., Brockett R., "Programming and Control of Kinematically Redundant Manipulators", Proc. 23rd IEEE Conf. on Decision and Control, Las Vegas, NV, 1984, pp. 768-774.

20. Hollerbach J., Suh K. C., "Redundancy Resolution of Manipulators through Torque Optimization", Proc. IEEE Int. Conf. Robotics and Automation, St. Louis, March 25-28, 1985, pp.1016-1021.

21. Nakamura Y., Hanafusa H., "Inverse Kinematic Solutions With Singularity Robustness for Robot Manipulator Control", ASME J. Dynamic Systems, Meas., Control, Vol. 108, September 1986, pp. 163-171.